

Aus dem Deutschen Krebsforschungszentrum (DKFZ) in der Helmholtz-Gemeinschaft
(Vorstandsvorsitzender und Wissenschaftlicher Vorstand: Prof. Dr. Michael Baumann)

Forschungsbereich Infektion, Entzündung und Krebs
Arbeitsgruppe Molekulare Therapie virusassoziierter Tumoren
(Arbeitsgruppenleiter: Prof. Dr. Felix Hoppe-Seyler)

Expression and Function of FAM57A (Family with Sequence Similarity 57 Member A) in Human Papillomavirus-Positive Cervical Cancer Cells

Inauguraldissertation
Zur Erlangung des medizinischen Doktorgrades
an der
Medizinischen Fakultät Heidelberg
der
Ruprecht-Karls-Universität
vorgelegt von
Dongyun Yang
aus
Anhui, China
2022

Dekan: Herr Prof. Dr. med. Hans-Georg Kräußlich

Doktorvater: Herr Prof. Dr. med. Felix Hoppe-Seyler

1. Table of Contents

1. Table of Contents	1
2. List of Figures	4
3. List of Tables	6
4. Abbreviations	7
5. Introduction	11
5.1 Cancer	11
5.2 Human papillomaviruses (HPVs) and cancer	11
5.2.1 HPVs and cervical cancer	11
5.2.2 The biology of HPV infection and HPV-associated carcinogenesis	12
5.2.3 The viral E6 and E7 oncoproteins	14
5.2.4 Cellular pathways related to biological characteristics of cervical cancer cells	15
5.2.5 Prevention and therapy of cervical cancer	16
5.3 Hypoxia and cancer	17
5.3.1 Hypoxia-inducible factors (HIFs)	18
5.3.2 Cellular metabolism under hypoxia	19
5.3.3 Hypoxia-induced resistance towards anti-cancer therapy	20
5.3.4 Hypoxia and HPV E6/E7 oncoproteins	21
5.4 FAM57A (family with sequence similarity 57 member A)	22
5.5 Research objectives	26
6. Materials and Methods	27
6.1 Reagents	27
6.2 Cellular biology techniques	27
6.2.1 Cell culture	27
6.2.2 Cell cryopreservation and thawing	28
6.2.3 Treatment with chemical compounds	28
6.2.4 Transfection of plasmid DNA	29
6.2.5 Transfection of synthetic small interfering RNAs (siRNAs)	29
6.2.6 CheckMate™ Mammalian Two-Hybrid System	31
6.2.7 Colony formation assays	32
6.2.8 Cell growth analyses	32

1. Table of Contents

6.2.9 Wound healing assays	33
6.3 DNA-based techniques	33
6.3.1 Transformation of bacteria	33
6.3.2 DNA preparation and sequencing validation	34
6.3.3 Molecular cloning strategies	35
6.4 RNA-based techniques	40
6.4.1 RNA extraction from cultured cells	40
6.4.2 Reverse transcription PCR (RT-PCR)	40
6.4.3 Quantitative real-time PCR (qRT-PCR)	40
6.5 Protein-based techniques	42
6.5.1 Development of a monoclonal mouse anti-FAM57A antibody	42
6.5.2 Protein extraction from cultured cells	42
6.5.3 Sodium dodecyl sulfate-polyacrylamide gel electrophoresis (SDS-PAGE)	43
6.5.4 Western transfer	43
6.5.5 Immunodetection of proteins	44
6.6 Statistical analyses	45
7. Results	46
7.1 Analysis of FAM57A expression	46
7.1.1 Development and validation of an antibody for FAM57A detection	46
7.1.2 FAM57A expression is induced under hypoxia	47
7.1.3 Cell density is a key regulator of FAM57A protein expression	48
7.1.4 Hypoxia-induced FAM57A protein expression is predominantly a result of decreased cell density	50
7.1.5 HPV <i>E6/E7</i> suppression induces FAM57A expression in a cell density-dependent manner.....	53
7.2 Phenotypic effects of FAM57A in HPV-positive cancer cells	54
7.2.1 FAM57A promotes the proliferation of HPV-positive cancer cells	54
7.2.2 FAM57A promotes the migration of HPV-positive cancer cells	55
7.3 Potential factors mediating FAM57A functions	59
7.3.1 SLC3A2 and FAM57A	59
7.3.2 FAM57A may be an upstream regulator of YAP/TAZ signaling	63
8. Discussion	68
8.1 Regulation of FAM57A expression	68

8.2 Phenotypic effects of FAM57A in HPV-positive cancer cells	69
8.2.1 FAM57A promotes the proliferation of HPV-positive cancer cells	69
8.2.2 FAM57A promotes the migration of HPV-positive cancer cells	72
8.2.3 Expression levels of factors involved in YAP/TAZ signaling are downregulated following <i>FAM57A</i> suppression	73
8.3 Conclusions and perspectives	75
9. Summary	76
10. References	78
11. Curriculum Vitae	97
12. Acknowledgments	98
13. Eidesstattliche Versicherung	99

2. List of Figures

Figure 1. HPV16 genome organization	12
Figure 2. The HPV life cycle in squamous epithelium and cancer development	13
Figure 3. Schematic illustration of chronic hypoxia	18
Figure 4. Proteome analyses of differentially expressed proteins in SiHa cells, cultured under normoxia or hypoxia	22
Figure 5. FAM57A transcript variants and protein isoforms	23
Figure 6. Schematic representation of the CheckMate™ Mammalian Two-Hybrid System	31
Figure 7. Cloning strategy for the <i>FAM57A</i> -2 coding region	38
Figure 8. Schematic diagram of nested PCR	39
Figure 9. Validation of the anti-FAM57A antibody	46
Figure 10. Effects of hypoxia on FAM57A protein and transcript levels in HPV-positive and HPV-negative cells	47
Figure 11. Effects of cell density on FAM57A protein and transcript levels under normoxia	49
Figure 12. FAM57A protein stability and expression kinetics	50
Figure 13. FAM57A protein expression in dependence on cell density, normoxia/hypoxia and glucose supply	51
Figure 14. FAM57A expression upon <i>HIF1A</i> or <i>HIF2A</i> silencing	52
Figure 15. Putative HIF-1 α binding sites in the promoter region (-1056 - +64) of the <i>FAM57A</i> gene	52
Figure 16. Effects of <i>E6/E7</i> silencing on FAM57A expression in cervical cancer cells	53
Figure 17. Effects of <i>FAM57A</i> silencing on the colony formation capacity of HPV-positive cancer cells	54
Figure 18. Live cell imaging analyses of HPV-positive cancer cell growth following <i>FAM57A</i> silencing	56
Figure 19. Effects of FAM57A on the migration of cervical cancer cells	57
Figure 20. Effects of FAM57A on the migration and morphology of HeLa-2-mKate2 cells	58
Figure 21. Interaction between FAM57A and SLC3A2	60
Figure 22. Effects of <i>SLC3A2</i> suppression on the colony formation capacity of HPV-positive cancer cells	61

Figure 23. Effects of <i>SLC3A2</i> suppression on the growth of HPV-positive cancer cells in live cell imaging analyses	62
Figure 24. Cell density-dependent expression of key factors of YAP/TAZ signaling	63
Figure 25. Relation between FAM57A and YAP/TAZ signaling factors	65
Figure 26. <i>CYR61</i> and <i>CTGF</i> mRNA levels following <i>FAM57A</i> or <i>YAP/TAZ</i> silencing	66

3. List of Tables

Table 1. Chemical compounds	28
Table 2. Target sequences of siRNAs and shRNAs	30
Table 3. Primers for cloning	37
Table 4. Plasmids for the CheckMate™ Mammalian Two-Hybrid System	40
Table 5. Primers for qRT-PCR	41
Table 6. Recipe for SDS-polyacrylamide gels	43
Table 7. Antibodies for immunoblotting	44

4. Abbreviations

4E-BP1	eukaryotic translation initiation factor 4E-binding protein 1
ABP	actin-binding protein
AcCoA	acetyl-coenzyme A
ADA3	transcriptional adaptor 3
APS	ammonium persulfate
ARNT	aryl hydrocarbon receptor nuclear translocator
ATP	adenosine triphosphate
BES	N,N-bis(2-hydroxyethyl)-2-aminoethanesulfonic acid
BSA	bovine serum albumin
CBP	CREB-binding protein
CDKN1A/CDKN1B	cyclin dependent kinase inhibitor 1A/cyclin dependent kinase inhibitor 1B
cDNA	complementary DNA
CDS	coding sequence
CFA	colony formation assay
CHX	cycloheximide
CIP	calf intestinal alkaline phosphatase
co-IP	co-immunoprecipitation
CREB	cyclic adenosine monophosphate response element-binding protein
CTGF	connective tissue growth factor
CYR61	cysteine-rich angiogenic inducer 61
DMSO	dimethyl sulfoxide
DNA	deoxyribonucleic acid
DTT	dithiothreitol
<i>E.coli</i>	<i>Escherichia coli</i>
<i>e. g.</i>	<i>exempli gratia</i>
E6AP	ubiquitin ligase E6-associated protein
ECL	enhanced chemiluminescence
ECM	extracellular matrix
EDTA	ethylenediaminetetraacetic acid
EGTA	ethylene glycol-bis(β -aminoethyl ether)-N,N,N',N'-tetraacetic acid
ELISA	enzyme-linked immunosorbent assay
EMT	epithelial-mesenchymal transition
ENO1	enolase 1

4. Abbreviations

ERK	extracellular signal-regulated kinase
<i>et al.</i>	<i>et alii</i>
FAM57A	family with sequence similarity 57 member A
FAO	fatty acid oxidation
FBS	fetal bovine serum
GAPDH	glyceraldehyde-3-phosphate dehydrogenase
GGT	γ -glutamyltransferase
GLUT1/GLUT3	glucose transporter 1/glucose transporter 3
GPCR	G protein-coupled receptor
GSH	glutathione
HAT	heterodimeric amino acid transporter
HIF	hypoxia-inducible factor
HK	hexokinase
HNSCC	head and neck squamous cell carcinoma
HPV	human papillomavirus
HRE	hypoxia-responsive element
<i>i. e.</i>	<i>id est</i>
IGF1A	insulin-like growth factor 1A
LAT	L-type amino acid transporter
LB	Lysogeny Broth
LCR	long control region
LDHA	lactate dehydrogenase A
MAPK	mitogen-activated protein kinase
MCT4	monocarboxylate transporter 4
MDM2	mouse double minute 2 homolog
MMP	matrix metalloproteinase
MPA	membrane proximal F-actin
mRNA	messenger RNA
mTOR	mammalian target of rapamycin
mTORC1	mTOR complex 1
NCR	non-coding region
ORF	open reading frame
OXPHOS	oxidative phosphorylation
PAE	early polyadenylation site
PAL	late polyadenylation site

PBS	phosphate-buffered saline
PCR	polymerase chain reaction
PDK1	pyruvate dehydrogenase kinase 1
PDZ	PSD-95/DLG/ZO-1, post synaptic density protein 95 (PSD-95), disc large homolog (DLG), zonula occludens-1 (ZO-1)
PFKFB-3	fructose-2, 6-bisphosphatase
PFK-L	phosphofructokinase liver type
PGK1	phosphoglycerate kinase 1
P-gp	P-glycoprotein
pH	potential of hydrogen
PHD	prolyl hydroxylase
PI3K	phosphoinositide 3-kinase
PKC	protein kinase C
PKM2	pyruvate kinase isozyme M2
PNK	polynucleotide kinase
pRb	retinoblastoma protein
PVDF	polyvinylidene fluoride
qRT-PCR	quantitative real time-polymerase chain reaction
RASGRF1	Ras protein-specific guanine nucleotide-releasing factor 1
rel.	relative
RNA	ribonucleic acid
RNAi	RNA interference
ROS	reactive oxygen species
rRNA	ribosomal RNA
RT	room temperature
RTK	receptor tyrosine kinase
RT-PCR	reverse transcription-polymerase chain reaction
S6K1	ribosomal protein S6 kinase 1
SCC	squamous cell carcinoma
SDS	sodium dodecyl sulfate
shRNA	short hairpin RNA
siRNA	small interfering RNA
SLC3A2	solute carrier family 3 member 2
SNP	single-nucleotide polymorphism

4. Abbreviations

TAZ	transcriptional co-activator with PDZ-binding motif
TCA	tricarboxylic acid
TEAD	transcriptional enhancer factor
TEMED	tetramethylethylenediamine
TIMP2	tissue inhibitor of metalloproteinase 2
TMBIM6	transmembrane BAX inhibitor motif containing 6
UPS	ubiquitin-proteasome system
URR	upstream regulatory region
VLP	virus-like particle
vs.	versus
YAP	Yes1-associated protein

Unit

°C	degree Celsius
%	percent
µg	microgram
µL	microliter
µM	micromolar
µm	micrometer
<i>g</i>	centrifugal acceleration
g	gram
h	hour
kDa	kilodalton
L	liter
M	molar
min	minute
mL	milliliter
mM	millimolar
ng	nanogram
nM	nanomolar
rpm	revolutions per minute
sec	second
U	international unit
V	volt

5. Introduction

5.1 Cancer

Cancer is a leading cause of death worldwide and an important barrier to increasing life expectancy. Approximately 19.3 million new cases and almost 10.0 million cancer deaths occurred in 2020 according to the GLOBOCAN 2020 estimates. Moreover, cancer incidence is still increasing because of population aging and growth, as well as cancer-associated lifestyles. An estimated 28.4 million new cases of cancer are projected to occur in 2040 (Sung *et al.* 2021).

Cancer is defined as a group of diseases in which cells of the body grow abnormally and potentially spread to other tissues. Cancer starts with the accumulation of genetic changes, predominantly involving proto-oncogenes, tumor suppressor genes and DNA repair genes. During the multistep development of cancer, cells gain the potential to maintain inadequate proliferative signaling, evade growth-inhibitory pathways, resist cell death, induce replicative immortality, stimulate angiogenesis, activate cell invasion and metastasis, reprogram the cellular energy metabolism and escape from the host's immune response, which together have been designated "hallmarks of cancer" (Hanahan and Weinberg 2011).

5.2 Human papillomaviruses (HPVs) and cancer

Infections are one of the major risk factors for cancer and caused 13 % of all malignancies globally in 2018 (de Martel *et al.* 2020). Oncogenic HPV types belong to the best-characterized cancer-related infectious agents in humans and are closely linked to the development of cancers of the cervix, anus, vagina, vulva, penis, oropharynx, oral cavity and larynx (Schiffman *et al.* 2016). HPVs cause virtually all cases of cervical cancer, which accounts for around half of the infection-related cancers in women (Vineis and Wild 2014).

5.2.1 HPVs and cervical cancer

Cervical cancer is the fourth most commonly diagnosed cancer and the fourth leading cause of cancer mortality in women, resulting in approximately 604,000 new cases and 342,000 cancer deaths in 2020 (Sung *et al.* 2021). The disease is a particularly prominent problem in developing countries, where it is the second most prevalent cancer form in females and leads to nearly 90 % of the cervical cancer deaths occurring worldwide (Torre *et al.* 2015).

HPVs are non-enveloped double-stranded DNA viruses infecting human skin and mucosa, where they can cause benign warts or cancers. More than 200 HPV genotypes are known and classified into five genera -

5. Introduction

α , β , γ , μ , and ν . HPVs of the β , γ , μ , and ν genera have a cutaneous tropism. The best-studied oncogenic or, alternatively called high-risk HPV types (HPV16, 18, 31, 33, 35, 39, 45, 51, 52, 56, 58 and 59), all belong to the α genus. They possess a mucosal tropism and are associated with the development of anogenital and oropharyngeal cancers. The most common carcinogenic HPV types, HPV16 and HPV18, are responsible for approximately 70 % of cervical cancer cases (Schiffman *et al.* 2007).

5.2.2 The biology of HPV infection and HPV-associated carcinogenesis

The circular genome of HPVs consists of approximately 8000 base pairs encompassing up to 10 open reading frames (ORFs) (Harden and Munger 2017). In oncogenic HPV types, such as HPV16 or HPV18, the early (E) region possesses 6 ORFs: E1, E2, E4, E5, E6 and E7 (Figure 1). The early genes are expressed in the early stage of the viral life cycle and the proteins are necessary for viral replication. E1 is an ATP-dependent helicase recruited to a specific E1 binding site in the viral origin by E2, a DNA-binding protein that can contact the HPV DNA at multiple binding sites (#1, #2, #3 and #4 in Figure 1) in the transcriptional control region. E1 and E2 are expressed at the beginning of the infection and contribute to viral replication and transcription while E4 and E5 are mainly expressed in differentiating cells, where genomic replication is increased. Eventually, the virus is released from the uppermost cell layer of the epithelium (Figure 2). E6 and E7, which also represent the major oncogenes of the virus, affect various processes in the host cell, including cell cycle regulation, apoptosis control, cellular differentiation and immune evasion (Moody 2017). The late (L) region is located downstream of the E region and encodes the major (L1) and minor (L2) viral proteins, which form the viral capsid and are involved in viral entry and trafficking. The early and late regions are separated by a transcriptional control region, which is alternatively termed long control region (LCR), upstream regulatory region (URR) or non-coding region (NCR). This region contains the origin of viral replication and transcriptional regulatory elements, with a promoter controlling *E6/E7* expression located at the 3' end (P97 for HPV16, Figure 1) (Harden and Munger 2017).

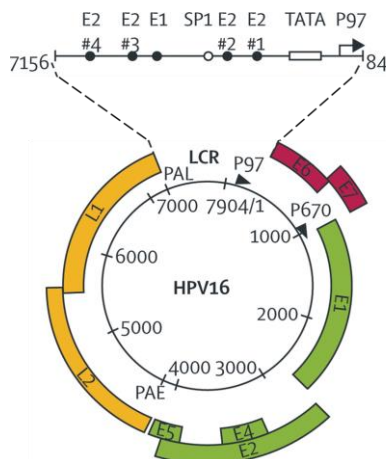


Figure 1: HPV16 genome organization. The HPV16 genome consists of a double-stranded circular DNA. Six early ORFs: E1, E2, E4, E5 (green) and E6, E7 (red), and two late ORFs: L1 and L2 (yellow), are expressed from the early and late promoters marked by arrowheads (P97 and P670, respectively). The binding sites for the viral E1 and E2 proteins (black dots) and the cellular SP1 transcription factor (black circle) in the transcriptional control region (LCR) are depicted. PAE = early polyadenylation site, PAL = late polyadenylation site. Modified from (Schiffman *et al.* 2007).

The development of cervical cancer is attributed to persistent oncogenic HPV infections. HPV genome replication relies on the host cell, due to the lack of a viral polymerase gene in HPVs. HPVs infect the basal layer of cutaneous or mucosal squamous epithelia through microwounds, and start their viral life cycle in proliferating basal keratinocytes. Infections by HPVs are usually cleared within a few months by the immune system (Plummer *et al.* 2007; Rodriguez *et al.* 2008). However, the HPV oncoproteins E6 and E7 (and to some extent E5) can support evasion from the immune surveillance of the host (Steinbach and Riemer 2018). Thus, these oncoproteins can create a cellular environment which promotes HPV persistence in the infected keratinocytes (Della Fera *et al.* 2021). Upon exiting the basal layer of the epithelium, differentiating cells usually withdraw from the cell cycle and do not support DNA synthesis. However, oncogenic HPVs can activate cellular DNA replication via expression of the multifunctional E6 and E7 oncoproteins, which allows viral DNA synthesis and can lead to the accumulation of genetic changes in the host cell, including chromosome abnormalities, point mutations and epigenetic alterations, ultimately contributing to the development and progression to cancer (Harden and Munger 2017; Schiffman *et al.* 2016).

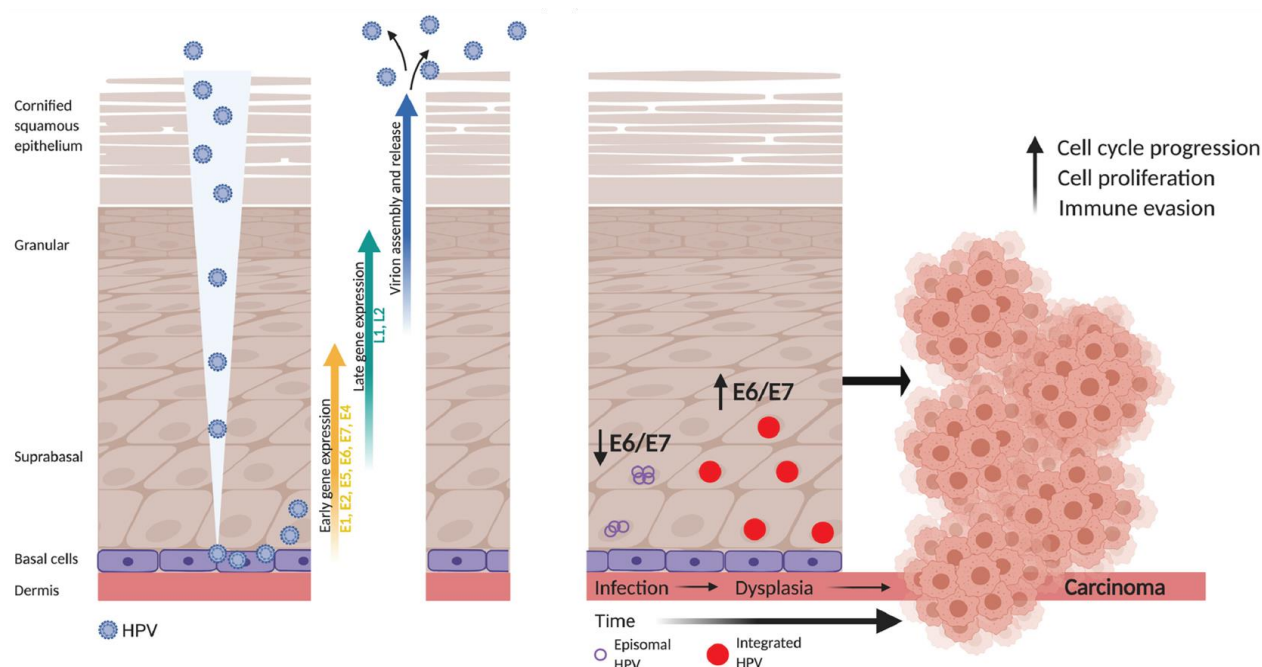


Figure 2: The HPV life cycle in squamous epithelium and cancer development. HPVs enter the basal layer of squamous epithelia through microwounds. The HPV early proteins (E1, E2, E4, E5, E6 and E7) initiate viral genome replication and promote host cell proliferation. As cells differentiate, the late HPV proteins (L1 and L2) are expressed to package newly replicated viral DNA into capsids which are subsequently released from the surface (left panel). Viral E6 and E7 gene expression is kept low in the episomal state. During cancer development, E6 and E7 expression is typically increased (*e. g.* following integration of the viral genes into the host cell genome). This can lead to the deregulation of cell proliferation, apoptosis resistance, genomic instability and immune evasion, which supports cancer development (right panel). Modified from (Cosper *et al.* 2021).

5.2.3 The viral E6 and E7 oncoproteins

The HPV E6 and E7 oncoproteins modulate the activity of many cellular proteins (Mantovani and Banks 2001; Munger *et al.* 2001), of which the tumor suppressor proteins p53 and pRb (retinoblastoma tumor suppressor protein) are the most prominent and best-studied examples. The E6 protein of oncogenic HPV types mediates the degradation of p53 via the ubiquitin-proteasome system (UPS) by forming a trimeric E6/E6AP (ubiquitin ligase E6-associated protein)/p53 complex. As a result, p53-induced growth inhibition and apoptosis induction in response to DNA damage are impaired, thereby allowing the accumulation of genomic mutations and promoting carcinogenesis (Mantovani and Banks 2001). The E6 oncoproteins can also interfere with the acetylation of p53 by binding to the histone acetyltransferases p300, CREB-binding protein (CBP) and transcriptional adaptor 3 (ADA3), thus blocking the acetylation of p53 and decreasing its stability (Kumar *et al.* 2002; Patel *et al.* 1999; Zimmermann *et al.* 1999). The E6 proteins from low-risk HPV types have been also reported to interfere with the growth-suppressive activity of p53, which is predominantly attributed to direct binding to p53 and interference with p53-mediated transcriptional regulation (Crook *et al.* 1994; Lechner and Laimins 1994). In addition to p53, the E6 proteins from oncogenic HPV types also associate with other cancer-relevant factors, such as PDZ (PSD-95/DLG/ZO-1) proteins via a PDZ binding motif (PBM), which interestingly is not found in the E6 proteins of non-oncogenic HPV types (Ganti *et al.* 2015; Thomas *et al.* 2008). It has been shown that the E6 oncoprotein can mediate the degradation of PDZ proteins or impair their functions through altering their subcellular localization (Ganti *et al.* 2016).

E7, among other targets, affects the pRb/E2F interaction in the host cell. In normal (uninfected) non-proliferating cells, unphosphorylated pRb binds to E2F transcription factors and thereby blocks the E2F-mediated transcriptional activation of a variety of cell cycle promoting target genes. For cell division, E2Fs are released from pRb upon pRb phosphorylation, and then can activate transcription of their target genes, leading to S-phase entry. In HPV-positive cells, this regulation is disturbed in that the E7 oncoprotein binds to pRb and mediates its degradation. Consequently, E2Fs are released from the negative regulation by pRb, leading to unscheduled cell cycle progression and cell division (Narisawa-Saito and Kiyono 2007).

Notably, there is also evidence that E6 and E7 cooperate in the transformation process since the abrogation of pRb function by high-risk E7 can sensitize infected cells to p53-dependent apoptosis, which is blocked by the concomitant E6 expression (Eichten *et al.* 2004; Jones *et al.* 1997).

5.2.4 Cellular pathways related to biological characteristics of cervical cancer cells

Oncogenic HPVs are necessary but not sufficient for the development of cervical cancers. This is indicated by the observation that only a small proportion of females infected with high-risk HPVs develop cancer. Moreover, cervical carcinogenesis is a process which typically evolves over several decades after initial infection with an oncogenic HPV type (Schiffman *et al.* 2016). This indicates that - besides an oncogenic HPV infection - additional genetic or epigenetic alterations in the cells are necessary for cervical cancer development (Fang *et al.* 2014; Soto *et al.* 2017). Indeed, a variety of pathways are deregulated in cervical cancer cells, which could be dependent or independent on the viral oncogenes. Among others, these include the phosphoinositide 3-kinase (PI3K)/AKT signaling pathway, the mitogen-activated protein kinase (MAPK)/extracellular signal-regulated kinase (ERK) cascade as well as Yes1-associated transcriptional regulator (YAP)/transcriptional co-activator with PDZ-binding motif (TAZ) dependent signaling (Olmedo-Nieva *et al.* 2020; Rasi Bonab *et al.* 2021).

The PI3K/AKT cascade is one of the most important signaling pathways, which is hyperactive in many cancers and affects different phenotypic characteristics of cancer cells, such as proliferation, apoptosis, metabolism, invasiveness and cytoskeleton remodeling (Deng *et al.* 2022; Engelman 2009; Noorolyai *et al.* 2019). It can be activated by a wide range of stimuli, including growth factors, cytokines and mechanical signals, and regulate numerous downstream proteins, thereby cross-connecting many signaling pathways in a complex manner (Deng *et al.* 2022; Manning and Cantley 2007; Revathidevi and Munirajan 2019). Aberrant activation of PI3K/AKT has been identified in cervical cancer (Bahrami *et al.* 2017; Millis *et al.* 2016), which can predict prognosis and serve as a biomarker for risk stratification (Bahrami *et al.* 2017). An important pathway regulated by AKT is the mTOR pathway, which enhances protein synthesis through the activation of downstream factors, such as ribosomal protein S6 kinase 1 (S6K1) and eukaryotic translation initiation factor 4E-binding protein 1 (4E-BP1) (Bahrami *et al.* 2017; Bossler *et al.* 2019a).

MAPK/ERK signaling is the most-studied of the MAPK signaling cascades and is essential for fundamental cell functions, such as the control of cell proliferation, cell cycle progression, differentiation or migration (Degirmenci *et al.* 2020). MAPK/ERK signaling transduces extracellular stimuli from receptor tyrosine kinases (RTKs) and G protein-coupled receptors (GPCRs) through RAS and RAF activation, and ultimately phosphorylated ERK regulates its targets in the cytosol or via nuclear translocation and subsequent phosphorylation of transcription factors (Ebner *et al.* 2007; Guo *et al.* 2020). Additionally, ERK is also activated by intracellular calcium and protein kinase C (PKC), which connects extracellular signals and intracellular networks (Guo *et al.* 2020). The deregulation of MAPK/ERK due to the gain-of-function mutations mainly in the RAS or RAF genes, which has also been reported in cervical cancers (Santarpia

5. Introduction

et al. 2012), can contribute to the resistance towards certain anti-cancer drugs, including RAF inhibitors (Degirmenci *et al.* 2020).

YAP and TAZ are transcriptional coactivators that can potently promote cell proliferation, potentially leading to organ overgrowth or to the development of cancer. Mechanistically, YAP and TAZ interact with DNA-binding factors of the transcriptional enhancer factor (TEAD) family, thus regulating the expression of numerous target genes in the nucleus (Pocaterra *et al.* 2020). As such, the nuclear translocation of YAP/TAZ is a key step for YAP/TAZ signaling, a process which is regulated by phosphorylation. In specific, YAP/TAZ phosphorylation results in their sequestration in the cytoplasm, where the proteins are proteasomally degraded, whereas non-phosphorylated YAP/TAZ enter the nucleus and transcriptionally activate target gene expression (Piccolo *et al.* 2014). YAP/TAZ can promote glycolysis by upregulating various glycolysis-related genes, including *HK2* (*hexokinase 2*), *GAPDH* (*glyceraldehyde-3-phosphate dehydrogenase*), *PGK1* (*phosphoglycerate kinase 1*) and *LDHA* (*lactate dehydrogenase A*) (Yamaguchi and Taouk 2020), thereby supporting the rapid growth of tumor cells. Moreover, YAP and TAZ are involved in the cellular response towards mechanical stress from cell shape, polarity and cytoskeleton structures (Dupont *et al.* 2011; Totaro *et al.* 2018) and in turn affect cell-cell contacts and cell adhesion (Totaro *et al.* 2018). In line, YAP/TAZ signaling has been linked to cell migration by limiting the maturation of the cytoskeleton and focal adhesions (Mason *et al.* 2019).

The role of YAP/TAZ in cervical squamous cell carcinoma (SCC) is still controversial. Several investigations reported that YAP and TAZ are highly expressed in cervical SCC compared to normal tissues, which is correlated to a highly malignant phenotype and poor clinical prognosis (Maehama *et al.* 2021; Wang *et al.* 2020; Zhang *et al.* 2020). In contrast, it was also reported that the nuclear localization of YAP/TAZ is absent in cervical SCC, indicating inactivation of YAP/TAZ signaling and an inverse association between YAP/TAZ expression and cancer progression (Liu *et al.* 2013; Liu *et al.* 2018).

5.2.5 Prevention and therapy of cervical cancer

Prophylactic vaccination protecting against the infection with oncogenic HPV types effectively prevents the development of cervical pre-neoplasia and cancers (Falcaro *et al.* 2021). Three prophylactic HPV vaccines have been licensed: the bivalent Cervarix (GlaxoSmithKline (GSK), London, UK), the quadrivalent Gardasil and the nonavalent Gardasil9 (both Merck, Kenilworth, New Jersey, USA). All these vaccines are based on the major HPV capsid protein L1 which forms virus-like particles (VLPs). Thus, these VLPs are free of viral DNA and cannot initiate a viral life cycle, but can provoke an immune response (Stanley *et al.* 2012). Cervarix contains VLPs from HPV16 and HPV18. Gardasil provides protection against low-risk HPV6 and HPV11 as well as against high-risk HPV16 and HPV18 whereas Gardasil9 additionally contains

VLPs from HPV31, HPV33, HPV45, HPV52 and HPV58, thus protecting against infections which are related to approximately 90 % of the cervical cancer incidence (Castellsague *et al.* 2015; Einstein *et al.* 2011; Giuliano *et al.* 2011; Joura *et al.* 2015).

Secondary prevention also plays a major protective role against cervical cancer development. Currently, three options are primarily used for cervical cancer screening: analyzing cervical cytology (Papanicolaou (Pap) test), HPV detection as a primary test, or a cotest which combines cytology and HPV detection (Fontham *et al.* 2020). According to the American Cancer Society (ACS) Guidelines 2020, the primary HPV test alone is preferentially recommended for individuals aged between 25-65 years. Following the initial screening at the age of 25 years, these individuals should undergo the HPV test every 5 years. Cotesting every 5 years and Pap test alone every 3 years are also considered to be acceptable options. Cervical cancer screening can be discontinued in individuals above 65 years old, who have no history of precancerous lesions (cervical intraepithelial neoplasia grade 2 or higher) or cancer within the past 25 years, and who have adequate negative prior screening (Fontham *et al.* 2020).

It should be noted, however, that - on a worldwide scale - both the vaccination and screening rates are disappointingly low, especially in low- and middle-income countries, which have the highest incidence of and mortality from cervical cancer (Sung *et al.* 2021). Thus, HPV-induced cancers are likely to remain a major medical problem worldwide for many years to come.

Therapeutically, surgery is recommended for most patients with more progressed precancerous lesions or early cervical cancers. For advanced cervical cancers, patients receive concurrent cisplatin-based chemoradiation regimens as a primary treatment, which are adopted worldwide (Koh *et al.* 2015; Small *et al.* 2017). Unfortunately, advanced or recurrent cervical carcinomas still show rather poor survival rates (Marth *et al.* 2017). Therefore, novel and more effective therapeutic strategies for the treatment of HPV-associated cancers need to be developed, which may profit from an improved understanding of the molecular mechanisms contributing to the malignant phenotype of HPV-positive cancer cells. This includes analyses under hypoxic conditions, which are linked to increased therapy resistance.

5.3 Hypoxia and cancer

The term “hypoxia” refers to low oxygen contents which are often present in subregions of solid cancers and are usually defined as an O_2 concentration $\leq 2\%$ O_2 . There are two major forms of hypoxia in tumors. Chronic hypoxia is often caused by limitations of O_2 diffusion. This can be due, for example, to the rapid and uncontrolled proliferation of tumors, resulting in enlarged distances between tumor blood vessels and tumor cells (Figure 3). Moreover, tumor blood vessels are often structurally and functionally impaired,

5. Introduction

which also limits oxygen supply to the surrounding tumor tissue. As a matter of fact, the poor structure of tumor vessels can also lead to a second major form of hypoxia in cancers, called cycling hypoxia. This form of hypoxia is typically due to perfusion perturbations, for example through recurrent changes in the erythrocyte flux which exposes neighboring tumor cells to repeated cycles of hypoxia and reoxygenation (Hoppe-Seyler *et al.* 2017b; Jing *et al.* 2019).

The term normoxia refers to the oxygen level in standard tissue culture *in vitro*, which is approximately 20 % O₂, whereas physoxia is used to describe physiological oxygen levels, which for most organs vary between 3.4 % to 6.8 %. The mean O₂ concentration in normal cervical tissue lies around 5.5 % O₂ and is reduced to about 1.2 % O₂ in cervical cancer (McKeown 2014).

Hypoxia has been associated with poor prognosis for many cancers, including cervical cancer, head and neck cancer, breast cancer and lung cancer (Vaupel and Mayer 2007). In part, this is attributed to alterations in gene expression under the transcriptional control of hypoxia-inducible factors (HIFs), which can lead to pro-tumorigenic alterations of the cellular metabolism and increased resistance to anti-cancer treatments, such as chemo- and radiotherapy (Albadari *et al.* 2019; Semenza 2010).

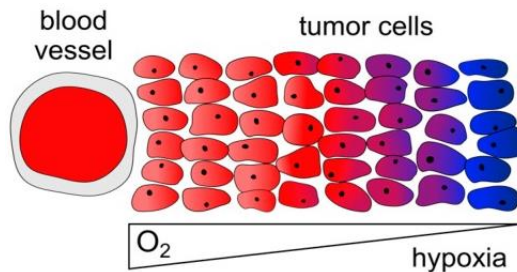


Figure 3: Schematic illustration of chronic hypoxia. Hypoxic cells (blue) are inadequately supplied with oxygen due to the large distance to tumor blood vessels (starting at a distance of approximately 100 μm (Al Tameemi *et al.* 2019)). Modified from (Hoppe-Seyler *et al.* 2017b).

5.3.1 Hypoxia-inducible factors (HIFs)

HIF-1 is a pivotal transcriptional activator that mediates the cellular response to hypoxia. It consists of an O₂-sensitive subunit HIF-1 α and an O₂-insensitive subunit HIF-1 β . HIF-1 α is prone to be degraded by the UPS in the presence of sufficient oxygen. Under normoxic conditions, HIF-1 α is hydroxylated at the proline residues 564 and/or 402 by the prolyl hydroxylase domain proteins PHD1-3, using oxygen as substrate. This results in binding to an E3 ligase component - the von Hippel-Lindau protein - which ubiquitinates HIF-1 α and leads to its degradation by the proteasome. Under hypoxic conditions, PHDs are inactive, which prevents the proteasome-dependent degradation of HIF-1 α (Bruick and McKnight 2001; Epstein *et al.* 2001; Ivan *et al.* 2001; Jaakkola *et al.* 2001; Maxwell *et al.* 1999). Hence, HIF-1 α is stabilized and forms a heterodimer with HIF-1 β that translocates into the nucleus to activate the transcription of target genes via

binding to hypoxia-responsive elements (HREs). The HIF-1 β protein, also designated as aryl hydrocarbon receptor nuclear translocator (ARNT), is stable and constitutively expressed regardless of the oxygen availability (Mandl and Depping 2014), although there is some evidence indicating that HIF-1 β can be upregulated in response to hypoxia in certain cell lines (Mandl and Depping 2014). In contrast to the respective proteins, *HIF1A* and *ARNT* are constitutively expressed at the mRNA level in various human tissues (Huang *et al.* 1996).

HIF-2 α and HIF-3 α are two homologues of HIF-1 α that can also form heterodimers with HIF-1 β . HIF-2 α shares 48 % homology in amino acid sequence with HIF-1 α and activates the transcription of hypoxia-responsive genes (Ema *et al.* 1997; Flamme *et al.* 1997; Tian *et al.* 1997). However, HIF-1 α is ubiquitously expressed while HIF-2 α is predominantly expressed in vascular endothelial cells during embryonic development. Besides common target genes, HIF-1 α and HIF-2 α also show some differences in the spectrum of their transcriptional activities. For example, HIF-1 α , but not HIF-2 α , is associated with the upregulation of glycolytic genes while HIF-2 α preferentially enhances expression of erythropoietin and is involved in the regulation of iron metabolism genes (Hu *et al.* 2003; Kapitsinou *et al.* 2010). HIF-3 α is subject to alternative splicing. Although six splice variants have been reported, none of them directly acts as a transcription factor, but some of them can maximize the transcriptional activation of target genes in the presence of adequate amounts of HIF-1 β . When HIF-1 β is limited, these HIF-3 α variants bind to HIF-1 α and HIF-2 α and inhibit their transcriptional activity (Heikkila *et al.* 2011; Pasanen *et al.* 2010).

5.3.2 Cellular metabolism under hypoxia

To survive under hypoxic stress, cancer cells tend to increase intracellular oxygen delivery and decrease oxygen consumption, which to a large part depends on the activity of HIF-1. HIF-1 upregulates the expression of glucose transporters, such as GLUT1 (SLC2A1) and GLUT3 (SLC2A3), to increase glucose levels inside cells (Semenza 2010). In addition, hypoxic cancer cells reduce O₂-dependent mitochondrial oxidative phosphorylation (OXPHOS) and promote glycolysis, characterized by higher glucose consumption and lactate production (Denko 2008).

HIF-1 mediates this metabolic switch by upregulating the expression of a series of genes encoding for glycolytic enzymes, including hexokinase 1 and 2 (HK1, HK2), phosphofructokinase liver type (PFK-L), aldolase A and C (ALD-A, ALD-C), phosphoglycerate kinase 1 (PGK1), enolase 1 (ENO1), pyruvate kinase isozyme M2 (PKM2), and fructose-2, 6-bisphosphatase (PFKFB-3) (DeBerardinis *et al.* 2008; Kierans and Taylor 2021; Semenza 2003; Wigerup *et al.* 2016). Pyruvate, a product of glycolysis, is an intermediate in several metabolic pathways, including the tricarboxylic acid (TCA) cycle, gluconeogenesis, and anabolic

synthesis of fatty acids and amino acids (Chaneton *et al.* 2012; Zahra *et al.* 2020). Lactate dehydrogenase A (LDHA), which catalyzes the conversion from pyruvate to lactate, and pyruvate dehydrogenase kinase 1 (PDK1), which hinders acetyl-coenzyme A (AcCoA) conversion from pyruvate, are both induced by HIF-1, which contributes to the suppression of OXPHOS under hypoxic conditions (Denko 2008; Kierans and Taylor 2021). Lactate, as a product of glycolysis, can be removed by monocarboxylate transporter 4 (MCT4), a plasma membrane transporter which is induced by HIF-1 as well (Ullah *et al.* 2006).

Further, HIF-1 also inhibits fatty acid oxidation (FAO), another major source of AcCoA, thereby reducing the production of reactive oxygen species (ROS) by OXPHOS (Huang *et al.* 2014). Notably, the HIF-1-induced PDK1 can in turn promote HIF-1 α activation dependent on the accumulation of glycolytic metabolites, suggesting a feed-forward loop of cellular metabolism under hypoxia (McFate *et al.* 2008). Moreover, HIF-1 can reduce the respiratory capacity via the induction of mitochondrial autophagy (Zhang *et al.* 2008) and the regulation of cytochrome c oxidase (Fukuda *et al.* 2007), which also limits the production of ROS, thereby further protecting hypoxic cells from cell death. An additional mechanism by which HIF-1 can protect against oxidative stress is its promotion of glutathione (GSH) synthesis, which makes hypoxic cells more tolerant to ROS production (Bouthelier and Aragonés 2020; Lu 2013).

5.3.3 Hypoxia-induced resistance towards anti-cancer therapy

Of high clinical relevance is the finding that the presence of hypoxic areas in cancers is linked to increased resistance towards chemo- and radiotherapy. Reasons underlying this observation include the notion that the efficacy of chemotherapy depends on efficient delivery of chemotherapeutic agents to cancer cells. Thus, the abnormal distribution and inadequate perfusion of cancer blood vessels does not only lead to inadequate O₂ supply, but can also interfere with drug delivery (Viallard and Larrivee 2017). In addition, many chemotherapeutic drugs kill cells by the oxidation of free radicals, a process which is oxygen-dependent. Therefore, the efficiency of chemotherapy can be reduced under hypoxic conditions due to the deficiency in oxygen molecules and the reduction of cytotoxic ROS production, which is further supported by HIF-1 induction (see above), eventually protecting cancer cells from DNA damage, and ultimately cell death (Jing *et al.* 2019). Furthermore, the acidic microenvironment of tumors caused by hypoxia disrupts the activity of pH-dependent chemotherapeutic agents, such as doxorubicin and docetaxel (Thews *et al.* 2014). Moreover, the cellular drug efflux pump P-gp, which can remove intracellular chemotherapeutic drugs, is activated by HIF-1 (Li *et al.* 2016; Shi *et al.* 2021). The resistance of hypoxic cancer cells to chemotherapy can be also a consequence of hypoxia-induced cell cycle arrest, which is a state of reduced proliferation that can protect cells from extracellular stress and provide resistance towards chemotherapeutic agents which preferentially attack proliferating cells (Rohwer and Cramer 2011).

The anti-cancer effects of radiotherapy rely to a large part on the induction of DNA strand breaks. In the presence of oxygen, the ionizing radiation-induced DNA damage can be fixed by oxygen molecules, which have a higher affinity to react with various radicals that provoke irreversible DNA damage, preventing cells from DNA damage repair (Wang *et al.* 2019). The accumulation of unrepaired DNA damage then results in cell death. In hypoxic cancer cells, however, the temporary DNA damage can be repaired and cells can recover more effectively from radiation-induced DNA damage (Boulefour *et al.* 2021). In addition, HIF-1 can mediate radioresistance under hypoxia by interfering with apoptosis, activating autophagy, supporting DNA damage repair and through its antioxidant effects, *e. g.* by decreasing ROS levels and increasing reduced GSH levels (Kabakov and Yakimova 2021).

5.3.4 Hypoxia and HPV E6/E7 oncoproteins

In view of the key role of hypoxia for the phenotype of cancer cells, it is important to assess the consequences of hypoxia for the cellular behavior of cervical cancer cells. It was found that hypoxia leads to a strong downregulation of the HPV oncogenes (Hoppe-Seyler *et al.* 2017a), an effect which is mediated by hypoxia-induced PI3K/AKT signaling (Bossler *et al.* 2019b). Strikingly, whereas HPV E6/E7 repression under normoxia rapidly and efficiently induces senescence, this regulation is abolished under hypoxia. Rather, hypoxic cervical cancer cells induce a reversible growth arrest, which is reverted by reoxygenation and thus may potentially contribute to tumor recurrence after treatment. Mechanically, the anti-senescent effect of hypoxia in cervical cancer cells is, at least in part, due to the interference of hypoxia with pro-senescent mTORC1 signaling (Bossler *et al.* 2019a). Since hypoxia interferes with senescence induction, hypoxic HPV-positive cancer cells were found to become resistant to pro-senescent chemotherapeutic agents. The chemotherapy resistance of these cells could be further supported by the anti-proliferative effects of hypoxia (Bossler *et al.* 2019b; Hoppe-Seyler *et al.* 2017a).

In order to gain insights into the factors determining the phenotypic response of cervical cancer cells towards hypoxia, a proteome analysis comparing normoxic and hypoxic HPV16-positive SiHa cells was performed (Bossler *et al.* 2019b). Notably, FAM57A, a thus far very poorly investigated cellular factor, was the top hit among the proteins, which were significantly upregulated in hypoxic cervical cancer cells (Figure 4). Thus, FAM57A expression inversely correlates with the strong decrease in HPV E6/E7 oncoprotein expression under hypoxia (Bossler *et al.* 2019b). These findings raise the questions: (i) whether FAM57A is a *bona fide* hypoxia-responsive factor, (ii) whether FAM57A expression is connected to the HPV oncogenes and (iii) whether alterations in FAM57A expression play a role for the phenotypic behavior of cervical cancer cells.

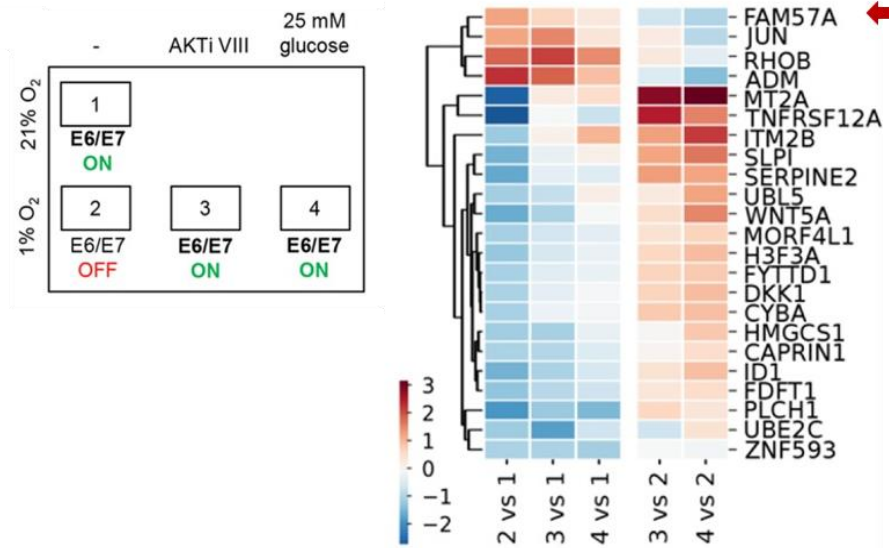


Figure 4. Proteome analyses of differentially expressed proteins in SiHa cells, cultured under normoxia or hypoxia. Left panel: Schematic illustration of the four treatment conditions. Cells were grown under normoxia (1), hypoxia (2) or hypoxia in the presence of 10 mM AKTi VIII, an AKT inhibitor (3), or of 25 mM glucose (4). E6/E7 expression under the different treatment conditions is indicated as ON/OFF. Right panel: Heat map (hierarchical clustering) depicting changes in protein expression levels (log₂-transformed fold changes). FAM57A is indicated by an arrow. Modified from (Bossler *et al.* 2019b).

5.4 FAM57A (family with sequence similarity 57 member A)

FAM57A, also known as CT120 or TLCD3A (TLC domain containing 3A), is a plasma membrane-associated protein with seven transmembrane domains, which is expressed in most human tissues (He *et al.* 2002). The *FAM57A* gene spans over 10373 nucleotides on chromosome 17p13.3 and encompasses five exons. Due to alternative splicing, the *FAM57A* gene can produce four transcript variants (Figure 5). Variant 1 (reported as *CT120A* (He *et al.* 2002)) represents the longest transcript and encodes the FAM57A-1 protein isoform of 257 amino acids in length. Variant 2 (referred to as *CT120B* (He *et al.* 2002)) lacks the fourth in-frame exon compared to variant 1 and produces a 32-amino acid shorter protein isoform, containing the same N- and C- termini. Transcript variants 3 and 4 lack the third exon or both the third and fourth exons, respectively (Figure 5). So far, there is no published data which has detected the predicted protein products of transcript variants 3 or 4.



Figure 5: FAM57A transcript variants and protein isoforms. Upper panel: FAM57A transcript variants. Light blue and dark blue rectangles represent single exons. Lower panel: Alignment of FAM57A protein isoforms. Sequences with shading are the putative transmembrane domains predicted by an online tool (<http://www.cbs.dtu.dk/services/TMHMM/>). Amino acid sequences specific for FAM57A-1 (light blue), FAM57A-3 (orange) and FAM57A-4 (red) are indicated.

There is very limited data available in the literature about FAM57A (only 13 references in Pubmed for FAM57A or its alternative name CT120, as of May 23, 2022 (Baltaci *et al.* 2015; Baltaci *et al.* 2017; Brill *et al.* 2010; He *et al.* 2002; He *et al.* 2004; Li *et al.* 2010; Lin *et al.* 2005; Pan *et al.* 2006; Pan *et al.* 2005; Ramanand *et al.* 2020; Ren *et al.* 2021; Wang *et al.* 2016; Wei *et al.* 2021)). FAM57A has been reported to act as a putative oncogene, promoting proliferation and inhibiting apoptosis of lung cancer cells *in vitro* (He *et al.* 2003; Li *et al.* 2010; Pan *et al.* 2006). In hepatocellular carcinoma (HCC), high FAM57A expression levels, as assessed by immunohistochemistry, were described to correlate with poor clinicopathological characteristics and with the expression of immune checkpoint genes, suggesting that FAM57A could serve

5. Introduction

as a predictor of poor prognosis and the immunotherapy response for HCC patients (Wei *et al.* 2021). Moreover, prostate cancer patients with high *FAM57A* expression levels have a shorter disease-specific survival period (Ren *et al.* 2021). In head and neck squamous cell carcinomas (HNSCCs), *FAM57A* has been reported to be a c-Myc target gene (Baltaci *et al.* 2017) and *FAM57A* transcript levels were found to be higher in tumors compared to the corresponding normal tissues (Baltaci *et al.* 2015). On the other hand, overexpression of *FAM57A*-2 isoform in lung cancer cells appears to inhibit proliferation by delaying G1/S phase transition, of which the underlying mechanism is unclear (Pan *et al.* 2005). No data is available concerning the function of *FAM57A* in cervical cancer.

At the molecular level, interactions of the *FAM57A* protein with the SLC3A2 (solute carrier family 3 member 2) and GGTL3B (a novel isoform of γ -glutamyltranspeptidase-like 3, also known as GGT7, γ -glutamyltransferase 7) proteins have been detected in yeast two-hybrid and co-immunoprecipitation (co-IP) assays (He *et al.* 2002). SLC3A2 is the heavy chain protein forming diverse heterodimeric amino acid transporters (HATs) by associating with different light chain subunits, such as LAT (L-type amino acid transporter) 1/SLC7A5, LAT2/SLC7A8, y^+ LAT1/SLC7A7, y^+ LAT2/SLC7A6, xCT/SLC7A11 and Asc1/SLC7A10 (Broer *et al.* 2001; Fort *et al.* 2021; Kantipudi *et al.* 2020; Palacin *et al.* 2004; Rodriguez *et al.* 2021; Yan *et al.* 2019). As a scaffold protein of HATs, SLC3A2 plays an important role for trafficking of transporters to the plasma membrane, thereby regulating amino acid metabolism and cellular GSH homeostasis (Liu *et al.* 2020). Additionally, SLC3A2 participates in cell adhesion, mechanotransduction and tumorigenesis mediated by integrins (Estrach *et al.* 2014; Feral *et al.* 2005; Henderson *et al.* 2004; Prager *et al.* 2007).

The putative *FAM57A* interaction partner GGT7 is a member of γ -glutamyltransferase (GGT) family and is reported to act as an anti-tumorigenic factor in glioblastoma cells by protecting cells from ROS (Bui *et al.* 2015). On the other side, GGT7 is overexpressed in hepatocellular carcinoma and correlates to a poor clinical outcome, suggesting pro-tumorigenic activities (Tian *et al.* 2021). Notably, the better-characterized GGT1 protein, a related enzyme of GGT family, cleaves the γ -glutamyl moieties from GSH, which are transferred to a variety of amino acids and dipeptide receptors (Hanigan 2014; Heisterkamp *et al.* 2008). Collectively, *FAM57A* may affect the GSH metabolism through the interaction with SLC3A2 and, possibly, GGT7, and thus be involved in the cellular redox homeostasis.

Further, two major growth-promoting pathways, the MAPK/ERK and the PI3K/AKT signaling cascades have been reported to be activated following ectopic expression of *FAM57A* in NIH3T3 fibroblasts (He *et al.* 2004). These potentially oncogenic pathways may underlie pro-tumorigenic effects of *FAM57A* and, as described above (chapter 5.2.4), both of these pathways are also hyperactive in cervical cancer cells (Rasi Bonab *et al.* 2021).

In specific, FAM57A leads to an enhanced phosphorylation of MEK1/2 and ERK1 in NIH3T3 cells, as well as to an increased expression of MAPK/ERK pathway-associated genes, such as *Myc*, *RAB2* (*Ras-related protein*), and to a decreased expression of *RASGRF1* (*Ras protein-specific guanine nucleotide-releasing factor 1*) (He *et al.* 2004). Further, FAM57A overexpression results in AKT activation (as indicated by increased AKT phosphorylation) and is accompanied by corresponding changes in the expression of a series of genes linked to AKT signaling, such as *14-3-3*, *MDM2* (*mouse double minute 2 homolog*), *CDKN1A* (*cyclin dependent kinase inhibitor 1A*), *CDKN1B* (*cyclin dependent kinase inhibitor 1B*) and *IGF1A* (*insulin-like growth factor 1A*) (He *et al.* 2004). The observation that the AKT inhibitor (AKTi VIII) downregulates FAM57A protein level under hypoxia (Figure 4) (Bossler *et al.* 2019b) also raises the possibility that there could be an interplay between FAM57A and the AKT pathway.

Besides, FAM57A may also provide a link to cell migration and tumor metastasis, suggested by the effects of FAM57A overexpression on the expression of *cathepsin B/D/L* (*CTSB/CTSD/CTSL*), *MMP* (*matrix metalloproteinase*)-2/14 and *TIMP2* (*tissue inhibitor of metalloproteinase 2*) in NIH3T3 cells (He *et al.* 2004). However, there is no functional data available which addresses the question whether FAM57A may affect cell motility, migration or invasiveness.

5.5 Research objectives

The *E6/E7* genes of oncogenic HPV types are essential for cervical cancer development. Yet, they are not sufficient for carcinogenesis and additional cellular alterations are required. It is thus important to gain insights into the cellular mechanisms which determine the malignant phenotype of cervical cancer cells. In a proteome screen, the FAM57A protein emerged as the most prominently induced factor in hypoxic cervical cancer cells. This thesis aims to uncover the regulation and function of FAM57A in cervical cancer cells by addressing three major questions:

- (i) Which molecular mechanisms control FAM57A expression and how does hypoxia lead to the strong increase of FAM57A levels? Here, specific antibodies for FAM57A detection will be developed. FAM57A expression will be analyzed both at the protein and transcript level in normoxic and hypoxic cells, under various experimental conditions (including differences in glucose supply and cell density). A possible role of the HPV *E6/E7* oncogenes for the regulation of FAM57A will be investigated as well as the functional significance of the hypoxia-induced transcription factors HIF-1 α and HIF-2 α .
- (ii) What is the function of FAM57A in cervical cancer cells? Here, the phenotypic effects of *FAM57A* repression by RNA interference will be analyzed through investigating possible changes in the cellular proliferation rate by performing live cell imaging analyses and colony formation assays. Furthermore, effects of FAM57A on cellular migration will be analyzed by wound healing assays.
- (iii) Which factors may mediate phenotypic effects exerted by FAM57A? Here, the selection of candidate factors to be analyzed will depend on the nature of the FAM57A-dependent cellular effects. In addition, the role of the SLC3A2 protein will be assessed, which has been proposed to interact with FAM57A.

Overall, this thesis aims to improve our current concepts of cervical carcinogenesis by determining the function of FAM57A in cervical cancer cells and to assess the suitability of FAM57A to serve as a potential novel therapeutic target for cervical cancer treatment.

6. Materials and Methods

6.1 Reagents

Molecular biology grade reagents were applied where available. All standard reagents for buffers and media were supplied by AppliChem (Darmstadt, Germany), BD Biosciences (Heidelberg, Germany), Bio-Rad (Munich, Germany), Carl Roth (Karlsruhe, Germany), Enzo Life Sciences (Lörrach, Germany), Merck (Darmstadt, Germany), New England Biolabs (NEB, Frankfurt, Germany), Promega (Madison, WI, USA), Sigma-Aldrich (St. Louis, M, USA) and Thermo Fisher Scientific (Waltham, MA, USA). Manufacturers of non-standard reagents are specified in the text.

Buffers and solutions were prepared with H₂O if not stated otherwise.

6.2 Cellular biology techniques

6.2.1 Cell culture

HPV18-positive HeLa-1 and HeLa-2 (RRID: CVCL_0030), HPV16-positive SiHa (RRID: CVCL_0032) and CaSki (RRID: CVCL_1100) cervical cancer cells, HPV-negative HaCaT (RRID: CVCL_0038) keratinocytes as well as Sp2/0 murine myeloma cells (RRID: CVCL_2199) were obtained from the German Cancer Research Center (DKFZ) tumor bank (Heidelberg, Germany). These cell lines have been authenticated within the last 3 years by single-nucleotide polymorphism (SNP) profiling (Multiplexion GmbH, Heidelberg, Germany). Cells were cultivated in Dulbecco's minimal essential medium (DMEM, Gibco, Thermo Fisher Scientific) supplemented with 10 % fetal bovine serum (FBS, PAN-Biotech, Aidenbach, Germany), 100 U/mL penicillin, 100 µg/mL streptomycin and 2 mM L-glutamine (all from Sigma-Aldrich). Standard cell culture was performed with medium containing 1 g/L (5.5 mM) glucose at 37 °C, 5 % CO₂ and 21 % O₂ (if not state otherwise). For hypoxia experiments, cells were cultivated at 37 °C, 5 % CO₂ and 1 % O₂ using the InvivoO₂ 400 physiological oxygen workstation (Ruskin Technology Ltd, Bridgend, UK).

HeLa-1-mKate2, HeLa-2-mKate2, SiHa-mKate2 and CaSki-mKate2 cells stably express the red fluorescent protein mKate2 in their nuclei and were generated from HeLa-1, HeLa-2, SiHa and CaSki cell lines, respectively. The stock culture of HeLa-1-mKate2, HeLa-2-mKate2, SiHa-mKate2 and CaSki-mKate2 cells was kept under selection using the complete medium mentioned above, additionally supplemented with puromycin (Table 1).

6. Materials and Methods

Cells were passaged every 3-4 days before reaching confluent using 0.25 % Trypsin-EDTA solution (Gibco). All experiments were performed with mycoplasma-free cells.

The trypan blue method (Phelan and Lawler 2001) was used for viable cell counting with the Countess™ Automated Cell Counter (Invitrogen, Thermo Fisher Scientific).

6.2.2 Cell cryopreservation and thawing

For cryopreservation, cells were trypsinized and centrifuged for 3 min at 800 g. The pellets were resuspended in cryotubes (#72.379, Sarstedt, Nümbrecht, Germany) containing medium supplemented with 20 % FBS and 5 % DMSO. The cryotubes were transferred into an isopropanol-filled Cryo 1 °C Freezing Container (NALGENE, Thermo Fisher Scientific) at room temperature (RT) and sequentially kept at -80 °C for several days, and finally stored in liquid nitrogen.

For thawing, cells were rapidly defrosted in a 37 °C water bath, resuspended in fresh complete medium and transferred into a new cell culture T-75 flask (TPP, Sigma-Aldrich). Medium was changed the following day.

6.2.3 Treatment with chemical compounds

Cells were treated with inhibitors or small molecule compounds (Table 1) as described in the text. The chemical compounds were added into the medium and the equal volume of the solvent was applied as control.

Table 1. Chemical compounds.

Compound	Solvent	Final concentration	Supplier
Cycloheximide	DMSO	10 µg/mL	Sigma-Aldrich
Mitomycin C	DMSO	5 µg/mL	Enzo Life Sciences
Puromycin	DMEM	HeLa-1-mKate2: 1 µg/mL	Sigma-Aldrich
		HeLa-2-mKate2: 1 µg/mL	
		SiHa-mKate2: 1 µg/mL	
		CaSki-mKate2: 0.5 µg/mL	
Hygromycin B	DMEM	HeLa-1: 200 µg/mL	Invitrogen
		HeLa-2: 250 µg/mL	
		SiHa: 300 µg/mL	
		CaSki: 75 µg/mL	

6.2.4 Transfection of plasmid DNA

Plasmid DNA was transfected by calcium phosphate co-precipitation technique described by Chen and Okayama (Chen and Okayama 1987). Cells were seeded in 6 cm dishes (Greiner Bio-one, Frickenhausen, Germany) the day before transfection and cultivated with 3 mL complete medium. When cells reached 30-40 % confluency, a total amount of 6 µg plasmid DNA were transfected per dish. If necessary, pBlueScript II vector (Stratagene, Heidelberg, Germany) was supplemented. Prior to transfection, 0.25 M CaCl_2 solution and 2x BES buffer (50 mM BES, 280 mM NaCl, 1.5 mM Na_2HPO_4 , pH 6.95) were warmed up to RT. DNA was mixed with 150 µL CaCl_2 solution followed by adding 150 µL of 2x BES buffer. The transfection mix was incubated at RT for 15 min and then added to cells covered with 3 mL fresh complete medium. After an incubation at 35 °C, 3 % CO_2 for 16-18 h, cells were washed twice with phosphate-buffered saline (PBS, 137 mM NaCl, 2.7 mM KCl, 4.3 mM Na_2HPO_4 , 1.4 mM KH_2PO_4 , pH 7.4) and afterwards cultivated under standard conditions until harvesting or splitting for subsequent experiments. Cell harvesting was usually performed 72 h after transfection of short hairpin RNA (shRNA)-expressing plasmids or 48 h after transfection of overexpression plasmids. Efficiency of knockdown was verified by detecting transcript expression using qRT-PCR (quantitative real time-polymerase chain reaction) and/or protein expression applying immunoblot analyses. The efficiency of ectopic overexpression of factors was evaluated by detecting their protein levels by immunoblot analyses.

6.2.5 Transfection of synthetic small interfering RNAs (siRNAs)

Synthetic siRNAs (Ambion, Thermo Fisher Scientific) supplied in form of lyophilized powder were dissolved in RNase-free water and diluted to 10 µM for long-term storage at -20 °C. For the transfection of siRNAs, cells were seeded in 6 cm dishes to reach 30-40 % confluence. Prior to transfection, the standard medium was replaced by 1.6 mL standard cell medium lacking penicillin and streptomycin. For each dish 4 µL (for HeLa-1) or 6 µL (for HeLa-2, SiHa and CaSki) of transfection reagent DharmaFECT I (Horizon Discovery, Cambridge, UK) and 6 µL stock siRNA (10 µM) were pre-incubated with reduced serum medium Opti-MEM I (Gibco) separately in a total volume of 200 µL for 5 min at RT. Afterwards, Dharmafect I solution and siRNA solution were mixed and incubated for 20 min at RT. The 400 µL transfection mix was then added to cells to reach a final siRNA concentration of 30 nM. Medium was removed and replaced by standard medium 24 h after transfection, and harvesting was performed 72 h after transfection.

For the experiments performed at low cell density, cells were transfected as mentioned above. Subsequently, medium was removed and cells were split 24 h after transfection. HeLa-1, HeLa-2 and SiHa cells were

6. Materials and Methods

seeded at a density of 2×10^5 cells per 6 cm dish and CaSki cells were seeded at a density of 4×10^5 per dish. After another 48 h, all tested cells were harvested.

Reverse transfection was performed in 96-well plates (#3596, Corning, NY, USA) for cell growth analyses. For HeLa-2-mKate2 and CaSki-mKate2 cells, 0.3 μ L transfection reagent DharmaFECT I and 0.3 μ L stock siRNAs (10 μ M) were pre-incubated with 10 μ L Opti-MEM I separately before being pooled. A volume of 0.1 μ L or of 0.2 μ L of DharmaFECT I were applied for SiHa-mKate2 or HeLa-1-mKate2 cells, respectively. A total volume of 20 μ L transfection mix were distributed to a well of 96-well plates and incubated at RT for 20 min. Then 80 μ L cell suspension containing 5×10^3 cells were added to each well. Medium was removed after 24 h and 200 μ L DMEM containing 1.8 mM glucose were replenished. Efficiency of siRNAs was validated at the transcript and the protein levels using qRT-PCR and immunoblot analyses, respectively.

Listed are the target sequences of siRNAs and shRNAs employed in this dissertation (Table 2). For siRNA transfection, a pool of several siRNAs targeting the same transcript(s) at equimolar concentrations was applied. Two different negative control siRNAs, referred as siCon.1 and siNeg, were applied and contain at least four mismatches to all known human genes.

Table 2. Target sequences of siRNAs and shRNAs.

Target transcript	si/shRNA designation	si/shRNA target sequence
<i>FAM57A</i> (variant-1/2/3/4)	si/shFAM57A-E1	5'-GCACCGACUGCGUGAUGAU-3'
	si/shFAM57A-E52	5'-GGAAGGCAGUCCGGCUCUU-3'
<i>FAM57A</i> (variant-1/2)	siFAM57A-AB1	5'-CUCUGUGAAUGGUGCCGAA-3'
	siFAM57A-AB2	5'-CCCUCACUCUUCGAAACUU-3'
<i>HIF-1α</i>	siHIF1A-1	5'-CUAACUGGACACAGUGUGU-3'
	siHIF1A-2	5'-CUGAUGACCAGCAACUUGA-3'
<i>HIF-2α</i>	siHIF2A-1	5'-CAGCAUCUUUGAUAGCAGU-3'
	siHIF2A-2	5'-GCGACAGCUGGAGUAUGAA-3'
<i>HPV16 E6</i>	si16E6 (4)	5'-ACCGUUGUGUGAUUUGUUA-3'
	si16E6 (246)	5'-GGGAUUUAUGCAUAGUAUA-3'
	si16E6 (321)	5'-UUAGUGAGUAUAGACAUUA-3'
<i>HPV16 E6/E7</i>	si16E6/E7 (2)	5'-CCGGACAGAGCCCAUUA-3'
	si16E6/E7 (575)	5'-CACCUACAUUGCAUGAAUA-3'
	si16E6/E7 (617)	5'-CAACUGAUCUCUACUGUUA-3'
<i>HPV18 E6</i>	si18E6 (340)	5'-GACAUUUAUUCAGACUCUGU-3'
	si18E6 (349)	5'-CAGACUCUGUGUAUGGAGA-3'
	si18E6 (353)	5'-CUCUGUGUAUGGAGACACA-3'
<i>HPV18 E6/E7</i>	si18E6/E7	5'-CCACAACGUCACACAAUGU-3'
	si18E6/E7 (563)	5'-CAGAGAAACACAAGUAUAA-3'

	si18E6/E7 (846)	5'-UCCAGCAGCUGUUUCUGAA-3'
SLC3A2	si/shSLC3A2-1	5'-GCAUCCGUGUCAUUCUGGA-3'
	shSLC3A2-2	5'-GCCUGAAACUGGAGCCUCA-3'
	si/shSLC3A2-3	5'-AGCUCAUACCUGUCUGAUU-3'
TAZ	siTAZ	5'-AGGUACUCCUCAAUACACA-3'
TEAD1/3/4	siTEAD1/3/4	5'-GAUCAACUUCAUCCACAAG-3'
YAP	siYAP	5'-GACAUCUUCUGGUCAGAGA-3'
-	si/shCon.1	5'-CAGUCGCGUUUGCGACUGG-3'
-	si/shNeg	5'-UACGACCGGUCUAUCGUAG-3'

6.2.6 CheckMate™ Mammalian Two-Hybrid System

The CheckMate™ Mammalian Two-Hybrid System (Promega) was used to investigate the intracellular protein-protein interaction between FAM57A and SLC3A2. In this system, a DNA-binding domain fused to protein X is expressed together with a transcriptional activation domain fused to protein Y. The interaction between protein X and protein Y results in the reconstitution of a complete transcription factor capable of activating the *Firefly luciferase* reporter gene of the pG5luc vector (Figure 6).

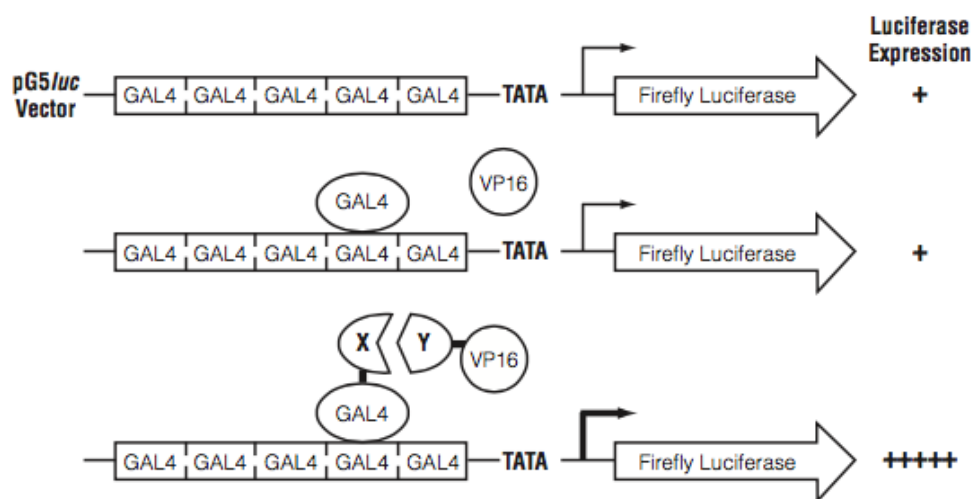


Figure 6. Schematic representation of the CheckMate™ Mammalian Two-Hybrid System. The pG5luc Vector contains five GAL4 binding sites upstream of a minimal TATA box, controlling expression of a *Firefly luciferase* gene. An interaction between the two proteins, which are expressed as GAL4-X and VP16-Y fusions, result in the stimulation of *Firefly luciferase* expression (adapted from the Technical Manual of the CheckMate™ Mammalian Two-Hybrid System, Promega Corporation).

To this end, the *FAM57A* and *SLC3A2* genes were cloned into pBIND2 or pACT2 vectors in order to express fusion proteins with the DNA-binding domain of GAL4 or with the activation domain of VP16, respectively.

6. Materials and Methods

The p-BIND2 vector contains a *Renilla luciferase* gene, which allows normalizing the transfection efficiency.

Transfection of plasmid DNA was performed as described in chapter 6.2.4. Each transfection was performed with a mixture containing 2 µg pACT2, 2 µg pBIND2 and 2 µg pG5luc plasmids. After 48 h cells were lysed using 200 µL trisphosphate buffer (25 mM Trisphosphate pH 7.8, 4 mM EGTA, 10 % glycerol, 1 % Triton X-100) on ice. Total lysates were centrifuged at 12,000 *g* and 4 °C for 5 min followed by transferring the supernatants to clean 1.5 mL tubes (Eppendorf, Sigma-Aldrich) kept on ice. For the luciferase activity measurement conducted by a luminometer (LB943 Mithras2, Berthold Technologies, Bad Wildbad, Germany), 50 µL supernatant were pipetted into white 96-well plates (#3600, Corning) and 50 µL lysis buffer were used as blank. For measuring Firefly luciferase activity, 200 µL luciferase buffer (25 mM glycylglycine pH 7.8, 15 mM MgSO₄, 15 mM K₃PO₄, 4 mM EGTA, 80 µM luciferin, 2 mM ATP, freshly prepared) were injected by the luminometer; for determining Renilla luciferase activity, 200 µL Renilla buffer (25 mM glycylglycine pH 7.8, 15 mM MgSO₄, 15 mM K₃PO₄, 4 mM EGTA, 1.6 µM coelenterazine, freshly prepared) were added per well. To account for the transfection efficiency, Firefly luciferase values were normalized to the respective values of the Renilla luciferase activity.

6.2.7 Colony formation assays

Colony formation assay is an *in vitro* cell survival assay based on the proliferative capacity of a single cell. To assess the capacity of cell proliferation, cells were seeded in 6 cm dishes for transfection with pCEP4-sh plasmids. Transfection was performed as mentioned in chapter 6.2.4. After 48 h cells were split into new 6 cm dishes at ratios ranging from 1:5 to 1:200. To select for successfully transfected cells, medium was replaced by standard medium supplemented with hygromycin B (Table 1) after another 24 h and changed every 3-4 days. Depending on the cell line, cells were fixed and stained after 10-15 days with a formaldehyde-crystal violet solution (12 mM crystal violet, 29 mM NaCl, 3.7 % formaldehyde, 22 % ethanol) for 5 min at RT. Then dishes were washed with water and dried at 37 °C overnight.

6.2.8 Cell growth analyses

Cell growth was evaluated using the IncuCyte® S3 Live-Cell Analysis System (Sartorius, Göttingen, Germany). The red fluorescent protein mKate2-expressing cells, HeLa-1-mKate2, HeLa-2-mKate2, SiHa-mKate2 and CaSki-mKate2, were seeded in 96-well plates in quintuplicates at a density of 5x10³ cells per well, in parallel with the implementation of reverse transfection (chapter 6.2.5). Medium was replaced

by 200 μ L DMEM containing 1.8 mM glucose 24 h after seeding. Cell number was determined as red object count.

6.2.9 Wound healing assays

The wound healing assay is one of the most widely used methods to study cell migration *in vitro*, detecting cell migration into a cell-free region generated by scratching of a cell monolayer (“wound”) (Rodriguez *et al.* 2005). In my assays, 4×10^4 cells were seeded in each well of the 96-well plates 48 h after transfection in octuplicates. Medium was replaced after 24 h and cells were treated with 5 μ g/mL mitomycin C for 3 h before scratching. The Incucyte® Woundmaker Tool (Sartorius) was applied to create homogeneous wounds in all wells simultaneously. Subsequently, medium was discarded and cells were carefully washed with PBS, followed by adding DMEM containing 2 % FBS (for HeLa-1-mKate2 and HeLa-2-mKate2 cells) or 10 % FBS (for SiHa-mKate2 cells). Images were obtained for wound width measurement using the IncuCyte® S3 Live-Cell Analysis System.

6.3 DNA-based techniques

6.3.1 Transformation of bacteria

For the production of competent bacteria, *Escherichia coli* (*E.coli*) strain TG2 was cultivated in Lysogeny Broth (LB) medium (1 % Bacto trypton, 0.5 % yeast extract, 170 mM NaCl, pH 7.0) at 37 °C overnight, then pelleted and resuspended in transformation buffer (10 % polyethylene glycol 8000, 5 % DMSO, 50 nM MgCl₂, 15 % glycerol in LB medium, pH 6.5). Bacteria suspension was frozen in liquid nitrogen and aliquots were stored at -80 °C for further use.

Transformation of competent *E.coli* TG2 with plasmid DNA was performed as described in the protocol of Hanahan (Hanahan 1983). For transformation, bacteria were thawed on ice. Approximately 50-100 ng plasmid DNA were incubated with 100 μ L bacteria suspension for 30 min on ice. Bacteria were then heat-shocked at 42 °C for 1 min in a water bath, followed by being chilled on ice for 1 min. Subsequently, 900 μ L LB medium without antibiotics were added to the bacteria, the mixture was shaken at 37 °C and 800 rpm for 1 h by using the Eppendorf® Thermomixer (Eppendorf). A fraction of the transformation reaction was streaked on a LB agar plate (1.5 % bacteriology agar (Gerbü, Heidelberg, Germany) in LB medium) and cultivated at 37 °C overnight. Alternatively, the transformation product was inoculated to an overnight culture of LB medium. The LB agar plates and LB medium were supplemented with the appropriate antibiotic (100 μ g/mL ampicillin for all applied plasmids).

6.3.2 DNA preparation and sequencing validation

6.3.2.1 Isolation of plasmid DNA

A colony of transformed bacteria grown on the LB agar plates were inoculated into 3 mL LB medium, cultured at 37 °C overnight using a SM-30 shaker (Edmund Bühler, Hechingen, Germany). Approximately 1 mL of the bacteria suspension was used for isolation of plasmid DNA applying the PureLink™ Quick Plasmid Miniprep Kit (Invitrogen) following the manufacturer's protocol to prepare a small amount of plasmid DNA. Alternatively, transformed bacteria were inoculated into 50 mL LB medium and incubated at 37 °C overnight for a larger amount of plasmid DNA preparation using the PureLink™ HiPure Plasmid Filter Midiprep Kit (Invitrogen). DNA concentrations were determined using the Nanodrop® ND-1000 spectrophotometer (Thermo Scientific, Thermo Fisher Scientific).

6.3.2.2 Restriction digestion

Restriction endonucleases (NEB) were chosen appropriately and applied according to the manufacturer's guidelines. For analytical digestion, 0.5-1 µg plasmid DNA were incubated in a final volume of 20 µL for 2 h at 37 °C in a water bath. For cloning purposes, 10 µg plasmid DNA were digested in a final volume of 50 µL.

6.3.2.3 Dephosphorylation of 5' termini

To prevent self-ligation of linearized plasmids, terminal 5' phosphate groups were removed from DNA using the calf intestinal alkaline phosphatase (CIP, NEB). To this end, digested plasmid DNA was incubated with 5-30 units CIP in a final volume of 50 µL for 1 h at 37 °C in a water bath, prior to gel purification.

6.3.2.4 DNA precipitation with ethanol

When a second digestion was required or plasmids needed to be concentrated, a precipitation of plasmid DNA was performed. Approximately 3 volumes of ethanol and 0.1 volume of 3 M sodium acetate (pH 5.2) were added to plasmids and incubated at -20 °C for 10 min. DNA was pelleted by centrifugation at 12,000 g and 4 °C for 30 min. The supernatant was removed and the DNA pellet was air-dried before dissolving in water.

6.3.2.5 Agarose gel electrophoresis and purification of DNA fragments

Digested DNA was separated by horizontal agarose gel electrophoresis. Depending on expected fragment lengths, 1-2 % agarose gel was prepared with electrophoresis buffer (40 mM Tris, 5 mM sodium acetate, 1 mM EDTA, pH 7.8), supplemented with PeqGREEN non-toxic DNA/RNA dye (Peqlab, Erlangen, Germany) at a dilution of 1:20,000. The gel was then put into an electrophoresis chamber (Peqlab) that was filled with the electrophoresis buffer. DNA samples were mixed with 6x DNA loading buffer (0.25 % bromphenol blue, 0.25 % xylencyanol, 30 % glycerol), loaded on the gel and run at 80-100 V. A total volume of 5 µL of SmartLadder (Eurogentec, Seraing, Belgium) were used as size marker. DNA was visualized by ultraviolet transillumination in a gel documentation system (Intas Science Imaging Instruments, Göttingen, Germany).

To extract DNA fragments from the agarose gel, the QIAquick Gel Extraction Kit (Qiagen, Hilden, Germany) was applied following the manufacturer's instructions.

6.3.2.6 Ligation

To ligate DNA inserts into CIP-treated vectors, 50-100 ng vector were mixed with a 3-7 molar fold excess of the DNA insert, 1 unit of T4 DNA ligase (Thermo Scientific) and the supplied 10x reaction buffer in a final volume of 20 µL. The ligation reaction was incubated at 21 °C for 2 h and inactivated at 65 °C for 5 min. The ligation mixture was used to transform competent *E.coli* TG2 as aforementioned.

6.3.2.7 Plasmid DNA sequencing

After the analytical digestion and the agarose gel electrophoresis, plasmid DNA samples with the expected lengths of DNA fragments were sent to Eurofins Genomics (Ebersberg, Germany) for sequencing. The sequencing results were analyzed using the Basic Local Alignment Search Tool (BLAST) provided by the National Center for Biotechnology Information (NCBI).

6.3.3 Molecular cloning strategies

6.3.3.1 Cloning of shRNAs into pSUPER plasmids

pSUPER is a mammalian expression vector that directs the intracellular synthesis of shRNA using the H1-RNA polymerase-III promoter (Brummelkamp *et al.* 2002). These transcripts can be further processed

to functional siRNAs in mammalian cells. To clone a shRNA into the pSUPER vector, synthetic oligonucleotides (Sigma-Aldrich) that contain the respective 19-nucleotide siRNA target sequence in sense and antisense orientation, separated by a hairpin sequence, was designed. Additionally, the oligonucleotides contained the appropriate 5'-overhangs required for cloning into the pSUPER vector. To anneal the oligonucleotides for ligation, the sense and antisense oligonucleotides were mixed and incubated at 95 °C for 5 min, followed by incubation at 70 °C for 10 min in a water bath, before slowly cooling down to 40 °C. The 5'-termini of the annealed oligonucleotides were phosphorylated by employing T4 polynucleotide kinase (PNK, NEB) in the presence of 1 mM ATP in the supplied T4 PNK buffer at 37 °C for 30 min. Enzyme inactivation was then performed at 70 °C for 10 min in a water bath. The kinase-treated double-stranded oligonucleotides were subsequently ligated to the BglII/HindIII-digested and CIP-treated pSUPER plasmid.

6.3.3.2 Cloning of shRNAs into pCEP4-sh plasmids

pCEP4-sh plasmids were applied for stable transfections in this project. These plasmids are derived from pCEP4 vector (Invitrogen), which contains a CMV promoter, a hygromycin resistance cassette, and the gene encoding for the Epstein Barr nuclear antigen (EBNA-1) and the EBNA ori-P sequence, thus allowing episomal replication of the plasmids within cells (Parham *et al.* 2001). For cloning shRNAs into the pCEP4 vector, the BamHI/XhoI fragments from pSUPER plasmids encompassing the H1-promoter and the shRNA sequences were inserted into BglII/XhoI-digested pCEP4 vector, thereby replacing the CMV-promoter of pCEP4 vector.

6.3.3.3 Cloning of FAM57A expression plasmids

The four isoforms of FAM57A were ectopically expressed as N-terminal Flag-tagged fusion proteins by transfections with pcDNA3-Flag-based plasmids. For cloning the four transcript variants of *FAM57A* into the pcDNA3-Flag vector, *FAM57A-1* transcripts were amplified by reverse transcription PCR (RT-PCR) from HeLa-1 cells by using primers with suitable restriction sites for cloning. All primers are listed in Table 3. For PCR, 100 ng cDNA, 0.25 µM forward primer, 0.25 µM reverse primer, 0.2 µM dNTPs and 2 units of Phusion DNA polymerase (Thermo Scientific) were mixed with the supplied Phusion buffer to a final volume of 100 µL. PCR was run in the MJ Research PTC-200 Peltier Thermal Cycler (Global Medical Instrumentation, Ramsey, USA) by applying 40 cycles of the following program: 98 °C for 30 sec, 60 °C for 30 sec, and 72 °C for 1 min. After the last cycle, a further extension step at 72 °C for 10 min was performed. The PCR products were ethanol-precipitated and digested with EcoRI and XhoI at 37 °C

overnight. The digested fragments were purified by agarose gel electrophoresis and ligated into EcoRI/XhoI-digested and dephosphorylated pcDNA3-Flag vector. Sequences were verified by analytic restriction analysis and sequencing.

Table 3. Primers for cloning.

Primer designation forward (for)/reverse (rev)	Primer sequence	PCR product
FAM57A(EcoRI/NdeI) for	5'-TAGGAATTCATATGCTGCTGACG CTGGCCG-3'	<i>FAM57A-1</i> <i>FAM57A-2</i> (PCR3)
FAM57A(XbaI/XhoI) rev	5'-GCTCTAGACTCGAGTTAGCCATC CTTTTGGCTTGG-3'	<i>FAM57A-3/4</i> (2 nd round of nested PCR)
FAM57A(2) for	5'-CCTTGTGCCAGTCGCACAGCTA AAGCAGCAGCACAC-3'	<i>FAM57A-2</i> (PCR1, PCR2)
FAM57A(2) rev	5'-GTGTGCTGCTGCTTTAGCTGTG CGACTGGCACAAGG-3'	
FAM57A ext3 for	5'-CAGCCCCGATGCTGCTGAC-3'	(1 st round of nested PCR)
FAM57A ext rev	5'-GGAATGCTGAGTGGAGGAGG-3'	
SLC3A2(EcoRI/BglII) for	5'-ATGGAATTCAGATCTATGGAGCT GCAGCCACCTGA-3'	<i>SLC3A2</i>
SLC3A2(XhoI/XbaI) rev	5'-GCCTCGAGTCTAGATCAGGCGG CATATGGAAATCTCAG-3'	

For cloning *FAM57A-2* transcripts, which lack the in-frame exon 4 compared to *FAM57A-1*, a PCR-based *in vitro* mutagenesis strategy, depicted in Figure 7, was applied. *FAM57A-1*-containing vector pcDNA-Flag-FAM57A-1 was used as template for the generation of two PCR products 1 and 2, encompassing the 5' or the 3' part of *FAM57A-1*, respectively, but missing the exon 4. Due to an overlap in primer sequences (Table 3), both PCR products share sequences of the exon3/exon5 junction. Thus, a third PCR with PCR1 and PCR2 products as template resulted in the generation of *FAM57A-2*. PCR1, PCR2 and PCR3 were performed as described above. For cloning, the PCR3 product was digested with EcoRI and XhoI at 37 °C overnight followed by gel purification and ligation into EcoRI/XhoI-digested pcDNA3-Flag vector.

6. Materials and Methods

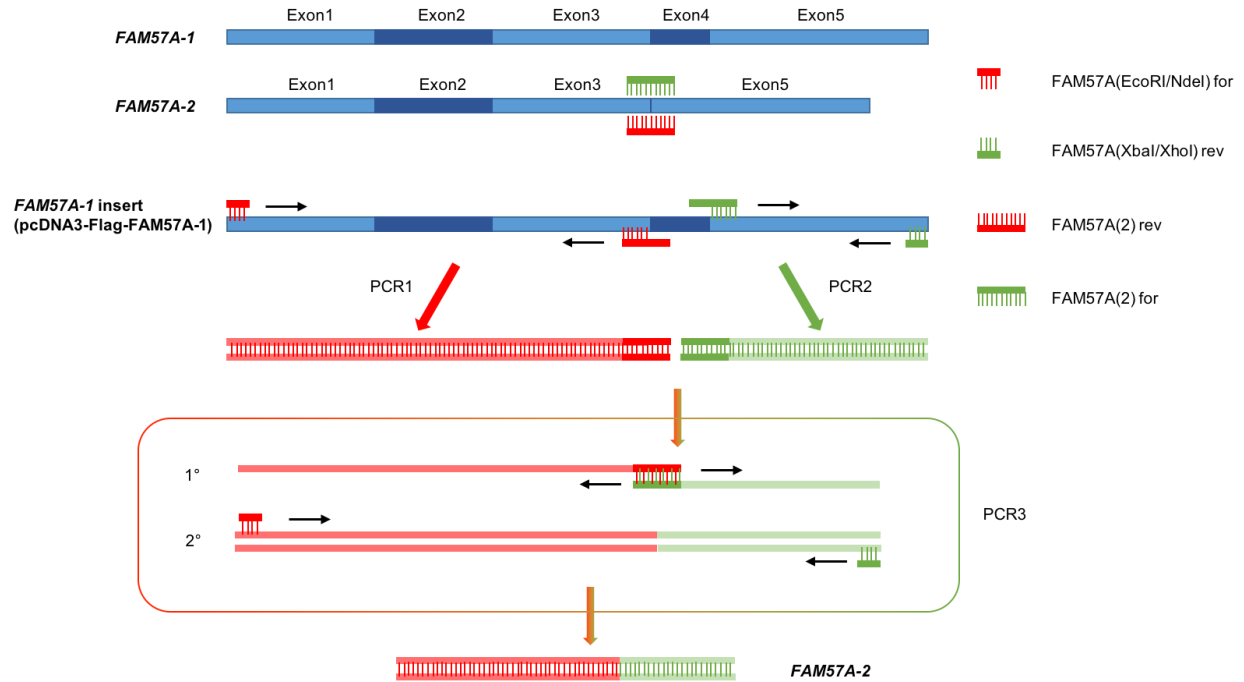


Figure 7: Cloning strategy for the *FAM57A-2* coding region. The constitution of the *FAM57A-1* and *FAM57A-2* coding regions (CDS) are shown as rectangles in light blue and dark blue. The DNA strands containing exon 1-3 and a shared sequence of the exon3/exon5 junction (PCR1) were generated from *FAM57A-1* insert with the primer pair of FAM57A(EcoRI/NdeI) for (short comb in red) and FAM57A(2) rev (long comb in red). The DNA strands containing exon 5 and the shared sequence of the exon3/exon5 junction (PCR2) were amplified with the FAM57A(2) for (long comb in green) and FAM57A(XbaI/XhoI) rev (short comb in green) primer pair. In PCR3, the single DNA strands from PCR1 (red) and PCR2 (green) were annealed with the shared sequence (dark red and dark green regions), and each strand was extended (1°). For further cycles of PCR, the elongated strands were applied as template and the FAM57A(EcoRI/NdeI) for and FAM57A(XbaI/XhoI) rev primers (2°) were employed, leading to the amplification of the *FAM57A-2* CDS fragment.

FAM57A-3 lacks the exon 3 of *FAM57A-1* while the exon 3 and exon 4 are missing in the *FAM57A-4* variant, which leads to frameshifts and consequently encodes for protein isoforms with shorter and distinct C-termini compared to *FAM57A-1*. Due the rarity of *FAM57A-3* and *FAM57A-4* transcripts in cultured cells compared to *FAM57A-1*, a nested PCR approach with cDNA from HeLa-1 cells, which were depleted of *FAM57A-1* and *FAM57A-2*, was necessary for obtaining signals for *FAM57A-3* and *FAM57A-4*. For a specific *FAM57A-1/2* knockdown, cells were transfected with siFAM57A-AB1/siFAM57A-AB2 (Table 2). For nested PCR (Figure 8), an additional external primer pair (FAM57A ext3 for and FAM57A ext rev) was applied for the first round of PCR, followed by a second PCR with the standard cloning primers (FAM57A(EcoRI/NdeI) for and FAM57A(XbaI/XhoI) rev, Table 3). The PCR products digested with EcoRI and XhoI and yielding the expected size were gel purified for ligation. Eventually, all plasmids were verified by analytic digestion and sequencing.

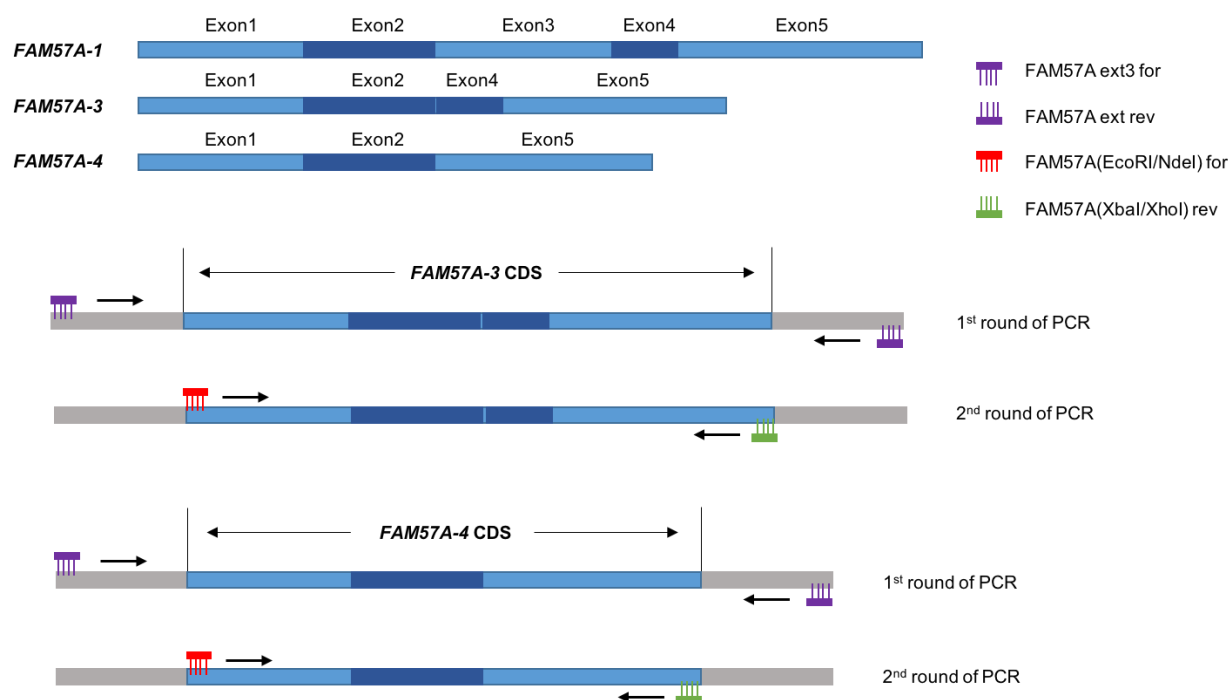


Figure 8: Schematic diagram of nested PCR. Nested PCR was used for the enrichment of *FAM57A-3* and *FAM57A-4* transcripts. The external primer pair (purple) recognizing sequences upstream or downstream (grey region) of the coding region (CDS) of *FAM57A-3/4* (light and dark blue region) was used for the 1st round of PCR with the cDNA template from *FAM57A-1/2* downregulated cells. The product from 1st PCR was mixed with *FAM57A*(EcoRI/NdeI) for (red) and *FAM57A*(XbaI/XhoI) rev (green) primers for the 2nd PCR. The inserts of *FAM57A-3* and *FAM57A-4* were then isolated from the product of 2nd PCR by agarose gel electrophoresis.

6.3.3.4 Cloning of CheckMate™ Mammalian Two-Hybrid plasmids

Following the technical manual of the CheckMate™ Mammalian Two-Hybrid System, the *FAM57A* and *SLC3A2* cDNAs were introduced into pBIND2 or pACT2 vectors to generate fusion proteins with the DNA-binding domain of GAL4 or with the transcriptional activation domain of VP16, respectively (Table 4). *FAM57A* was amplified by PCR using pcDNA3-Flag-FAM57A-1 plasmid as template. For *SLC3A2* cloning, pDONR221-SLC3A2 plasmid (#132213, Addgene, USA) containing a codon-optimized open reading frame (ORF) of *SLC3A2* was used as template. The respective primers for PCR were designed as listed in Table 3. PCR was performed as described in chapter 6.3.3.3. The PCR products were precipitated followed by an overnight digestion with NdeI/XbaI (for *FAM57A*) or EcoRI/XbaI (for *SLC3A2*) at 37 °C. The digested fragments were purified and ligated into the corresponding digested pBIND2 and pACT2 vectors. All plasmids were verified by analytic digestion and sequencing.

Table 4. Plasmids for the CheckMate™ Mammalian Two-Hybrid System.

Vector	Comment
pACT2*	VP16-fusion protein construction
pACT2-FAM57A	VP16-FAM57A fusion protein expression
pACT2-SLC3A2	VP16-SLC3A2 fusion protein expression
pBIND2*	GAL4-fusion protein construction
pBIND2-FAM57A	GAL4-FAM57A fusion protein expression
pBIND2-SLC3A2	GAL4-SLC3A2 fusion protein expression
pG5luc*	GAL4 binding site, TATA box, Firefly luciferase gene

* Plasmids were kindly provided by Karin Hoppe-Seyler & Claudia Lohrey.

6.4 RNA-based techniques

6.4.1 RNA extraction from cultured cells

Total RNA isolation was performed applying the PureLink™ RNA Mini Kit (Invitrogen). For the RNA harvesting from 6 cm dishes, cells were washed with PBS and lysed with 600 µL supplied RNA lysis buffer freshly supplemented with 1 % β-mercaptoethanol. The lysates were transferred to 1.5 mL tubes for storage at -20 °C or directly proceeded for RNA isolation according to the manufacturer's protocol. The PureLink™ DNase Set (Invitrogen) was used to prevent DNA contaminations. The concentration of purified RNA was measured using the NanoDrop® ND-1000 spectrophotometer, and RNA samples were stored at -80 °C.

6.4.2 Reverse transcription PCR (RT-PCR)

cDNA was synthesized using the ProtoScript® II First Strand cDNA Synthesis Kit (NEB). A total amount of 500 ng RNA was mixed with 0.5 µL randomized primer mix and 0.5 µL oligo-d(T) primer, and complemented by RNase-free water to a volume of 4 µL. The mix was incubated at 70 °C for 5 min for denaturation, followed by adding 5 µL of 2x reaction mix and 1 µL 10x enzyme mix. The 10 µL reaction mix was then first incubated at 25 °C for 5 min, followed by an incubation at 42 °C for 1 h and finally at 80 °C for 5 min. The cDNA product was stored at -20 °C.

6.4.3 Quantitative real-time PCR (qRT-PCR)

qRT-PCR was performed for the analyses of gene expression at the mRNA level. For each pair of primers, a reaction mix was prepared, which comprises of 10 µL SYBR™ Green PCR Master Mix (Applied Biosystems, Thermo Fisher Scientific), 0.4 µL forward primer (5 µM) and 0.4 µL reverse primer (5 µM),

complemented with 7.2 μL nuclease-free water to a total volume of 18 μL . The sequences of qRT-PCR primers are listed in Table 5. To the 18 μL reaction mix, 2 μL of the 1:5 diluted cDNA were added per well in a 96-well PCR plate (Biozym, Hessisch Oldendorf, Germany). As negative control, instead of cDNA, 2 μL nuclease-free water were added to the reaction mix. All PCRs were run in duplicates applying the 7300 Real Time PCR System (Applied Biosystems), according to the following program.

Initiation	50 °C	2 min	
Polymerase activation	95 °C	10 min	
Denaturing	95 °C	15 sec	} 40 cycles
Annealing and elongation	60 °C	1 min	
Dissociation curves	95 °C	15 sec	
	60 °C	1 min	
	95 °C	15 sec	
	60 °C	15 sec	

The $2^{-\Delta\Delta C_t}$ method (Livak and Schmittgen 2001) was applied to calculate the relative mRNA expression with normalization to the *18S rRNA* (Kozera and Rapacz 2013) or *TMBIM6* (Fjeldbo *et al.* 2016) reference genes. All primer pairs were initially validated for amplification efficiencies between 90-110 %. In parallel, the dissociation curves were generated as a quality control for unspecific amplifications.

Table 5. Primers for qRT-PCR.

Target gene	Sequence of forward (for) and reverse (rev) primer
<i>18S rRNA</i>	for: 5'-CATGGCCGTTCTTAGTTGGT-3'
	rev: 5'-ATGCCAGAGTCTCGTTCGTT-3'
<i>CTGF</i>	for: 5'-CACCCGGGTTACCAATGACA-3'
	rev: 5'-GGATGCACTTTTGGCCTTCTTA-3'
<i>CYR61</i>	for: 5'-AAGGAGCTGGGATTTCGATGC-3'
	rev: 5'-CATTCCAAAAACAGGGAGCCG-3'
<i>FAM57A</i>	for: 5'-AGTGTGGCCAAGAGATCAGC-3'
	rev: 5'-GCCATCATTTACGCTTCCC-3'
<i>SLC3A2</i>	for: 5'-AGCTGGAGTTTGTCTCAGGC-3'
	rev: 5'-GGCCAATCTCATCCCCGTAG-3'
<i>TAZ</i>	for: 5'-TGGCAGTATCCCAGCCAAAT-3'
	rev: 5'-GTCAGCGCATTGGGCATACT-3'
<i>TEAD1</i>	for: 5'-CTCAGGACAGGCAAGACGAG-3'
	rev: 5'-GAGACGATCTGGGCTGAGGA-3'

6. Materials and Methods

TMBIM6	for: 5'-GTGGTCATGTGTGGCTTCGT-3'
	rev: 5'-GGAAAGGCTGGATGGTCACT-3'
YAP	for: 5'-TTAGCCCTGCGTAGCCAGTT-3'
	rev: 5'-ACACTGTAGCTGCTCATGCTT-3'

6.5 Protein-based techniques

6.5.1 Development of a monoclonal mouse anti-FAM57A antibody

A monoclonal anti-FAM57A antibody recognizing all four isoforms was developed with the support of the Genomics and Proteomics Core Facility (GPCF) Antibody Unit of the German Cancer Research Center (DKFZ) according to the principles of Köhler and Milstein's hybridoma technology (Kohler and Milstein 1975). In brief, BALB/c mouse immunization was performed with a synthetic peptide antigen TWALRRSQPGWSRTDC (PSL GmbH, Heidelberg, Germany), which was C-terminally-conjugated through a cysteine residue to Keyhole Limpet Hemocyanin (KLH). Anti-sera were tested for a specific immune reaction by immunoblotting with protein lysate obtained after overexpression of FAM57A-1 in HeLa-1 cells. Anti-FAM57A antibody-producing B lymphocytes isolated from positively-reacted mice were fused with Sp2/0 murine myeloma cells to produce hybridoma cell clones. After 7 days, the cell supernatant was screened for the presence of specific antibodies to the protein of interest by enzyme-linked immunosorbent assay (ELISA) followed by immunoblotting analysis. Validated mother clones were subcloned by limited dilution to obtain monoclonal cell clones.

6.5.2 Protein extraction from cultured cells

Whole cell lysates were used for immunoblot analyses. In brief, cells were washed with ice-cold PBS and 200 µL of 1x Laemmli buffer (10 % glycerol, 1 % SDS, 0.02 M Tris, 0.1 % Bromphenol blue sodium salt, 0.05 M DTT, pH 6.8) were added to 6 cm dishes directly. The 1x Laemmli buffer was prepared from 3x Laemmli stock solution freshly supplemented with DTT followed by a 1:3 dilution with water. In addition, 125 units Benzonase® (Millipore, Merck) were added per dish to degrade DNA and RNA. Cells were scraped using a rubber policeman and transferred into 1.5 mL tubes, followed by a 5-min incubation at RT for nucleic acid digestion. The lysates were subsequently boiled at 95 °C for 3-5 min and used for immunoblot analyses or stored at -80 °C. Protein concentrations were determined after a 1:10 dilution with water applying the NanoDrop® ND-1000 spectrophotometer, with 1:10 diluted 1x Laemmli buffer used as blank.

6.5.3 Sodium dodecyl sulfate-polyacrylamide gel electrophoresis (SDS-PAGE)

SDS-PAGE is a commonly used method to separate proteins based on their molecular weight (Matsumoto *et al.* 2019). SDS-polyacrylamide gels were prepared as described in Table 6 using glass plates sealed with 1 % agarose.

Table 6. Recipe for SDS-polyacrylamide gels.

Components for separating gel (10 %)	For 2 gels	Components for stacking gel (5 %)	For 2 gels
Water	6.2 mL	Water	3.5 mL
3 M Tris-HCl (pH 8.9)	1.6 mL	0.47 M Tris-HCl (pH 6.7)	620 µL
30 % Acrylamide/bisacrylamide	4 mL	30 % Acrylamide/bisacrylamide	830 µL
10 % SDS	125 µL	10 % SDS	50 µL
10 % APS (ammonium persulfate)	62.5 µL	10 % APS	100 µL
TEMED (tetramethylethylenediamine)	12.5 µL	TEMED	5 µL

Gels were installed into the XCell SureLock™ Mini-Cell Electrophoresis System (Life Technologies, Thermo Fisher Scientific). Equal amounts of protein extract per lane were loaded on the gel placed in Tris-glycine SDS running buffer (2.5 mM Tris, 19.2 mM glycine, 0.1 % SDS). The PageRuler™ Prestained Protein Ladder (Thermo Scientific) was used as size standard in parallel. SDS-PAGE was performed at 90-120 V for 1-2 h.

6.5.4 Western transfer

Semi-dry blotting was employed for protein transfer to immunoblotting membranes. To prepare the transfer sandwich for each gel, 8 pieces of Whatman paper (GE Healthcare, Buckinghamshire, UK) were soaked in Towbin transfer buffer (2.5 mM Tris, 19.2 mM glycine, 20 % methanol, pH 8.3) and a polyvinylidene fluoride (PVDF) membrane (Immobilon-P membrane, 0.45 µm, Millipore) was activated in methanol. A wet sandwich comprised of 4 pieces of Whatman paper at the bottom (anode), followed by the activated PVDF membrane, the gel disassembled from glass plates and the other 4 pieces of Whatman paper on the top (cathode) was assembled into a Trans-Blot® SD Semi-Dry Electrophoretic Transfer Cell (Bio-Rad). Proteins were subsequently electrotransferred at 20 V for 1 h.

6. Materials and Methods

6.5.5 Immunodetection of proteins

To saturate unspecific binding sites, the PVDF membrane was incubated with blocking solution (5 % skimmed milk powder, 1 % BSA, 0.2 % Tween-20 in PBS) at RT for 1 h once the electrotransfer was completed. The membrane was then incubated with the primary antibody (Table 7) diluted in blocking solution at 4 °C overnight. For FAM57A probing, the supernatant from hybridoma cell culture was used for overnight incubation (Table 7). Prior to the incubation with the secondary antibody, the membrane was washed 3 times with PBS-T (0.2 % Tween-20 in PBS) for 10 min. A suitable secondary antibody (Table 7) was diluted in blocking solution and used for incubation at RT for 1 h. Afterwards, the membrane washing procedure described above was repeated. For protein visualization, enhanced chemiluminescence (ECL) was applied with ECL™ Prime Western Blotting Detection Reagent (GE Healthcare) according to the manufacturer's instruction. Images were acquired by the Fusion SL Detection System (Vilber Lourmat, Eberhardzell, Germany). All immunoblot analyses were repeated at least twice with consistent results.

Table 7. Antibodies for immunoblotting.

Primary antibodies			
Specificity	Source	Dilution	Supplier
anti-β-actin	mouse	1:50000	Santa Cruz sc-47778
anti-FAM57A	mouse	hybridoma supernatant	Developed in cooperation with the GPCF Antibody Unit, DKFZ, Heidelberg
anti-GAPDH	rabbit	1:5000	Santa Cruz sc-25778
anti-HIF-1α	mouse	1:500	BD Pharmingen #610959
anti-HIF-2α	mouse	1:500	Santa Cruz sc-46691
anti-HPV 16E6	mouse	1:3000	Arbor Vita Corporation (#849)
anti-HPV 16E7	mouse	1:1000	Kind gift of Dr. Müller, DKFZ, Heidelberg
anti-HPV 18E6	mouse	1:2000	Arbor Vita Corporation (#399)
anti-HPV 18E7	chicken	1:1000	Zentgraf, DKFZ, Heidelberg; ID: B (28) #47 31.10-11.11.95
anti-SLC3A2	rabbit	1:1000	Cell Signaling Technology #13180
anti-TAZ	rabbit	1:1000	Cell Signaling Technology #70148
anti-TEAD1	mouse	1:500	Santa Cruz sc-376113
anti-α-tubulin	mouse	1:5000	Calbiochem CP06
anti-YAP	rabbit	1:1000	Cell Signaling Technology #14074
anti-YAP phospho (Ser127)	rabbit	1:1000	Cell Signaling Technology #4911
Secondary antibodies			
Specificity	Source	Dilution	Supplier
anti-chicken IgG	goat	1:5000	Santa Cruz sc-2428
anti-mouse IgG	goat	1:5000	Jackson ImmunoResearch 111-035-003
anti-rabbit IgG	goat	1:5000	Jackson ImmunoResearch 111-035-071

6.6 Statistical analyses

All experiments were performed at least in three biological replicates if not stated otherwise. Fold change analyses of qRT-PCR and of the CheckMate™ Mammalian Two-Hybrid assays were performed following \log_2 -transformation. Mean values and standard deviations were calculated using Microsoft Excel software. Statistical significant differences of the data were evaluated by applying one-way ANOVA with SigmaPlot software and indicated by *P* values < 0.05 (*), < 0.01 (**), or < 0.001 (***).

7. Results

7.1 Analysis of FAM57A expression

7.1.1 Development and validation of an antibody for FAM57A detection

In order to investigate cellular FAM57A expression, a monoclonal antibody against FAM57A was generated with support by the GPCF (Genomics and Proteomics Core Facility) Antibody Unit of the German Cancer Research Center (DKFZ) (experimental details in chapter 6.5.1). For antibody validation, the four FAM57A isoforms (Figure 9) linked to a Flag tag were ectopically expressed in a highly transfectable HeLa laboratory variant, which in the following is termed HeLa-1 (chapter 6.2.1). Expression of the different FAM57A isoforms was validated by using an anti-Flag antibody (Figure 9A). As shown in Figure 9B, the anti-FAM57A antibody used in the subsequent experiments in this thesis recognizes all four ectopically expressed FAM57A isoforms (Figure 9B, right part). At the endogenous level (untransfected cells), FAM57A-1 was by far the predominant isoform detectable in HPV18-positive HeLa-1 and HeLa-2 cells as well as in HPV16-positive SiHa and CaSki cells (Figure 9B, left part). For reasons of simplicity, the FAM57A-1 isoform will be referred to as FAM57A in the following, if not indicated otherwise.

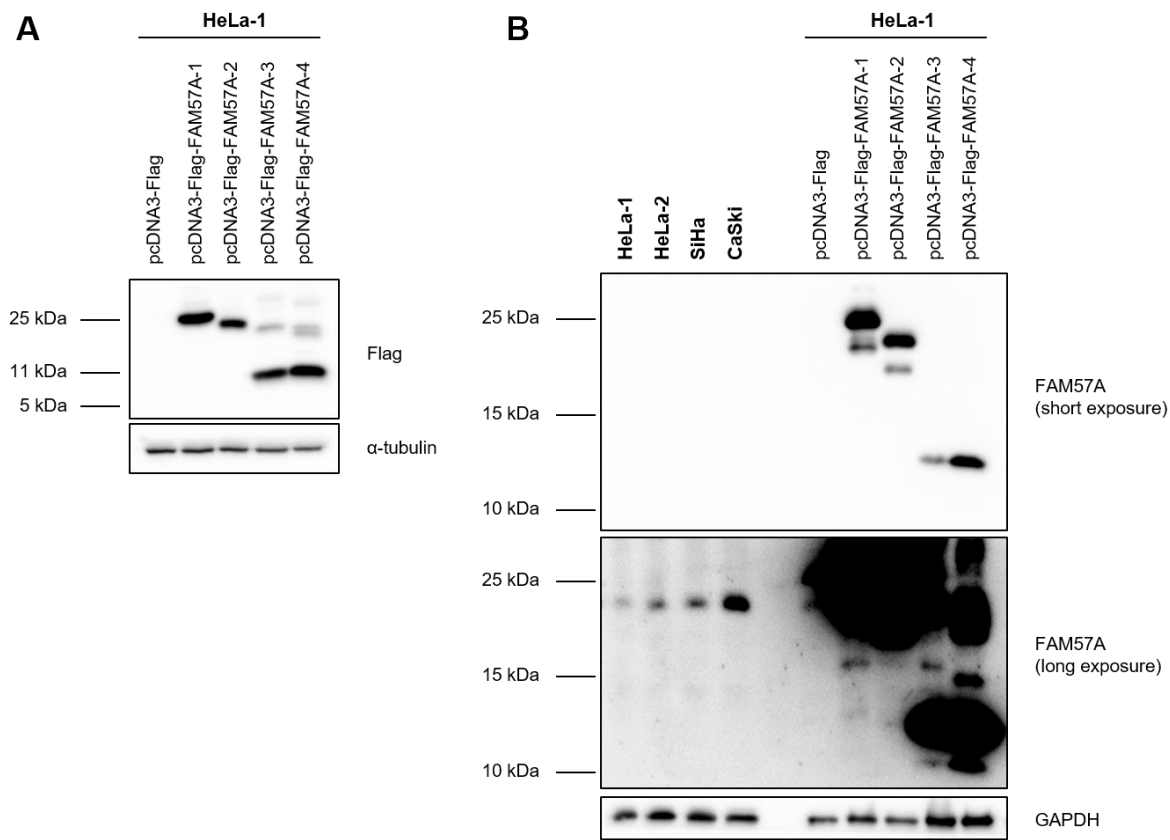


Figure 9 (previous page). **Validation of the anti-FAM57A antibody.** (A) The four FAM57A isoforms were ectopically expressed from pcDNA3-Flag-FAM57A-1/2/3/4 in HeLa-1 cells and analyzed by immunoblot using an anti-Flag antibody. α -tubulin: loading control. (B) Detection of endogenous and ectopic FAM57A expression by immunoblot employing the anti-FAM57A antibody developed in this thesis. Endogenous FAM57A expression is analyzed in HeLa-1, HeLa-2, SiHa and CaSki cells. Short and long exposures of the immunoblot are shown. GAPDH: loading control.

7.1.2 FAM57A expression is induced under hypoxia

Next, the hypoxic regulation of FAM57A expression was investigated by comparing FAM57A protein and transcript levels in HPV-positive cancer cell lines (HeLa-1, SiHa and CaSki) as well as in HPV-negative HaCaT keratinocytes, which were cultivated under normoxia (21 % O₂) or hypoxia (1 % O₂) for 24 h. The hypoxia-inducible factor HIF-1 α was used as hypoxia marker.

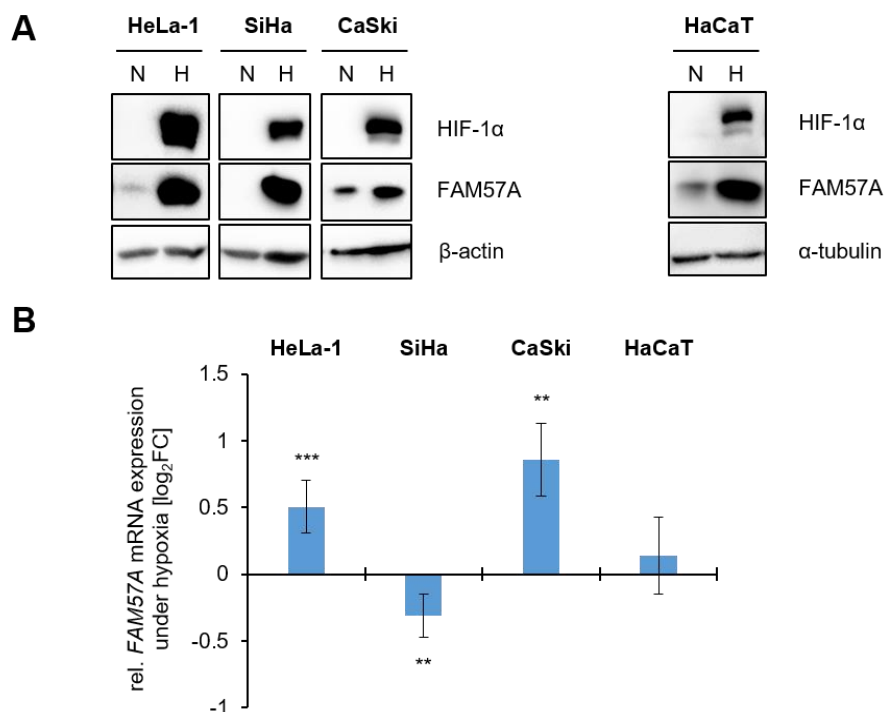


Figure 10. Effects of hypoxia on FAM57A protein and transcript levels in HPV-positive and HPV-negative cells. (A) Representative immunoblot analyses of HPV-positive HeLa-1, SiHa and CaSki cells as well as of HPV-negative HaCaT cells, after 24 h cell culture under normoxia (N) or hypoxia (H). HIF-1 α : hypoxia marker. β -actin, α -tubulin: loading controls. (B) Concomitant qRT-PCR analyses of the hypoxic regulation of FAM57A transcript expression. Shown are the log₂-transformed fold changes (log₂FC) of mean expression levels under hypoxia relative to normoxia with standard deviations from at least 3 independent experiments (HeLa-1: n=5, SiHa: n=6, CaSki: n=4, HaCaT: n=3). Statistically significant differences compared to the respective normoxic cells (log₂FC=0) are determined by one-way ANOVA, **: $P < 0.01$, ***: $P < 0.001$.

7. Results

Notably, expression of FAM57A was strongly induced under hypoxia compared to normoxia in all investigated cell lines, regardless of their HPV status (Figure 10A). In comparison, *FAM57A* transcript levels, which were quantified by qRT-PCR with the primer pair recognizing all four transcript variants, were considerably less affected under hypoxia (Figure 10B). The pronounced differences in the FAM57A response towards hypoxia on the protein and transcript levels indicate that the hypoxic induction of FAM57A expression mainly occurs at the protein level.

7.1.3 Cell density is a key regulator of FAM57A protein expression

During the course of my experiments, a possible impact of cell density on FAM57A protein levels under normoxic conditions was observed. To examine this issue in detail, the protein and transcript levels of FAM57A were assessed in different HPV-positive cancer cell lines and in HaCaT cells plated at different densities. To this end, 2×10^5 , 1×10^6 and 1×10^7 HeLa (both HeLa-1 and HeLa-2) and SiHa cells were seeded per 6 cm dish as low (LD), middle (MD) and high density (HD), respectively. For CaSki and HaCaT cells, 4×10^5 , 2×10^6 and 1×10^7 cells were seeded for LD, MD and HD, respectively. Microscopic images obtained after 48 h cell culture depict the different cell densities before harvesting (Figure 11A). Importantly, FAM57A protein levels were strongly declining in parallel with the increase of cell densities in all investigated cell lines (Figure 11B). Contrary to the regulation of FAM57A protein amounts, *FAM57A* transcript levels were only modestly affected, if at all, by the different cell densities (Figure 11C). Hence, the strong effect of cell density on FAM57A expression levels predominantly occurs at the protein level, as is observed for the hypoxic induction of FAM57A expression (Figure 10).

These results reveal that the cell density-dependent regulation of FAM57A expression primarily occurs at the protein level. Since there is no data available in the literature about the regulation of FAM57A protein stability, first pilot experiments were performed to address this issue. To this end, SiHa cells were cultivated under different cell densities, treated with the protein synthesis inhibitor cycloheximide (CHX) (Schneider-Poetsch *et al.* 2010), and FAM57A expression was assessed by immunoblot analyses in time course experiments. SiHa cells seeded at LD and cultivated for 24 h express FAM57A at a detectable level, in contrast to SiHa cells seeded under HD (please refer to the first 2 lanes in the immunoblot in Figure 12A, corresponding to time point 0). Subsequently, the cells seeded at LD were treated with 10 μ g/mL CHX for up to 24 h. Notably, FAM57A protein levels were not appreciably reduced even after 24 h CHX treatment, indicating that FAM57A has a relatively long half-life of more than 24 h under these experimental conditions. In contrast, the levels of p53, which is a protein with a short half-life of 5-20 min (Giaccia and Kastan 1998) and serves as a control for my experimental conditions, were quickly downregulated following CHX treatment.

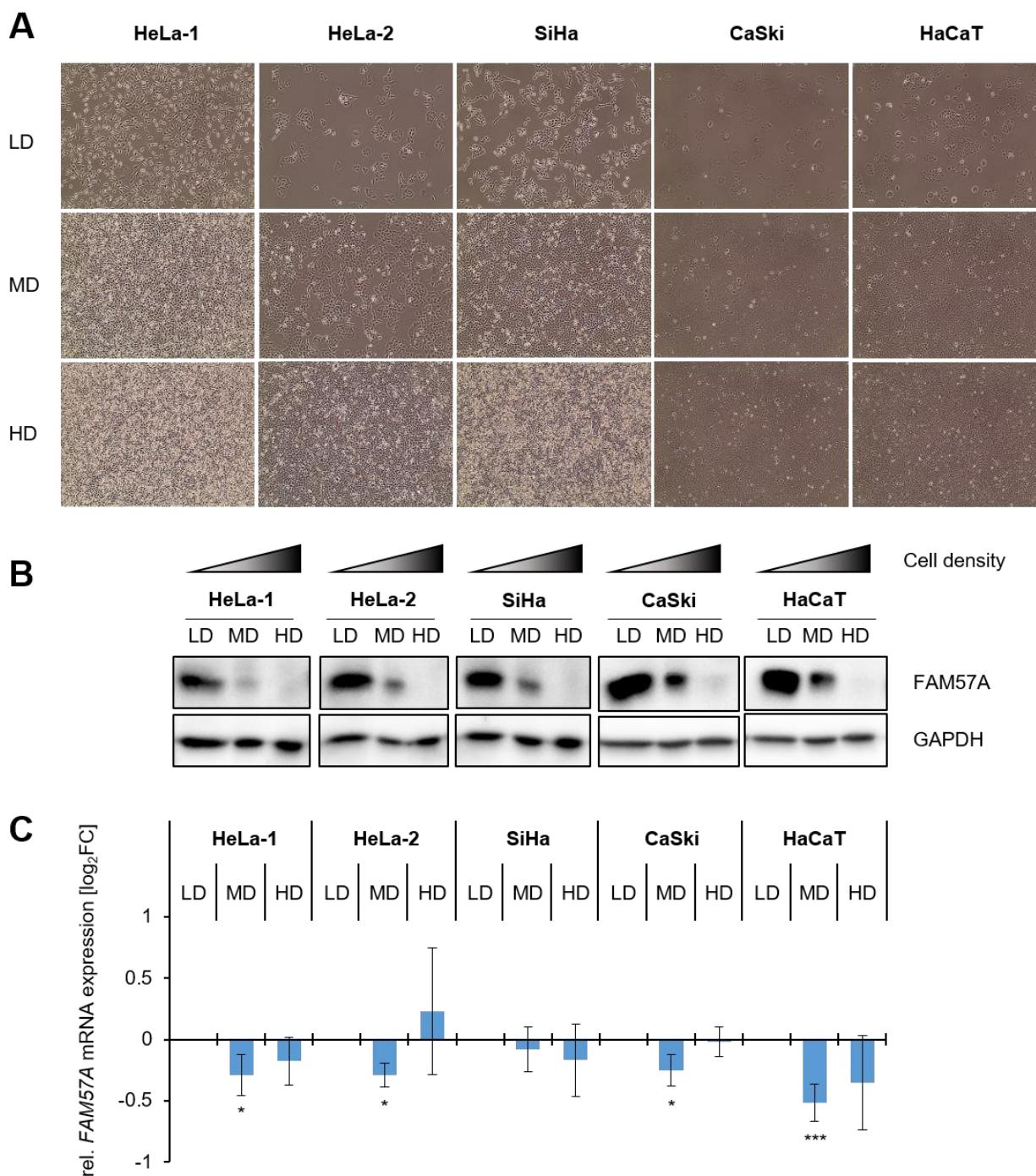


Figure 11. Effects of cell density on FAM57A protein and transcript levels under normoxia. (A) Microscopic visualization of cell densities before harvesting of the cells. LD: low density; MD: middle density; HD: high density. (B) Immunoblots visualizing FAM57A expression at the protein level under different cell densities. GAPDH: loading control. (C) Relative *FAM57A* mRNA levels under different cell densities, assessed by qRT-PCR. Shown are the \log_2FC of mean expression levels under MD and HD relative to LD with standard deviations from at least 3 independent experiments (HeLa-1: $n=5$, HeLa-2: $n=3$, SiHa: $n=4$, CaSki: $n=3$, HaCaT: $n=5$). Statistically significant differences compared to the respective LD cells ($\log_2FC=0$) are determined by one-way ANOVA, *: $P < 0.05$, ***: $P < 0.001$.

7. Results

In addition, experiments were performed to determine the time course of FAM57A repression under HD. Confluent cells (0 h, HD) were split and seeded at LD and HD, and then harvested for further analyses after 6 h, 12 h, 24 h and 48 h (refer to the scheme in Figure 12B). Interestingly, FAM57A protein levels were upregulated 6 h after splitting in cells seeded either at LD or HD. Over the whole time course, FAM57A protein expression remained at high levels in LD cells, whereas it became almost undetectable in HD cells 12 h after seeding.

In future experiments, it will be interesting to gain further insights into the underlying biochemical mechanism mediating FAM57A degradation, for example by analyzing the effects of chemical inhibitors of proteasome- (*e. g.* MG132 and bortezomib (Kisselev 2021)) or lysosome- (*e. g.* bafilomycin A1 and chloroquine (Liu *et al.* 2020)) mediated protein degradation on this regulation.

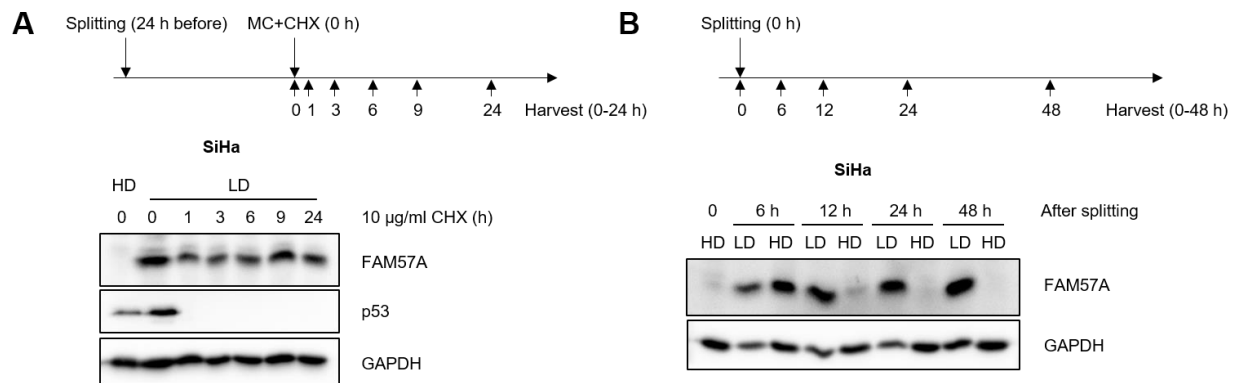


Figure 12. FAM57A protein stability and expression kinetics. (A) FAM57A protein levels in SiHa cells cultivated under HD and LD. Cells at LD were treated with 10 µg/mL CHX for different time periods, as indicated, and FAM57A and p53 protein levels were determined by immunoblot. (B) Immunoblot analysis depicting the kinetics of FAM57A protein expression. Cells were grown under HD, split and seeded at LD or HD conditions at time point 0 (0 h). FAM57A expression was analyzed after further cultivation of the cells for the indicated time periods. GAPDH: loading control.

7.1.4 Hypoxia-induced FAM57A protein expression is predominantly a result of decreased cell density

Hypoxia inhibits the proliferation of cervical cancer cells (Hoppe-Seyler *et al.* 2017a). In view of my findings presented above, the resulting lower cell density might thus contribute to the upregulation of FAM57A protein under hypoxia. Thus, in order to investigate whether the hypoxic induction of FAM57A expression is a direct effect of hypoxia or linked to the reduction of cell density, HPV-positive cancer cells were seeded under LD or HD, and FAM57A protein levels were analyzed upon cultivation of the cells under normoxic or hypoxic conditions. Moreover, the influence of glucose on FAM57A regulation under these different treatment conditions was analyzed, by supplying the cells with different glucose concentrations in the medium (0 mM, 5.5 mM and 25 mM).

Importantly, FAM57A expression was only detectable in cells seeded at LD for all investigated cell lines, but not in HD cells cultivated under all experimental conditions, including hypoxia (Figure 13). In addition, a slight increase in FAM57A levels was observed by comparing cells cultivated at LD under hypoxia to those grown under normoxia. In contrast to the striking effects of different cell densities, FAM57A regulation was not appreciably affected by the different tested glucose concentrations (Figure 13).

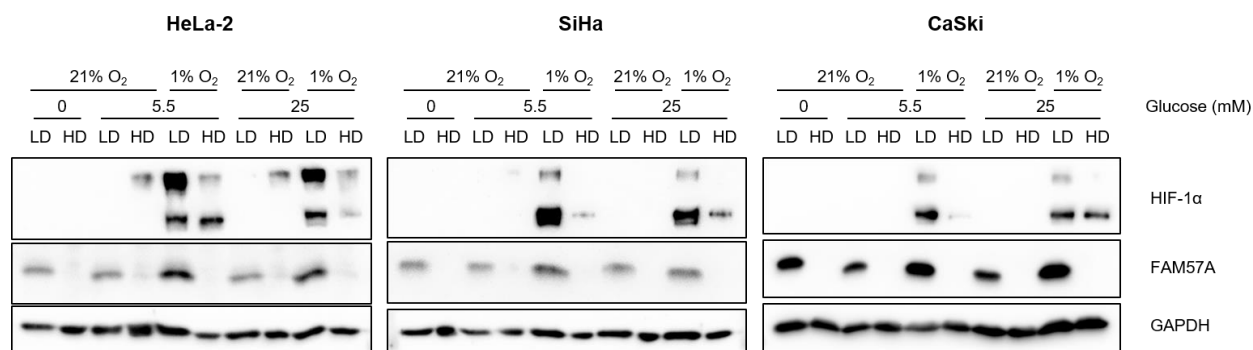


Figure 13. FAM57A protein expression in dependence on cell density, normoxia/hypoxia and glucose supply. HPV-positive cancer cells were seeded at LD or HD. After 24 h, cells were cultivated under normoxic (21 % O₂) or hypoxic (1 % O₂) conditions and under different glucose concentrations, as indicated, for another 24 h before harvesting. HIF-1α: hypoxia marker, GAPDH: loading control.

The slight increase in FAM57A protein levels in hypoxic versus normoxic cells cultivated under LD was most pronounced in HeLa-2 cells (Figure 13). Since this effect was accompanied by an approximately 2-fold upregulation of *FAM57A* mRNA levels (Figure 14A), I hypothesized that the modest increase of FAM57A protein levels in these cells might be related to HIF-linked transcriptional activation. Therefore, FAM57A expression in hypoxic HeLa-2 cells at LD was analyzed following RNA interference (RNAi)-mediated silencing of *HIF1A* and *HIF2A* expression, individually or in combination. It was found that the hypoxia-associated FAM57A induction under LD was diminished both at the protein (Figure 14B) and more pronounced, at the transcript (Figure 14C) levels when *HIF1A* was silenced alone or in combination with *HIF2A* silencing. In contrast, *HIF2A* silencing alone did not affect FAM57A expression (Figure 14B and 14C). This indicates that FAM57A expression can be activated by HIF-1α. In line with this possibility, putative binding sites for HIF-1α in the potential promoter region (-1056 - +64) of *FAM57A* gene were identified (Figure 15).

7. Results

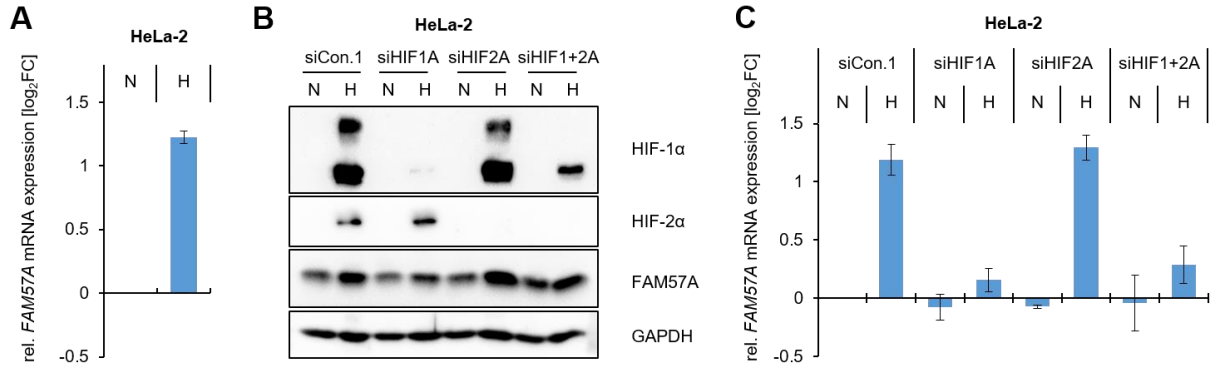


Figure 14. FAM57A expression upon *HIF1A* or *HIF2A* silencing. (A) *FAM57A* transcript levels in normoxic or hypoxic HeLa-2 cells. Depicted are the log₂FC of the mean expression levels under hypoxia relative to normoxia (log₂FC=0) with standard deviations of 2 independent experiments. (B) Immunoblot analyses of *FAM57A* levels following silencing *HIF1A* (siHIF1A) or *HIF2A* (siHIF2A) alone or in combination (siHIF1+2A). GAPDH: loading control. (C) Accompanying analysis of relative *FAM57A* transcript levels by qRT-PCR. Displayed are the log₂FC of mean expression levels relative to siCon.1 cells under normoxia (log₂FC=0) from 2 independent experiments with standard deviations. (A-C): N: normoxia, H: hypoxia.

Collectively, the results of these experiments indicate that the increase in *FAM57A* levels under hypoxia is predominantly cell density-dependent and this is likely a consequence of the hypoxia-related decrease in cell densities. In addition, there is a small contribution of HIF-1α to the effect.

5'- ...CAGAGTCCTGCTCTGTGGCCCCAGGCTGGAGTGCAGTGG**CGTG**ATCTCGGCTCACTGCAACCTC
 TGCCCTCCAGGTTCAAGCGATTCTCCTGCCTCAGCCTCCAGAGTAGCTGGGACTACAGACAGGCAC
 CACCACACCTGGCTAATTTTGTATTTTGTAGTAGAGACGGGGTTT**CACG**GGTGGTCAGGCTGGTCT
 CGAACTCCTGACGTCAAGTGATCTGCCCGCCTCGGCCTCCCCAAGTGCTGGGGTTACAGGCGCGCC
 CGACCCCGATACTTTTAAATAACGA**CACG**TTGTGAACAACACCACAGTCCCTACGCCTCTGGATGGT
 GTCTCCGGATAGATCCAAAGCCGAGAGGCGAGTAAGAGCCTGCAGCCTCCACAGTCCGCCTCCTGGT
 GCAGGTGGAGAGGGGCTGCTGGAGGCCCGGACCT**CACG**CTTCCTGAGGGCCACCCCGGAGCG
 GCTGCAGCCGCTGGCGGCACCGGGAAGCATCTCGGC**CGTG**CGGGGAGAGGCCACATCCTGAGG
 CCTCCACCGAGAAGCACCAGGGCTTGGTGGACGGGGCCCGCGAACCCAGGGCC**CACG**CCGCCT
 CCCTCCTTCCCTCCCGCGGGCCTCGCCCCACCCCGGAGGGGGTTCTACCTGGCTTCTCGGCC
 CGCGCCACCCCGCCCTTCGCCCGGGCGCGCGAGAAGAGCAGGTCGGGGAGGGGCGCGTCCG
 CTGACGGAACAGAAGCCGGAGCCGCGGCCCTTCCCGCCTCCGCCTGGGCCCGCGGCCGCTCG
 GGAGGGAGCGGCGGACTCGGAACGCGCGCGCGCCCGGCCACAGCCGCGCCTCGGTC
 CCCGCCTCCGCCCCCGCCACCCGCGCGGGGACGCGGGGAACCTCCGGGCCAGGGACC
 GCGAGAGACCCCGCCCCGCCCTATCGCAGCCGCCGGGCTGGT**CACG**CGCAGAGCCGCGCCGCG
 GGATCGGGGCCAGCGCCGGGCGGAGGCGGGACGGGGCGGAGGGTTGAAATCGCGCG
 GCCGGGCGGGGCGCGCC**G**AGCCGAACCCAGC**CACG**CGGCGCCAGCGAGGCGGCCGACCCGC
 AGCCCCG**ATGCTGCTGACG**...-3'

Figure 15. Putative HIF-1α binding sites in the promoter region (-1056 - +64) of the *FAM57A* gene. Potential HIF-1α binding motifs (5'-CGTG-3' or its reverse sequence 5'-CACG-3') are highlighted in bold. The predicted transcriptional start site (according to the NCBI database: <https://www.ncbi.nlm.nih.gov/gene/79850>) is marked in bold and italicized. The sequence with the single underline corresponds to the start of the coding sequence.

7.1.5 HPV E6/E7 suppression induces FAM57A expression in a cell density-dependent manner

The results obtained above show that FAM57A expression correlates with the lower cell densities. Thus, I reasoned that the inhibition of pro-proliferative stimuli should result in an increase of FAM57A expression levels. Suppression of the HPV *E6/E7* oncogenes in cervical cancer cells strongly inhibits their growth and results in senescence (Hoppe-Seyler *et al.* 2017a). To investigate the effect of *E6/E7* repression on FAM57A expression, FAM57A protein levels were analyzed following silencing of *E6/E7* by RNAi.

Figure 16A shows that *E6/E7* repression led to a strong induction of FAM57A protein levels in cervical cancer cells. To further assess the effects of cell density on this regulation, *E6/E7* expression was silenced, followed by seeding cells at LD and HD. In addition, possible effects of glucose supply were assessed by cultivating the cells under low (5.5 mM) or high (25 mM) glucose concentrations. Similarly as observed under hypoxia (Figure 13), FAM57A expression levels were again primarily density-dependent, since *E6/E7* repression in cell cultivated under LD only marginally, if at all, affected FAM57A expression levels (Figure 16B). Further, the regulation of FAM57A expression was also not affected by low or high glucose supply. Thus, as seen for the hypoxic induction of FAM57A, these findings indicate that the FAM57A increase upon *E6/E7* suppression in cervical cancer cells is predominantly a secondary response to the lower cell density resulting from the growth inhibitory effects of *E6/E7* silencing.

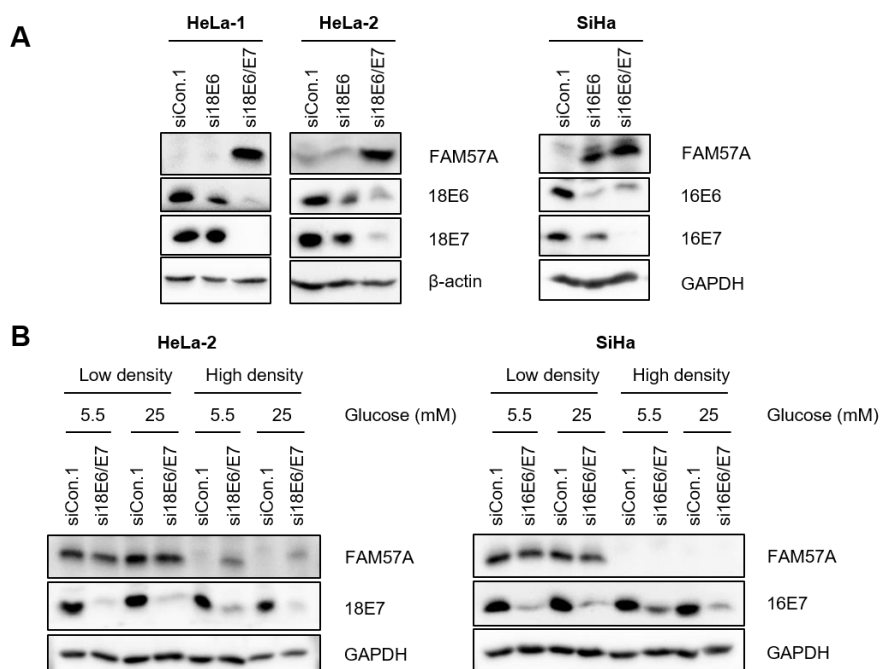


Figure 16: Effects of *E6/E7* silencing on FAM57A expression in cervical cancer cells. (A) Immunoblot analyses of FAM57A and viral E6/E7 protein expression in HPV-positive cancer cells after RNAi-mediated *E6* or *E6/E7* repression. β-actin, GAPDH: loading controls. (B) Immunoblot analyses of FAM57A and HPV E7 expression in HPV-positive cells seeded at LD or HD following *E6/E7* knockdown and subsequent cultivation under 5.5 mM or 25 mM glucose for 24 h. GAPDH: loading control.

7.2 Phenotypic effects of FAM57A in HPV-positive cancer cells

Next, the thus far unknown phenotypic effects of FAM57A in cervical cancer cells were investigated, focusing on cellular proliferation and migration.

7.2.1 FAM57A promotes the proliferation of HPV-positive cancer cells

To assess possible effects of FAM57A on the proliferation of cervical cancer cells, colony formation assays (CFAs) and live cell imaging analyses were performed following *FAM57A* silencing by RNAi.

For CFAs, two short hairpin RNAs (shRNAs), shFAM57A-E1 and shFAM57A-E52, were utilized which target different sequences that are conserved in the transcripts of all four *FAM57A* variants. Their efficiencies were validated at the transcript level (Figure 17A). In CFAs, the shRNA-mediated downregulation of *FAM57A* inhibited the colony formation capacity in all tested HPV-positive cancer cell lines (Figure 17B).

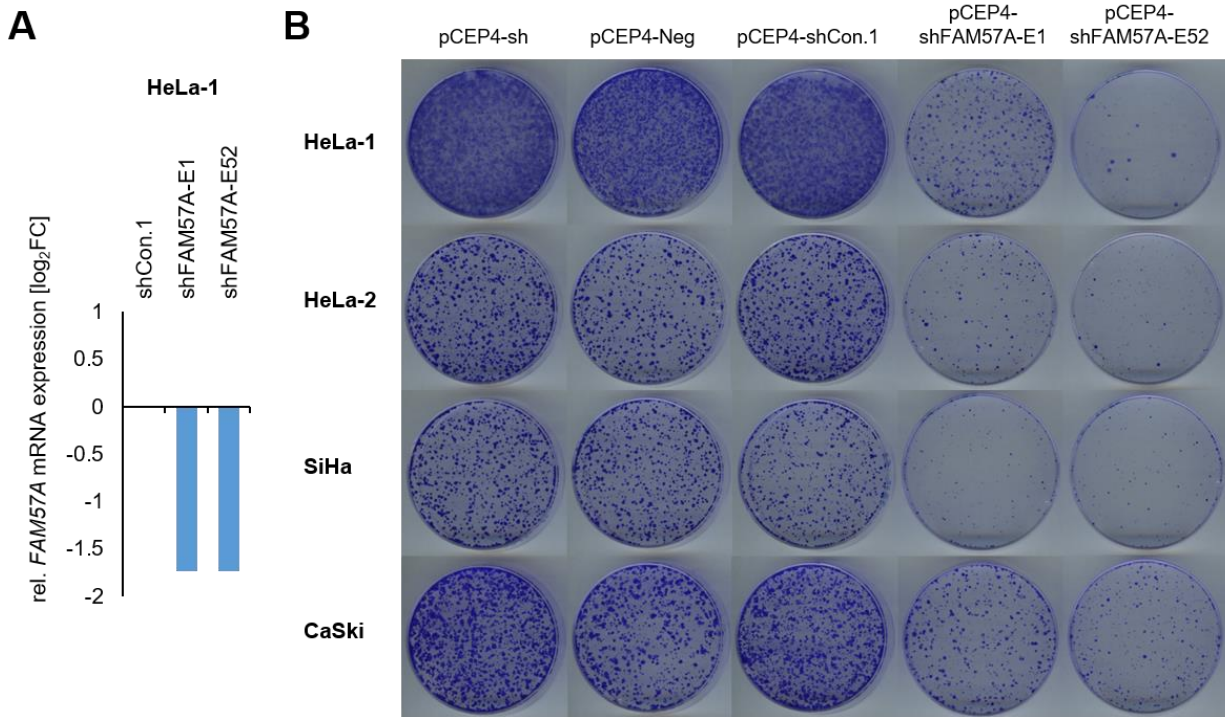


Figure 17. Effects of *FAM57A* silencing on the colony formation capacity of HPV-positive cancer cells. (A) qRT-PCR analyses of *FAM57A* transcript levels upon transfection of HeLa-1 cells with pSUPER plasmids expressing two different *FAM57A*-targeting shRNAs (shFAM57A-E1 or shFAM57A-E52), shCon.1: control shRNA. Shown are the log₂FC of the *FAM57A* levels following *FAM57A* silencing relative to shCon.1-transfected cells (log₂FC=0) from one experiment. (B) CFAs after transfection of the indicated cell lines with pCEP4-shFAM57A-E1 or pCEP4-shFAM57A-E52, or with three different control plasmids, pCEP4-sh, pCEP4-Neg or pCEP4-shCon.1.

Additionally, the short-term effects of *FAM57A* silencing on cell proliferation were examined by live cell imaging analyses using the IncuCyte® S3 Live-Cell Analysis System. *FAM57A* knockdown was performed by employing a pool of two different siRNAs (siFAM57A-E1, siFAM57A-E52) that contain the same target sequences as the corresponding shRNAs used in the CFAs (Figure 17). The efficiency of the *FAM57A*-targeting siRNA pool (siFAM57A-E1/E52) was validated in HPV-positive cells at the transcript (Figure 18A) and protein (Figure 18B) level. For their detection in the IncuCyte system, HPV-positive cancer cells were labelled with the red fluorescent protein, mKate2. Compared to control siRNA-transfected cells, the proliferation rate of cervical cancer cells transfected with the *FAM57A*-targeting siRNA pool was reduced (Figure 18C). This inhibitory effect can be further increased by repeated transfection of the *FAM57A*-targeting siRNAs (Karin Hoppe-Seyler, personal communication). As a further control, HPV *E6/E7*-silencing siRNAs were applied, which rapidly induce senescence and thus a stable and highly efficient proliferation block in cervical cancer cells.

Collectively, these results show that short-term inhibition of *FAM57A* expression in live cell imaging analyses and long-term inhibition of *FAM57A* expression in CFAs result in anti-proliferative effects in cervical cancer cells. These findings indicate that *FAM57A* supports the proliferation of cervical cancer cells.

7.2.2 *FAM57A* promotes the migration of HPV-positive cancer cells

The reported localization of *FAM57A* in the cell plasma membrane (He *et al.* 2002) and the strong inhibition of *FAM57A* expression under high cell density may provide a hint that *FAM57A* could be involved in cell-cell contacts, cell adhesion and/or migration and invasion. Therefore, a possible role of *FAM57A* in the process of cell migration was evaluated in wound healing assays, by applying the IncuCyte system.

mKate2-labelled cells were transfected with siRNA and then seeded into a 96-well plate. The cells were treated with mitomycin C before scratching. Mitomycin C is an antibiotic that inhibits DNA synthesis and thus is widely used to eliminate the “false positive” migration effects elicited by cell proliferation (Vang Mouritzen and Jenssen 2018). To allow exact comparisons between different wells, scratches were introduced with the standardized Incucyte® Woundmaker Tool, which generates precise and uniform cell free zones in the 96 wells. The migration capacity was evaluated by measuring the width of wound through the IncuCyte system. In parallel, total cell counts were also determined to exclude confounding effects caused by cell proliferation.

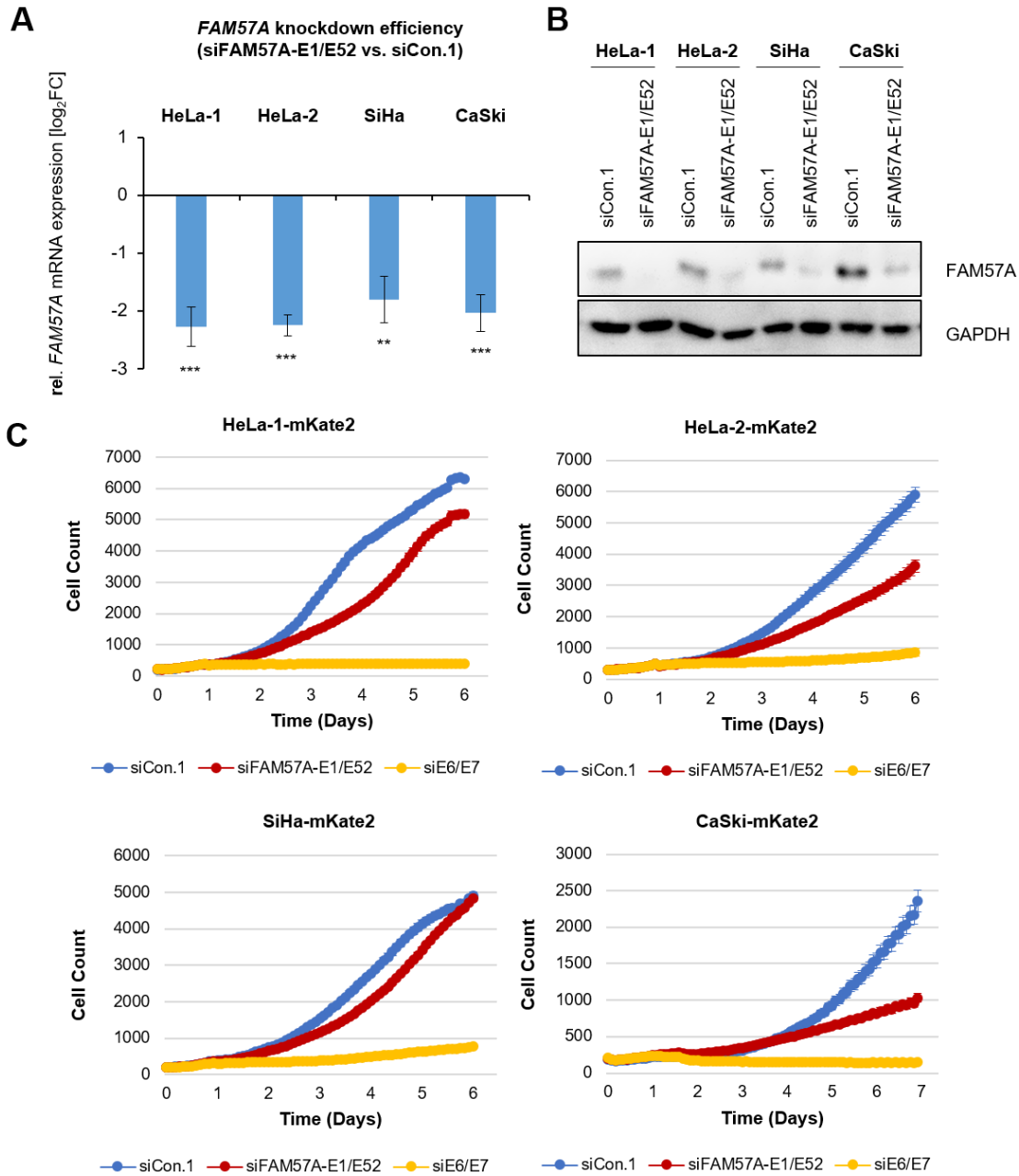


Figure 18. Live cell imaging analyses of HPV-positive cancer cell growth following *FAM57A* silencing. (A) Validation of pooled *FAM57A*-targeting siRNAs (siFAM57A-E1/E52) in different HPV-positive cancer cell lines at the transcript level by qRT-PCR. siCon.1: control siRNA. Shown are the \log_2FC values of mean *FAM57A* expression levels of siFAM57A-E1/E52-transfected cells relative to siCon.1-transfected cells ($\log_2FC=0$) with standard deviations from at least 3 independent experiments (HeLa-1, HeLa-2, SiHa: $n=3$, CaSki: $n=4$). Statistically significant differences to the respective siCon.1-transfected cells are determined by one-way ANOVA, **: $P < 0.01$, ***: $P < 0.001$. (B) Corresponding analyses on the protein level by immunoblot. GAPDH: loading control. (C) Growth curves of mKate2-labelled HPV-positive cancer cells in live cell imaging analyses employing the IncuCyte system. Cells were transfected with either control siRNA siCon.1 (blue curves), the *FAM57A*-targeting siRNA pool siFAM57A-E1/E52 (red curves) or siE6/E7 (yellow curves), which represents a pool of 3 different siRNAs blocking *E6/E7* expression (Hoppe-Seyler *et al.* 2021).

Interestingly, *FAM57A* silencing in SiHa-mKate2 cells inhibited cell migration, as indicated by the larger width of wound after 48 h (Figure 19A and 19B). Similarly, HeLa-1-mKate2 cells also migrated more slowly following *FAM57A* knockdown, an effect which was already visible 8 h after scratching (Figure 19A and 19B). The determination in parallel of cell numbers indicates that the proliferation of both SiHa-mKate2 and HeLa-1-mKate2 cells was almost completely blocked during the experiments (Figure 19A).

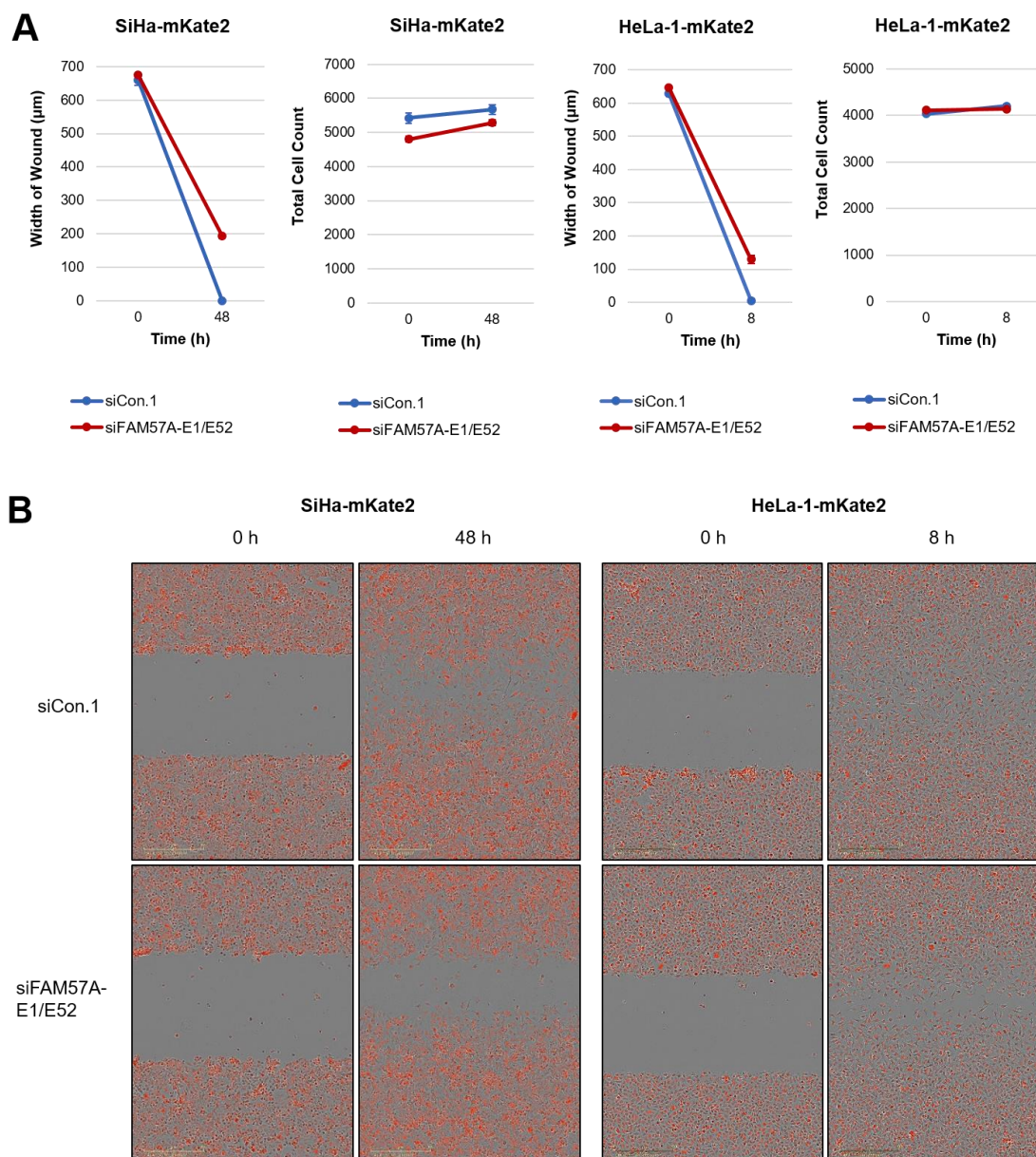


Figure 19. Effects of *FAM57A* on the migration of cervical cancer cells. Wound healing assays were performed after *FAM57A* silencing by siRNA. The IncuCyte® live-cell analysis system was employed for image acquirement and statistical analyses were performed by using the software provided by the supplier. Cells were seeded in octuplicates and treated with 5 μg/mL mitomycin C for 3 h before scratching. (A) Calculations of wound widths and total cell counts. (B) Images of the “wounds” after scratching (0 h) and after 48 h (SiHa-mKate2) or 8 h (HeLa-1-mKate2). siCon.1: control siRNA, siFAM57A-E1/E52: a pool of 2 siRNAs silencing *FAM57A*.

7. Results

As seen for HeLa-1-mKate2 cells, the migration capacity of HeLa-2-mKate2 cells (derived from HeLa cell variant 2) were also inhibited by *FAM57A* silencing (Figure 20A). Interestingly, however, contrary to the mesenchymal cell-like motility of HeLa-1-mKate2 cells, HeLa-2-mKate2 cells moved more collectively and the cells at the front edge of a cell sheet formed lamellipodia-like structures at the leading edge (Figure 20B, arrows). Upon *FAM57A* silencing, these lamellipodia-like structures as well as the cell-cell contacts of the leader cells were partly lost (Figure 20B, triangle).

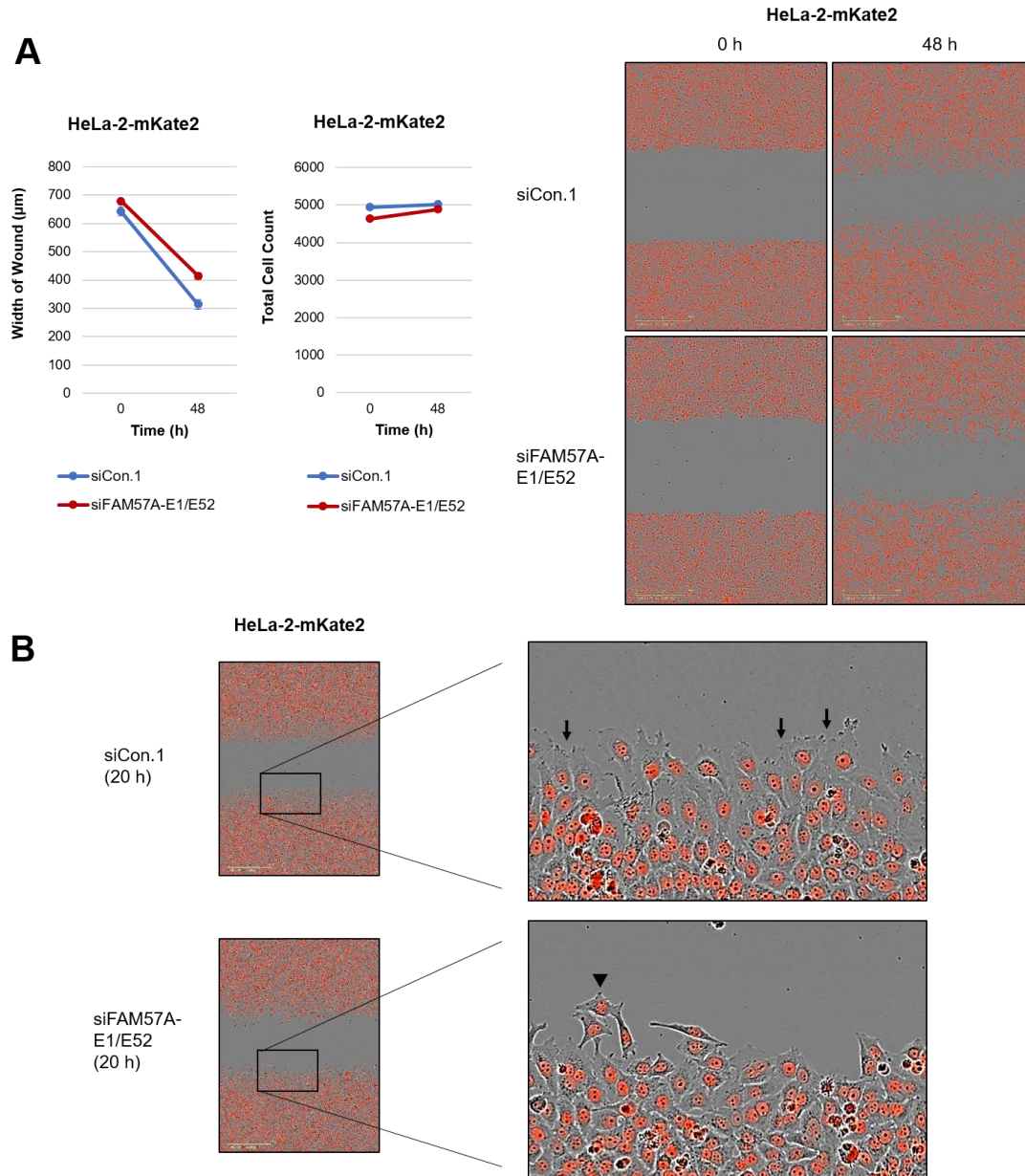


Figure 20. Effects of *FAM57A* on the migration and morphology of HeLa-2-mKate2 cells. (A) Wound healing assays were performed for 48 h, as further described in Figure 19. (B) Morphology of cells in the front edge 20 h after scratching. Arrows: lamellipodia-like structures at the leading edge and cell-cell contacts between leader cells in siCon.1-transfected cells (upper panel). Triangle: the cells partly lost the lamellipodia-like structures and cell-cell contacts following *FAM57A* silencing with siFAM57A-E1/E52 (lower panel).

7.3 Potential factors mediating FAM57A functions

7.3.1 SLC3A2 and FAM57A

7.3.1.1 FAM57A and SLC3A2 can interact with each other in cervical cancer cells

The reported interaction between FAM57A and SLC3A2 (please refer to chapter 5.4) in co-IP assays (He *et al.* 2002) raises the possibility that SLC3A2 could mediate FAM57A activities. In order to investigate whether the FAM57A-SLC3A2 interaction can indeed take place in cervical cancer cells, the CheckMate™ Mammalian Two-Hybrid System was applied. This method is basically a mammalian adaption of the more widely used Yeast Two-Hybrid system. In brief, two proteins are expressed from co-transfected expression vectors, one linked to a DNA-binding domain (here GAL4 in plasmid pBIND2), the other linked to a transcriptional activation domain (here VP16 in plasmid pACT2) (Stutz *et al.* 2015). If an interaction between the two factors takes place, this leads to the transcriptional stimulation of a co-transfected luciferase reporter plasmid carrying GAL4 recognition sites (for more technical details, please refer to chapter 6.2.6)

Notably, the co-expression of GAL4-FAM57A with VP16-SLC3A2 (pBIND2-FAM57A and pACT2-SLC3A2) in HeLa-1 cells led to a significant upregulation of luciferase activities, when compared to the co-expression of GAL4-FAM57A with VP16 only (pBIND2-FAM57A and pACT2) (Figure 21A). This supports the idea that FAM57A and SLC3A2 can interact *in vivo*. The *vice versa* experiment, in which SLC3A2 was linked to GAL4 and FAM57A to VP16 (pBIND2-SLC3A2 and pACT2-FAM57A), however, did not lead to the activation of the luciferase reporter, compared to the respective control (pBIND2-SLC3A2 and pACT2) (Figure 21A). This latter result may be explained, for example, by structural alterations of one binding partner due to its linkage to the GAL4 or VP16 fragment. Another possible scenario could be that the GAL4-SLC3A2 fusion protein can activate the luciferase reporter alone, which would not be further enhanced by the interaction with VP16-FAM57A.

In addition, the relation between FAM57A and SLC3A2 protein expression was analyzed in RNAi experiments. They revealed that neither SLC3A2 protein levels were affected upon *FAM57A* knockdown (Figure 21B) nor FAM57A protein levels upon *SLC3A2* knockdown (Figure 21C). Thus, although experimental evidence was obtained that an interaction between FAM57A and SLC3A2 can take place in cervical cancer cells, this does not result in changes of their expression levels.

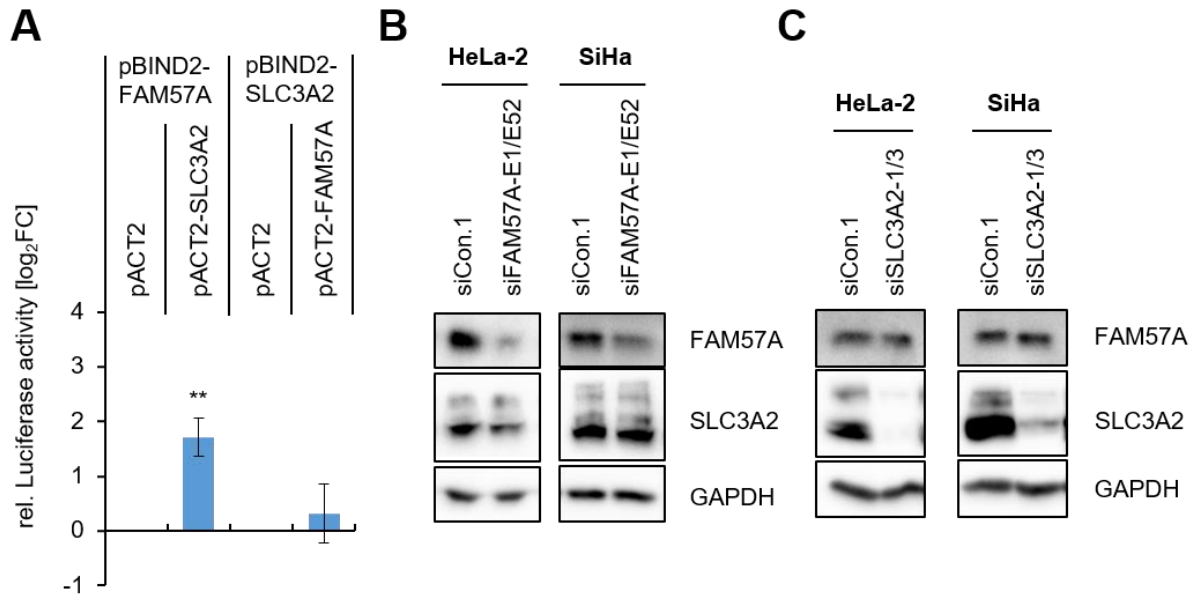


Figure 21. Interaction between FAM57A and SLC3A2. (A) CheckMate™ Mammalian Two-Hybrid analyses of the interaction between FAM57A and SLC3A2 in HeLa-1 cells. Indicated are relative luciferase activities upon co-transfection of pBIND2-FAM57A and pACT2-SLC3A2 or of pBIND2-SLC3A2 and pACT2-FAM57A above those of a co-transfected pACT2 vector. pACT2: VP16-expressing vector, used for normalization; pACT2-FAM57A, pACT2-SLC3A2: plasmids to generate VP16-FAM57A and VP16-SLC3A2 fusion proteins, respectively; pBIND2-FAM57A, pBIND2-SLC3A2: plasmids for producing GAL4-FAM57A and GAL4-SLC3A2 fusion proteins, respectively. Depicted are the \log_2 FC of mean values relative to the respective pACT2 co-transfection (\log_2 FC=0) with standard deviations from 3 independent experiments. Statistically significant differences are determined by one-way ANOVA, **: $P < 0.01$. (B) Immunoblot analyses of SLC3A2 protein levels after blocking *FAM57A* expression by RNAi (siFAM57A-E1/E52) in HeLa-2 and SiHa cells. (C) Immunoblot analyses of FAM57A protein levels after silencing *SLC3A2* (siSLC3A2-1/3, described in chapter 7.3.1.2) expression by RNAi in HeLa-2 and SiHa cells. (B-C): siCon.1: control siRNA, GAPDH: loading control.

7.3.1.2 SLC3A2 can stimulate the proliferation of cervical cancer cells

SLC3A2 plays an important role for the cellular metabolism as an auxiliary subunit of several amino acid transporters (Cano-Crespo *et al.* 2019; Liu *et al.* 2020; Yan *et al.* 2019), and may also affect cell adhesion and migration by modulating integrin signaling (Feral *et al.* 2005; Prager *et al.* 2007). In order to test possible effects of SLC3A2 on the proliferation of cervical cancer cells, CFAs and live cell imaging analyses were performed in a spectrum of cervical cancer cell lines, following *SLC3A2* repression by RNAi. The efficiencies of three different shRNAs were tested at the protein level by transfecting HeLa-1 cells (Figure 22A). Plasmids coding for shSLC3A2-1 and shSLC3A2-3, which showed the most pronounced *SLC3A2* knockdown (Figure 22A), were utilized for interfering with *SLC3A2* expression in CFAs (Figure 22B). In HeLa-2 and CaSki cell lines, silencing *SLC3A2* by either shRNA inhibited the capacity of colony formation, however, HeLa-1 and, to some extent, SiHa cells exhibited differential responses

(Figure 22B). In specific, whereas both shRNAs show a comparable inhibition of *SLC3A2* expression (Figure 22A), the anti-proliferative effects of shSLC3A2-1 were less pronounced in SiHa and, most notably, in HeLa-1 cells (Figure 22B). For live cell imaging analyses, *SLC3A2* was silenced by employing a siRNA pool (siSLC3A2-1/3) composed of siSLC3A2-1 and siSLC3A2-3 which target the same sequences as the corresponding shRNAs used in the CFAs (Figure 22). As shown in Figure 23A, the growth of SiHa-mKate2 and CaSki-mKate2 cells was inhibited following *SLC3A2* knockdown compared to control siRNA-transfected cells, whereas the proliferation of both mKate2-labelled HeLa variants (HeLa-1-mKate2 and HeLa-2-mKate2) was not influenced. Accompanying qRT-PCR analyses indicate that the knockdown efficiency of the siSLC3A2s pool was comparable in the analyzed cells (Figure 23B).

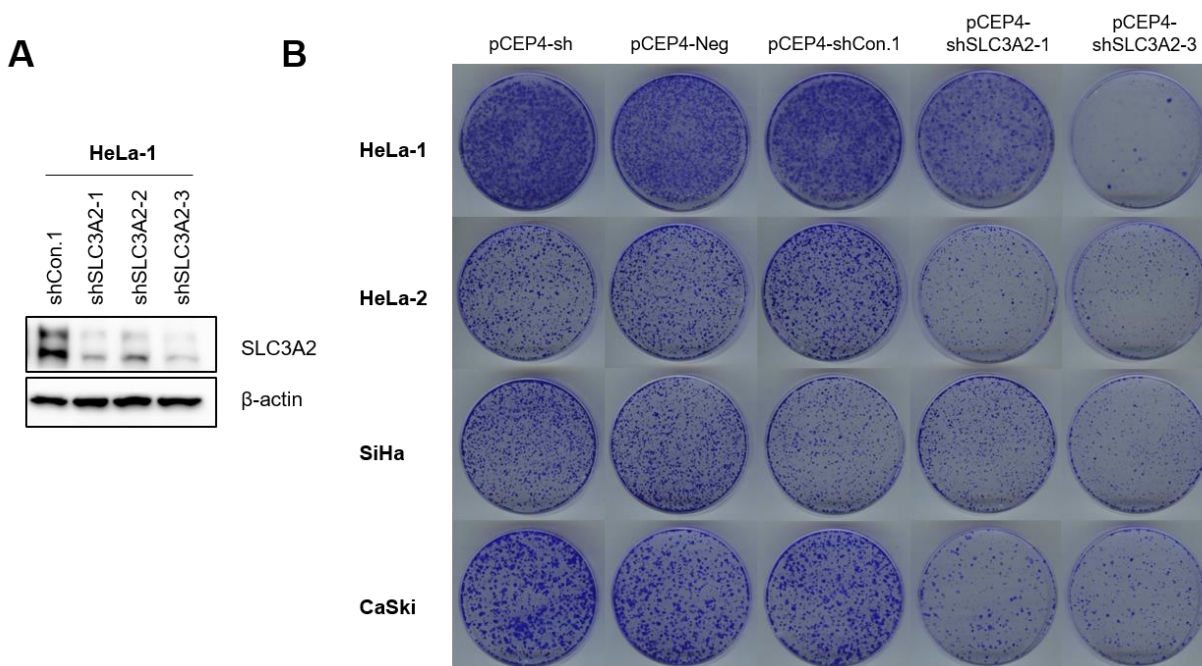


Figure 22. Effects of *SLC3A2* suppression on the colony formation capacity of HPV-positive cancer cells. (A) Efficiencies of shRNAs silencing *SLC3A2*, as assessed by immunoblot analyses. shCon.1: control shRNA, β-actin: loading control. (B) CFAs upon shRNA-induced *SLC3A2* downregulation. pCEP4-sh, pCEP4-Neg, pCEP4-shCon.1: control plasmids.

Collectively, these results indicate that *SLC3A2* can indeed interact with *FAM57A* at the intracellular level. This interaction does not affect the expression levels of either binding partner. In addition, *SLC3A2* silencing can exert anti-proliferative activities in cervical cancer cells. However, in contrast to the growth inhibition following *FAM57A* knockdown, which was consistently seen in all cell lines and under different experimental conditions, the anti-proliferative effects of *SLC3A2* silencing showed some cell type-dependency and also exhibited some variation between long-term inhibition by shRNAs in CFAs and

7. Results

short-term inhibition by siRNAs in live cell imaging. Thus, there appears to be not a straightforward connection between FAM57A and SLC3A2 in terms of the anti-proliferative effects of FAM57A.

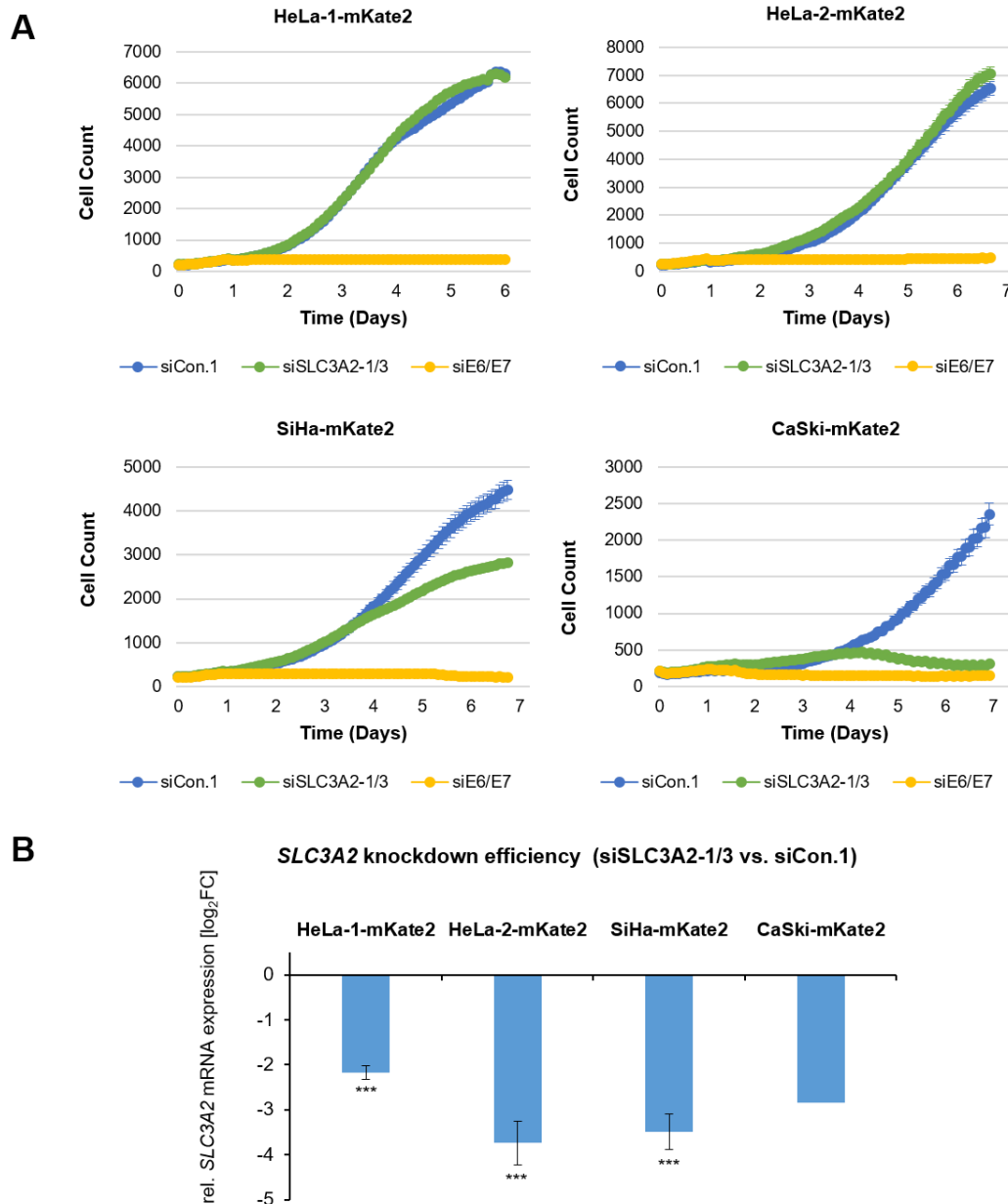


Figure 23. Effects of *SLC3A2* suppression on the growth of HPV-positive cancer cells in live cell imaging analyses. (A) Growth curves of HPV-positive cancer cells measured by employing the IncuCyte system upon silencing of *SLC3A2* expression by siSLC3A2-1/3 (green curves) and *E6/E7* expression by siE6/E7 (yellow curves). siCon.1: control siRNA (blue curves). (B) qRT-PCR analyses measuring the efficacy of *SLC3A2* knockdown through siSLC3A2-1/3 in different mKate2-labelled HPV-positive cell lines used for live cell imaging. Depicted are the \log_2FC of mean expression levels following *SLC3A2* repression relative to siCon.1 transfection ($\log_2FC=0$) with standard deviations from several independent experiments (HeLa-1-mKate2: n=3, HeLa-2-mKate2: n=5, SiHa-mKate2: n=4) or of the relative *SLC3A2* expression of siSLC3A2-1/3-transfected CaSki-mKate2 cells compared to siCon.1 from one experiment. Statistically significant differences to the respective siCon.1-transfected cells are determined by one-way ANOVA, ***: $P < 0.001$.

7.3.2 FAM57A may be an upstream regulator of YAP/TAZ signaling

Since the present work uncovered a link of FAM57A protein expression to cell density, a condition which alters cell-cell contacts and cell-ECM (extracellular matrix) contacts, the question arose whether FAM57A is connected to YAP/TAZ signaling. This pathway can sense the cellular structure, shape and polarity as well as respond to extracellular mechanical signals including cell-cell contacts and cell adhesion (Totaro *et al.* 2018) (please also refer to chapter 5.2.4).

7.3.2.1 YAP/TAZ signaling is downregulated under HD conditions

To assess the effects of cell density on the YAP/TAZ cascade, the protein levels of phosphorylated (p-)YAP (Ser127), total YAP (YAP), TAZ and TEAD1 were measured in different cervical cancer cell lines as well as in HaCaT cells, following plating at different cell densities. Immunoblots revealed that p-YAP, YAP, TAZ, TEAD1 all showed higher expression levels at LD compared to HD (Figure 24). This parallels the regulation of FAM57A expression (Figure 24), raising the possibility that FAM57A is connected to YAP/TAZ signaling, either acting upstream or being a downstream target.

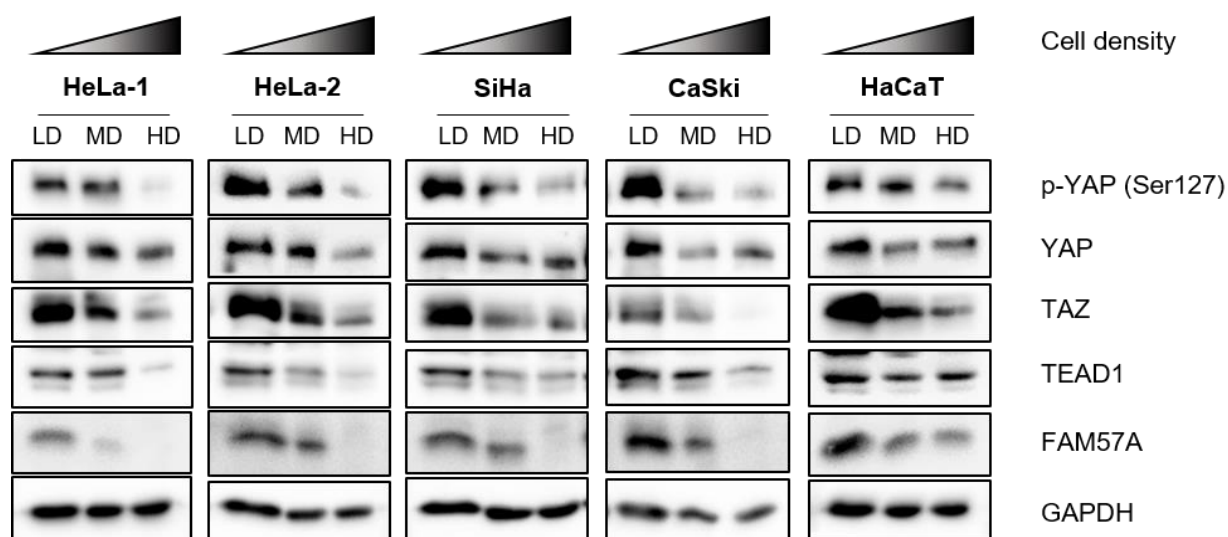


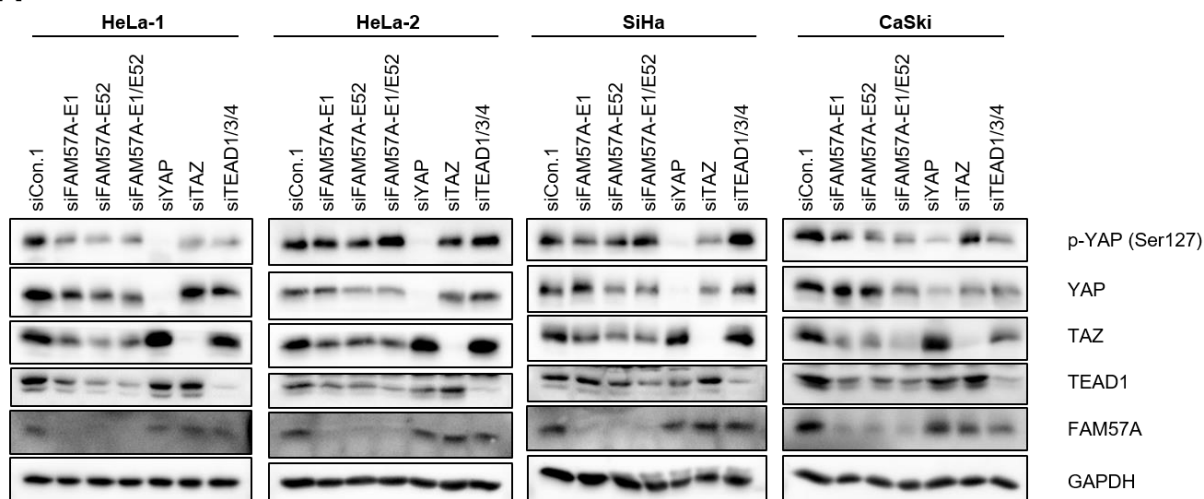
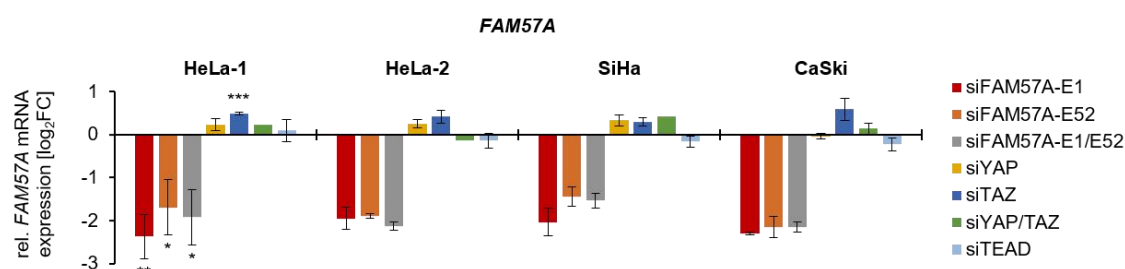
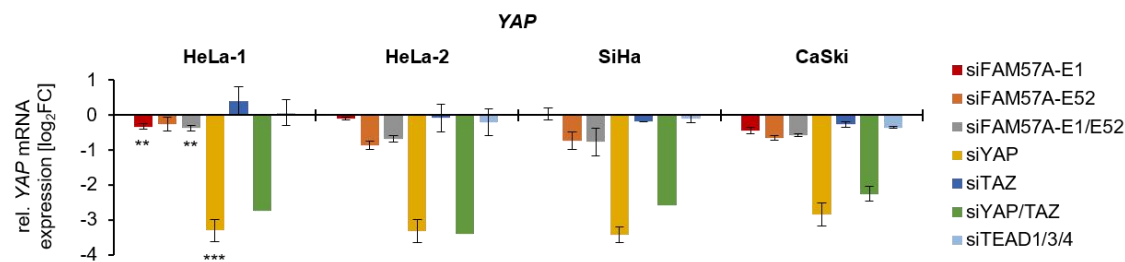
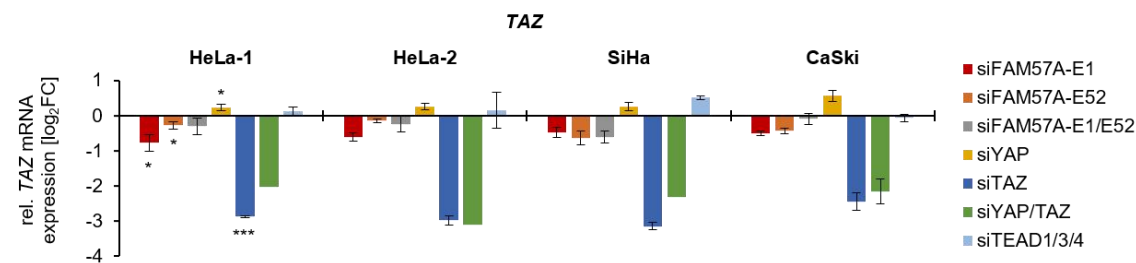
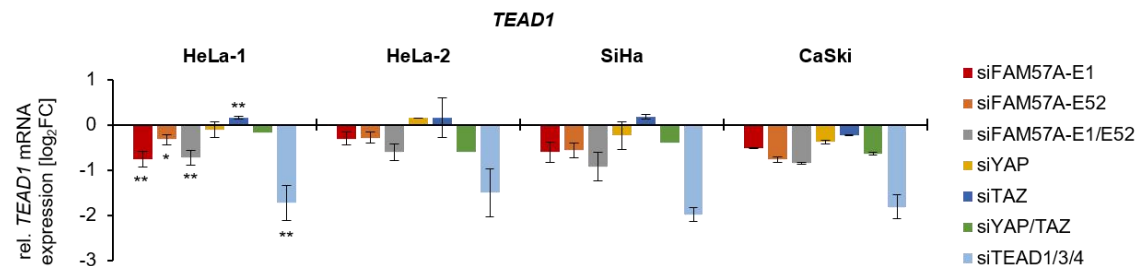
Figure 24. Cell density-dependent expression of key factors of YAP/TAZ signaling. Immunoblot analysis of the protein levels of phosphorylated YAP (Ser127), total YAP, TAZ and TEAD1 in HPV-positive and HPV-negative cells seeded at LD, MD and HD. In addition, FAM57A levels are shown. GAPDH: loading control.

7.3.2.2 *The expression levels of key factors of YAP/TAZ signaling are downregulated following FAM57A silencing*

To investigate whether FAM57A acts upstream or downstream of YAP/TAZ signaling, *FAM57A* was silenced in different cervical cancer cell lines by applying two siRNAs individually (siFAM57A-E1, siFAM57A-E52) or as a pool (siFAM57A-E1/E52). Also, siRNAs blocking expression of *YAP* (siYAP), *TAZ* (siTAZ) and *TEAD1*, 3 and 4 (siTEAD1/3/4) were introduced into the cells (Figure 25). The knockdown efficiencies of these siRNAs were validated both at the protein (Figure 25A) and transcript (Figure 25B-E) level.

Interestingly, immunoblot analyses revealed that *FAM57A* silencing consistently downregulated TAZ protein levels in all investigated cell lines (Figure 25A). TEAD1 levels were also downregulated in HeLa-1, HeLa-2 and CaSki cells upon *FAM57A* silencing. In addition, to some cell type-dependent extent, YAP levels also displayed a tendency to be downregulated upon *FAM57A* silencing (Figure 25A). On the other hand, silencing of *YAP*, *TAZ* or *TEAD1/3/4* expression did not appreciably modulate FAM57A expression in all investigated cell lines. Collectively, these results indicate that FAM57A repression is linked to a reduced expression of YAP/TAZ signaling factors, most prominently and consistently TAZ, raising the possibility that FAM57A may act as an upstream regulator of YAP/TAZ signaling. This issue awaits further experimental exploration, which is ongoing in the laboratory. In contrast, the observation that neither *YAP*, *TAZ* nor *TEAD1/3/4* repression affected FAM57A levels, indicates that FAM57A is not a downstream target of YAP/TAZ signaling, at least in regard of the regulation of FAM57A expression levels.

At the transcript level, *FAM57A* silencing in general reduced the mRNA levels of *YAP*, *TAZ* and *TEAD1*, but only to relatively modest extent (not more than 2-fold) (Figure 25C-E). Further, silencing of *YAP*, *TAZ* or *TEAD1/3/4* did not considerably affect *FAM57A* transcript amounts (Figure 25B).

A**B****C****D****E**

7. Results

Figure 25 (previous page). **Relation between FAM57A and YAP/TAZ signaling factors.** (A) Representative immunoblots of p-YAP (Ser127), YAP, TAZ, TEAD1 and FAM57A upon introducing the indicated siRNAs into different cervical cancer cell lines. GAPDH: loading control. (B-E) Corresponding analyses on the transcript level by qRT-PCR. Indicated are the \log_2FC of mean expression levels relative to siCon.1 ($\log_2FC=0$) with standard deviations from 2-3 independent experiments (HeLa-1: n=3, HeLa-2, SiHa, CaSki: n=2) or of data from a single experiment (double knockdown of YAP and TAZ - siYAP/TAZ - in HeLa-1, HeLa-2 and SiHa cells: n=1). Asterisks show statistically significant differences in HeLa-1 cells compared to control siRNA (siCon.1) as determined by one-way ANOVA. *: $P < 0.05$, **: $P < 0.01$, ***: $P < 0.001$.

7.3.2.3 FAM57A may activate the transcription of target genes for YAP/TAZ

Considering that YAP and TAZ as transcriptional co-activators exert their functions by binding to TEAD, which consequently leads to the transcriptional activation of specific genes, two well-established target genes for YAP/TAZ, *CYR61* (cysteine rich angiogenic inducer 61) and *CTGF* (connective tissue growth factor) (Pavel *et al.* 2018), were investigated.

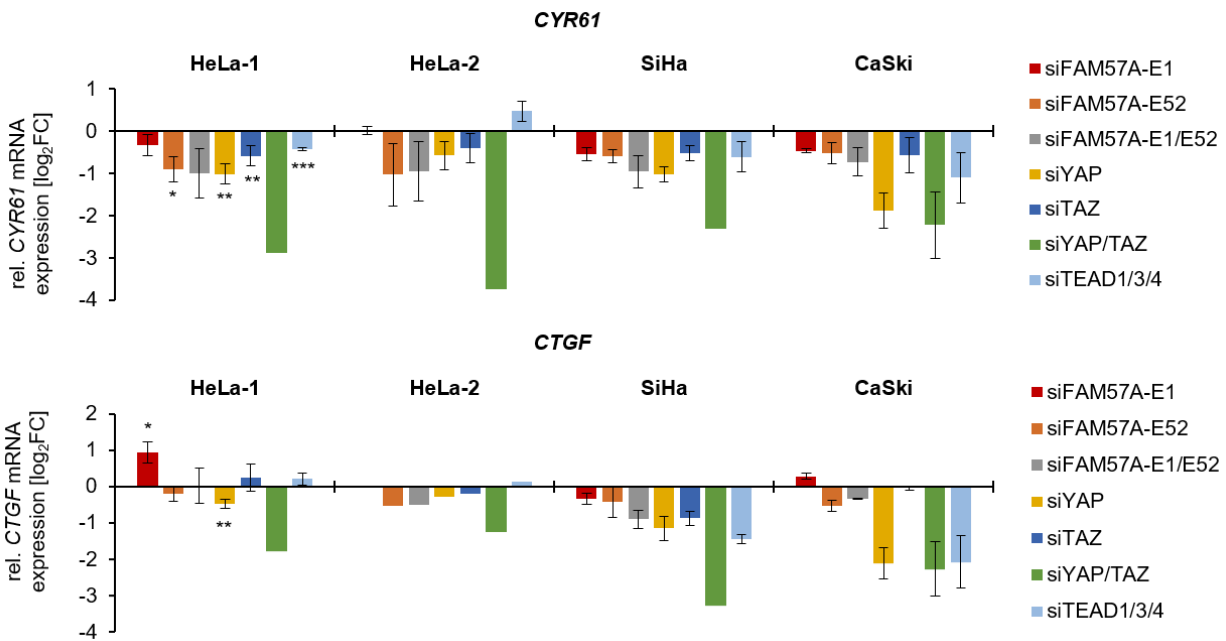


Figure 26. *CYR61* and *CTGF* mRNA levels following FAM57A or YAP/TAZ silencing. Indicated are the results of qRT-PCR analyses of the relative transcript levels of *CYR61* and *CTGF* following silencing of *FAM57A*, *YAP*, *TAZ* and *TEAD1/3/4* expression. Upper panels: relative *CYR61* transcript levels, shown are the \log_2FC of mean expression levels relative to siCon.1 ($\log_2FC=0$) with standard deviations from 2-3 independent experiments (HeLa-1: n=3, HeLa-2, SiHa, CaSki: n=2) or of data from a single experiment (double knockdown of YAP and TAZ - siYAP/TAZ - in HeLa-1, HeLa-2 and SiHa cells: n=1). Lower panels: relative *CTGF* transcript levels, shown are the \log_2FC of mean expression levels relative to siCon.1 ($\log_2FC=0$) with standard deviations from 2-3 independent experiments (HeLa-1: n=3, SiHa, CaSki: n=2) or of data from a single experiment (HeLa-2: n=1; siYAP/TAZ in HeLa-1, SiHa cells: n=1). Statistically significant differences in HeLa-1 cells compared to control siRNA (siCon.1) are determined by one-way ANOVA. *: $P < 0.05$, **: $P < 0.01$, ***: $P < 0.001$.

The mRNA levels of *CYR61* and *CTGF* were strongly reduced in all investigated cervical cancer cell lines by the double knockdown of *YAP* and *TAZ* (siYAP/TAZ), corroborating that these genes are downstream targets for YAP/TAZ signaling. *CYR61* transcript levels were downregulated by the *FAM57A*-targeting siRNA pool (siFAM57A-E1/E52) by 38-56 % (Figure 26, upper panels). There was also some tendency that *CTGF* transcript levels were decreased upon *FAM57A* silencing, however, this effect varied between cell lines and also between the different siRNA constructs (Figure 26, lower panels). Although these preliminary experiments warrant further exploration, they point at the possibility that not only the protein levels of YAP, TAZ and TEAD1 are influenced by FAM57A (Figure 25A), but possibly also the expression of downstream target genes of YAP/TAZ signaling.

Taken together, this part of my thesis provides a first indication that FAM57A expression and YAP/TAZ signaling could be functionally connected, in that FAM57A may act as an upstream activator of YAP/TAZ signaling. This finding is particularly interesting in the light that both FAM57A expression (this work) and YAP/TAZ signaling (Gumbiner and Kim 2014; Mason *et al.* 2019) are linked to cell density and cell migration. Future work is planned in the laboratory to explore this intriguing possibility in more depth.

8. Discussion

As main results, this thesis provides first insights into the regulation of FAM57A expression and the biological function of FAM57A in cervical cancer cells. It reveals that FAM57A expression is strongly dependent on cell density, being mainly regulated at the protein level. Moreover, FAM57A is a key factor for promoting cervical cancer cell proliferation and migration. Collectively, these findings identify a novel cellular factor which contributes to the malignant phenotype of cervical cancer cells. Moreover, in view of its growth- and migration-promoting activities, FAM57A may represent a novel therapeutic target in cervical cancer cells.

8.1 Regulation of FAM57A expression

In the present work, cell density is identified as a key regulator of FAM57A expression, since the protein is readily detectable in cervical cancer cells cultivated at low cell density while its expression is virtually abolished at high cell density. This cell density-dependent regulation of FAM57A is found to occur predominantly at the protein level, since *FAM57A* transcript levels are only marginally affected in cells cultivated at different cell densities. My analyses further indicate that FAM57A is a rather stable protein in cervical cancer cells, with a half-life of at least 24 h. Future studies are warranted to investigate in more detail the mechanisms of controlling the cell density-dependent FAM57A stability, which - among other possibilities - could include the analyses of proteasomal and lysosomal degradation pathways (Ciechanover 2005), of caspases (Julien and Wells 2017), of Ca^{2+} -dependent cysteine proteases calpains (Franco and Huttenlocher 2005; Goll *et al.* 2003) and of intramembrane proteolysis which can cleave membrane protein (Avci and Lemberg 2015; Kuhnle *et al.* 2019). Notably, the observed upregulation of FAM57A protein levels in a relatively short period (6 h) after splitting confluent cells suggests that the cell density-dependent FAM57A expression is rapidly induced and may be modulated by cell-cell contacts, which are reduced in freshly split cells.

The cell density-dependent regulation of FAM57A is also likely the main explanation for the observation that FAM57A levels are strongly upregulated in a proteome analysis comparing hypoxic with normoxic cervical cancer cells (Bossler *et al.* 2019b). In this scenario, the anti-proliferative effects of hypoxia in cervical cancer cells (Hoppe-Seyler *et al.* 2017a) result in decreased cell density, when compared to cells which continue to proliferate under normoxia. In line with this notion, when I analyzed cervical cancer cells plated at different cell densities and cultivated under either normoxia or hypoxia, FAM57A expression was closely linked to differences in cell density and only weakly affected by the differences in oxygen supply. My results further indicate that the latter, minor effect is linked to HIF-1 α -mediated transcriptional induction

of *FAM57A* expression, as it could be counteracted by RNAi-mediated *HIF1A* repression. Consistent with this interpretation, potential hypoxia-responsive elements are present in the *FAM57A* promoter region.

The strong dependence of *FAM57A* levels on cell density would predict that other anti-proliferative signals should also result in an upregulation of *FAM57A* protein levels. Indeed, I found that silencing expression of the strongly pro-proliferative HPV *E6/E7* oncogenes in cervical cancer cells also profoundly increases *FAM57A* protein levels.

My findings furthermore indicate that care should be taken in the interpretation of proteome studies aiming at the identification of hypoxia-induced factors, since the expression of cell density-regulated factors other than *FAM57A* could also be increased as a secondary effect of the reduced cell density under hypoxia, leading to the misclassification of such factors as “hypoxia-responsive”. Obviously, this obstacle could also be relevant for examining other pro- or anti-proliferative stimuli by proteome analyses or other comparative methods, and should be controlled, *e. g.* by assessing the effects of cell proliferation on the expression levels of candidate factors.

It is further noteworthy that the cell density-dependent regulation of *FAM57A* expression is not a peculiarity of HPV-positive cancer cells but also observed in HaCaT cells, which are HPV-negative, spontaneously immortalized but non-tumorigenic skin keratinocytes (Boukamp *et al.* 1988). Thus, this regulatory phenomenon appears to be conserved between cells of different histological origin and of different malignant potential.

8.2 Phenotypic effects of *FAM57A* in HPV-positive cancer cells

8.2.1 *FAM57A* promotes the proliferation of HPV-positive cancer cells

At the phenotypic levels, my results uncover that *FAM57A* promotes the proliferation of HPV-positive cancer cells. This is indicated by the anti-proliferative effects of *FAM57A* silencing in both short-term live cell imaging analyses and long-term CFAs (colony formation assays). These results are supported by reports on lung cancer and hepatocellular carcinoma cells, which also suggest a pro-proliferative role for *FAM57A* in these cancer entities (Li *et al.* 2010; Pan *et al.* 2006; Wei *et al.* 2021). In general, I observed that the anti-proliferative effects of *FAM57A* silencing appeared to be more pronounced in CFAs than in the live cell imaging analyses. This could be due to the possibility that - within the shorter time frame of the latter experiments - the relatively high stability of the *FAM57A* protein could lead to an underestimation of the inhibitory effects of RNAi-mediated *FAM57A* silencing.

Which pathways may be linked to the pro-proliferative activity of FAM57A in cervical cancer? My results raise the possibility that FAM57A repression is directly or indirectly linked to the downregulation of factors involved in YAP/TAZ signaling, which is a well-established pro-proliferative pathway in cancer cells (Piccolo *et al.* 2014) (further discussed in chapter 8.2.3). However, this may not be the only growth regulatory pathway affected by FAM57A, since preliminary data from ongoing work (Karin Hoppe-Seyler, personal communication) reveals that FAM57A can also stimulate the PI3K/AKT and MAPK/ERK signaling pathways, as indicated by a downregulation of phosphorylated AKT and phosphorylated ERK levels following silencing of endogenous *FAM57A* expression in cervical cancer cells. This idea is also supported by a report assessing the effects of ectopic FAM57A overexpression in NIH3T3 cells (He *et al.* 2004), which obtained evidence for an increase in the activities of both pathways. In the context of ERK signaling, it is also interesting that *FAM57A* expression has been reported to be transcriptionally stimulated by the c-Myc oncoprotein (Baltaci *et al.* 2015; Baltaci *et al.* 2017), which is stabilized via ERK signaling (Ciccarelli *et al.* 2018; Tsai *et al.* 2012). Thus, it would be interesting to investigate whether there may exist a positive feedback loop between FAM57A expression and MAPK/ERK signaling.

As outlined in chapter 5.2.4, both the PI3K/AKT and MAPK/ERK signaling cascades play a major role during carcinogenesis and have been reported to be hyperactive in cervical cancer cells. My results thus raise the question whether FAM57A could contribute to the stimulation of these potentially pro-oncogenic pathways, particularly in cells under low density conditions. Due to their pro-tumorigenic role, the PI3K/AKT and MAPK/ERK signaling cascades are both considered to represent targets for therapeutic interference. This notion extends also to cervical cancer cells. For example, LY294002, a reversible PI3K inhibitor, has been reported to sensitize HeLa cells towards radiation, and the prototypal compound quercetin, from which the LY294002 was designed, can inhibit the proliferation of HeLa cells as well as arrest or even reverse cervical neoplasia progression in mouse models (Manzo-Merino *et al.* 2014). In addition, a study reported that the MEK inhibitor cobimetinib can inhibit paclitaxel-induced ERK activation *in vitro* and in a xenograft model *in vivo*, suggesting that a combination therapy of cobimetinib and paclitaxel may bear potential for treating cervical cancer (Liu *et al.* 2022). Moreover, a recent study suggests that ERK plays a particularly important role in cervical cancer, as it has been reported to promote cervical carcinogenesis by stimulating HPV *E6/E7* oncogene expression (Luna *et al.* 2021). Thus, if a functional role of FAM57A for the stimulation of PI3K/AKT and MAPK/ERK signaling is further substantiated, this connection may provide a novel therapeutic opportunity, since FAM57A inhibition may interfere with at least two cellular pathways which are considered to be critical for cervical carcinogenesis and the development of many other tumor entities.

Little is known about potential FAM57A interaction partners which could mediate its biological function. One exception is the SLC3A2 protein, a component of amino acid transporters (Digomann *et al.* 2019b),

which has been identified as a FAM57A interaction partner by Yeast Two-Hybrid (Y2H) analyses and co-immunoprecipitation (Co-IP) assays (He *et al.* 2002). Both of these methods, however, have their limitations. The Y2H assay is performed in non-mammalian cells which cannot provide the complete arsenal of posttranslational protein modifications which are found in mammalian cells (Moesslacher *et al.* 2021) and which may influence protein-protein interactions. On the other hand, positive Co-IPs do not prove an intracellular interaction of two binding partners, as the binding may occur *in vitro* in the cellular protein extracts after harvesting. I therefore applied a mammalian two-hybrid assay (CheckMate™ Mammalian Two-Hybrid System) which detects protein-protein interactions intracellularly by transcriptionally activating a co-transfected reporter plasmid. These investigations indicate that FAM57A and SLC3A2 indeed have the potential to interact in cervical cancer cells. However, a limitation of the mammalian two-hybrid system is that both interaction partners are targeted to the nucleus to enable the transcriptional activation of the luciferase reporter. Thus, it cannot be excluded that the two factors still do not naturally interact, because they may physiologically localize to different cellular compartments. This issue could be addressed by co-localization studies, once a reliable anti-FAM57A antibody is available, which is suitable for immunofluorescence or immunohistochemistry analyses.

In my experiments, I did not detect an interdependency between SLC3A2 and FAM57A expression levels, since neither silencing of *SLC3A2* expression affected FAM57A levels, nor did the silencing of *FAM57A* expression affect SLC3A2 levels. Notably, however, I found that *SLC3A2* silencing can also exert anti-proliferative effects in cervical cancer cells. Yet, whereas *FAM57A* silencing inhibits cell proliferation in all tested cell lines, the anti-proliferative effect of *SLC3A2* silencing was cell line-dependent and showed more variations under different experimental conditions. Although these findings do not formally exclude that SLC3A2 may be linked to the growth promoting effects of FAM57A under certain conditions, this connection appears to be not straightforward.

Based on my observation that SLC3A2 can be critical for cervical cancer cell proliferation, it should be interesting to gain more insights into the significance of this factor in cervical cancer. Notably, SLC3A2 is increasingly gaining clinical importance in other cancer entities, such as head and neck squamous cell carcinoma (HNSCC), where SLC3A2 has been identified in several studies as a prognostic biomarker for radiotherapy and chemoradiotherapy (Liang and Sun 2021; Linge *et al.* 2016a; Linge *et al.* 2016b; Linge *et al.* 2016c; Lock *et al.* 2022; van der Heijden *et al.* 2019). In HNSCC cells, the overexpression of SLC3A2 increases amino acid metabolism and downregulates autophagy (Digomann *et al.* 2019a). SLC3A2 can also stabilize the GLUT1 protein, thereby increasing cellular glucose uptake (Ohno *et al.* 2011), and form the system xc⁻ - a cystine/glutamate antiporter - with SLC7A11. This antiporter is a critical molecule for cystine uptake and intracellular GSH synthesis, thus decreasing ROS level and promoting cell proliferation (Liu *et al.* 2020). Moreover, SLC3A2 can activate the PI3K/AKT and mTOR pathways to support cell

proliferation (Digomann *et al.* 2019a; Wu *et al.* 2022; Zhu *et al.* 2017) and the anti-proliferative effect resulting from SLC3A2 silencing in HNSCC cells has been closely linked to the repression of mTOR signaling (Digomann *et al.* 2019a). Thus, it should be interesting to analyze the role of these pathways for the pro-proliferative activity of SLC3A2 in cervical cancer cells. Moreover, in view of the proposed key significance of mTOR inhibition for the anti-proliferative effects of *SLC3A2* silencing (Digomann *et al.* 2019a), it will be also interesting to study whether its interaction partner FAM57A may also act growth-inhibitory through interference with the mTOR pathway. This could be assessed, for example, by measuring the levels of markers for active mTOR signaling following *FAM57A* silencing, such as the phosphorylation of p70S6 Kinase 1 (S6K1) or eIF4E Binding Protein (4E-BP1) (Saxton and Sabatini 2017).

8.2.2 *FAM57A promotes the migration of HPV-positive cancer cells*

Migration is an important step of tumor progression by preceding invasion and metastasis of cancer cells. In my studies, I found that FAM57A not only promotes the proliferation of cervical cancer cells, but also supports their migration capacity in wound healing assays. Live cell imaging analyses further revealed that the inhibitory effect of *FAM57A* silencing on cell migration was associated with distinct morphological changes of the cell, which were particularly obvious in the front edge of HeLa-2-mKate2 cells. In specific, in HeLa-2-mKate2 cells expressing FAM57A, the leader cells move orderly and collectively along a front-to-rear axis perpendicular to the wound. These cells contact each other and the contact-free edge forms protrusion structures, which possibly direct the collective migration of the cell sheet (Capuana *et al.* 2020). However, upon *FAM57A* silencing, cell-cell contacts are partly lost, as are the protrusion structures at the leading edge. These results form the basis for future studies which have been started in the laboratory, aiming to gain further insights into the possible link between cell-cell contacts and FAM57A protein levels. In addition, the effects of FAM57A on cell invasion will be assessed, *e. g.* by performing Transwell assays (Justus *et al.* 2014).

Migration relies on changes of the actin cytoskeleton. Its polarized assembly is dependent on the polymerization and depolymerization of actin filaments (Heckman and Plummer 2013). The actin cytoskeleton also contributes to the formation of cell protrusions (Schaks *et al.* 2019; Welf *et al.* 2020). Moving cells assemble and disassemble their actin cytoskeletons rapidly, particularly in protrusive actin structures, such as lamellipodia and filopodia (Machesky 2008). The observed rapid cell density-dependent regulation of FAM57A protein levels and the morphological alterations of FAM57A-deficient cells thus raise the question whether the reported plasma membrane-located FAM57A (He *et al.* 2002) may sense extracellular signals, leading to remodeling of actin cytoskeleton and thereby ultimately affecting cell migration. The formation of stress fibers consisting of actin filaments, myosin and various crosslinking

proteins play an important role in the migration process and can be visualized by immunofluorescence staining of F-actin (filamentous actin) (Chazotte 2010). Compared to cells under low cell density, F-actin stress fibers are drastically reduced in cells under high cell density (Pavel *et al.* 2018). During cell migration, F-actin is found at high concentrations in the front of migrating cells, while the membrane proximal F-actin (MPA) density is low in the front and high in the back of the cell. This allows the protrusions to selectively extend outward from the MPA density-reduced area due to the weaker membrane attachment (Bisaria *et al.* 2020). Moreover, F-actin stress fiber-mediated cell stiffening can drive cell proliferation (Tavares *et al.* 2017), which may explain the concomitant effects of FAM57A on both cell migration and proliferation. Hence, to assess a possible contribution of FAM57A in these processes, it will be interesting to analyze possible changes of the F-actin density and distribution in cervical cancer cells following FAM57A repression, *e. g.* by RNAi.

Cell migration can also be affected by various signaling pathways. For instance, the PI3K/AKT pathway can be activated by integrin overexpression (Sun *et al.* 2019; Wu *et al.* 2019) and induce epithelial-mesenchymal transition (EMT) (Xu *et al.* 2015), which promotes the invasiveness of cancer cells. Further, ERK activation can initiate the cell movement in response to mechanical signals by modulating actomyosin contractility, which is essential for the formation of stress fibers and focal adhesions. In this context, ERK phosphorylates key factors regulating these processes and can also transcriptionally modulate the expression of cytoskeleton components (Lavoie *et al.* 2020). Moreover, YAP/TAZ signaling also regulates cell migration in response to a variety of stimuli, including cell density, mechanical stress, cell adhesion, and signals transduced from a large number of G protein-coupled receptors (Koo and Guan 2018). As discussed, and newly found in my studies for YAP/TAZ, there is experimental evidence that FAM57A can affect the activity of all these three pathways linked to the control of cellular migration.

8.2.3 Expression levels of factors involved in YAP/TAZ signaling are downregulated following FAM57A suppression

YAP and TAZ are transcriptional co-activators that respond to the various signals received from the surrounding microenvironment, including physical stimuli from cell-cell adhesion and cell-ECM attachment (Mason *et al.* 2019; Pocaterra *et al.* 2020). YAP and TAZ are best known as downstream effector proteins of the Hippo signaling pathway, however, it becomes increasingly clear that additional, Hippo-independent upstream signals can lead to their activation (Piccolo *et al.* 2014). Nuclear YAP and TAZ transcriptionally regulate target genes involved in the control of a broad number of cellular processes, including cell proliferation and migration, mainly through associating with the transcriptional activator TEAD (Piccolo *et al.* 2014). At high cell density, YAP and TAZ are predominantly found in the cytoplasm (Aragona *et al.*

2013), where they are phosphorylated and proteasomally degraded (Piccolo *et al.* 2014). In line with this model, I observed lower YAP and TAZ expression levels in different HPV-positive cancer cells as well as in HPV-negative HaCaT cells, when the cells were cultivated at high density, compared to low density conditions. Moreover, the expression levels of TEAD1, a TEAD family member possibly playing a key role in cervical cancer (Ishiji *et al.* 1992; Mori *et al.* 2017), are also reduced in HPV-positive cancer cells cultivated at high cell density.

Furthermore, when cells are cultivated at low density, *i. e.* under conditions where FAM57A is expressed and YAP/TAZ signaling is activated, FAM57A silencing consistently resulted in a reduction of TAZ protein levels in all investigated cervical cancer cells. In addition, FAM57A silencing had the potential to reduce YAP and TEAD1 expression, however, this effect appeared to be somewhat cell type-dependent. The more pronounced reduction of TAZ compared to YAP levels could be due to the fact that the YAP is a relatively stable protein while TAZ is rather unstable with a half-life of < 2 h (Piccolo *et al.* 2014). Altogether, these results suggest that FAM57A repression can be linked to an interference with YAP/TAZ signaling, a notion which is further supported by the accompanying reduction of the transcript levels of the YAP/TAZ target genes *CYR61* and, to a lesser extent, *CTGF*, which encode components of the ECM and are related to cellular adhesion in various cell types (Chaour and Goppelt-Strube 2006; Kim *et al.* 2018).

Collectively, these findings indicate that FAM57A may have the potential to act as an upstream activator of YAP/TAZ signaling, which would be very interesting in the light of the high significance of this pathway in human cancer (Piccolo *et al.* 2014). Further work is required to analyze this issue in more depth. Particularly, it will be interesting to investigate whether the link between FAM57A and YAP/TAZ signaling is direct, *i. e.* whether FAM57A and YAP/TAZ are connected with each other in the same signaling cascade, or whether the effect is indirect, *i. e.* being a secondary consequence of the anti-proliferative or anti-migratory effects resulting from FAM57A repression. Whereas my data raises the possibility that FAM57A acts upstream on YAP/TAZ, I did not obtain evidence that FAM57A is positioned downstream of YAP/TAZ signaling, at least in terms of the regulation of its expression, since *YAP*, *TAZ* or *TEAD1/3/4* silencing did neither affect FAM57A protein nor *FAM57A* transcript levels.

A connection between FAM57A and YAP/TAZ signaling may not only be functionally relevant for the effect of FAM57A on cell proliferation and migration, since activation of YAP/TAZ has been also linked to increased resistance of tumor cells towards chemo- and immunotherapy in multiple cancers (Thompson 2020). Thus, the inhibition of YAP/TAZ might not only be an interesting therapeutic strategy *per se*, but also bear potential to be applied in combination with chemo- or immunotherapy. So far, attempts to inhibit the YAP/TAZ activities are mainly based on three approaches: (i) targeting upstream activators of YAP/TAZ, (ii) interfering with the formation of the YAP/TAZ-TEAD complex, or (iii) inhibiting oncogenic downstream targets which are transcriptionally activated by YAP/TAZ (Pobbati and Hong 2020). Thus,

targeting FAM57A for functional inhibition may provide a novel therapeutic opportunity to interfere with pro-tumorigenic activities of YAP/TAZ signaling, either as a monotherapy or in combination with radio-, chemo- or immunotherapy.

8.3 Conclusions and perspectives

The present study aims to gain new insights into the molecular mechanisms which control the phenotype of cervical cancer cells. Their elucidation should not only improve our current concepts of cervical carcinogenesis, but also may pave the way for novel therapeutic approaches. My results reveal that the activity of the FAM57A transmembrane protein is an important determinant for the phenotypic behavior of cervical cancer cells.

My investigations uncover that FAM57A exhibits a peculiar and strongly cell density-dependent expression pattern, being expressed at low cell density whereas its expression is almost undetectable when cells become confluent. This regulatory principle is conserved in different HPV16- or HPV18-positive cancer cell lines and also in HPV-negative cells, and predominantly occurs at the protein level. In line with the connection of FAM57A expression with low cell density, anti-proliferative stimuli, such as hypoxia or silencing of HPV *E6/E7* oncogene expression, also result in a pronounced increase of FAM57A protein levels. Moreover, my functional analyses reveal that FAM57A is a critical factor for promoting the growth of cervical cancer cells and their migration capacity. In addition, my preliminary data points at a possible connection between FAM57A and YAP/TAZ signaling, which provides an experimental basis for further experimental exploration. The here uncovered growth- and migration-promoting activities of FAM57A in cervical cancer cells also raise the question whether interference with its function may possess therapeutic potential, either as a monotherapy or in combination with radio-, chemo- or immunotherapy.

9. Summary

Oncogenic types of human papillomaviruses (HPVs) are important human carcinogens, causing cervical cancer and other major malignancies. Although HPV infections appear to be essential for cervical carcinogenesis, they are not sufficient. Thus, it is important to gain insights into the cellular mechanisms which may contribute to the transformed phenotype of HPV-positive tumor cells. This should not only increase our understanding of the carcinogenic process, but could also identify innovative therapeutic targets. In this thesis, the regulation and function of the thus far poorly investigated FAM57A protein was analyzed in cervical cancer cells. Previous work showed in proteome analyses that the expression levels of this factor are strongly increased in hypoxic cervical cancer cells, thereby inversely correlating with the downregulation of the HPV E6/E7 oncoproteins.

My work uncovers that the regulation of FAM57A expression is strongly dependent on cell densities: at low cell density, FAM57A is readily detectable, however, at high cell density, FAM57A expression is abolished. This regulation of FAM57A primarily occurs at the post-transcriptional level. The strong upregulation of FAM57A levels under hypoxia is found to be predominantly the result of the anti-proliferative effects of hypoxia and only to a minor part due to a HIF-1 α -linked transcriptional stimulation of *FAM57A* gene expression. In line with the connection between low cell density and FAM57A expression levels, other anti-proliferative stimuli, such as the inhibition of HPV *E6/E7* expression, also result in increased FAM57A levels in cervical cancer cells.

Functional analyses employing RNA interference reveal that silencing of FAM57A expression represses the proliferation of cervical cancer cells in both short-term live cell imaging analyses and long-term colony formation assays, indicating that FAM57A promotes cell proliferation. In addition, wound healing assays indicate that FAM57A repression results in a decreased migration capacity of cervical cancer cells. Mammalian Two-Hybrid analyses show that FAM57A can intracellularly interact with its putative binding partner SLC3A2. This interaction does neither lead to alterations in the expression levels of the two binding partners, nor does it appear to underlie the pro-proliferative activity of FAM57A. Notably, however, FAM57A repression is linked to a downregulation of factors involved in YAP/TAZ signaling, indicating that this pathway, which is involved in the control of cell proliferation and migration, could be directly or indirectly stimulated by FAM57A.

In summary, these findings reveal that FAM57A exhibits a strikingly cell density-dependent expression pattern in cervical cancer cells. This regulation also explains the highly elevated cellular FAM57A expression in hypoxic compared to normoxic cells. Mechanistically, FAM57A may stimulate YAP/TAZ signaling, an issue which warrants further exploration. The significant impact of FAM57A on the phenotype of cervical cancer cells not only identifies a novel factor which promotes their proliferation and migration, but also raises the possibility that FAM57A could serve as a novel target for therapeutic interference.

9. Zusammenfassung

Onkogene Typen humaner Papillomviren (HPVs) sind wichtige Karzinogene und verursachen das Zervixkarzinom und andere Krebsformen. Obwohl HPV-Infektionen für die Zervixkarzinogenese essentiell sind, sind sie nicht ausreichend. Es ist daher wichtig, Einblicke in die zellulären Mechanismen zu gewinnen, die zur Ausprägung des malignen Phänotyp HPV-positiver Tumorzellen beitragen. Dies könnte nicht nur unser Verständnis der Karzinogenese verbessern, sondern auch neue therapeutische Optionen eröffnen. In der vorliegenden Dissertation wird die Regulation und Funktion des FAM57A-Proteins in Zervixkarzinomzellen untersucht. Vorarbeiten zeigten in Proteomstudien, dass die FAM57A-Expressionsspiegel in hypoxischen Zervixkarzinomzellen stark erhöht werden und invers mit der Reduktion der HPV E6/E7-Onkoproteinspiegel korrelieren.

Meine Untersuchungen zeigen, dass die FAM57A-Expression stark von der Zelldichte abhängt: bei niedriger Zelldichte wird FAM57A exprimiert, bei hoher Zelldichte ist das Protein nicht mehr nachweisbar. Diese Regulation erfolgt in erster Linie auf der post-transkriptionellen Ebene. Auch die starke FAM57A-Induktion in hypoxischen Zellen ist primär das Resultat der anti-proliferativen Wirkung von Hypoxie und nur zu einem geringen Anteil durch eine HIF-1 α -abhängige Stimulierung der FAM57A-Genexpression verursacht. In Übereinstimmung mit der Zelldichte-abhängigen Regulation der FAM57A-Expression führen auch andere anti-proliferative Einflüsse, wie z. B. eine Hemmung der HPV E6/E7-Expression, in Zervixkarzinomzellen zu einem Anstieg der FAM57A-Spiegel.

Funktionsstudien mittels RNA-Interferenz ergeben, dass eine FAM57A-Hemmung die Proliferation von Zervixkarzinomzellen in Lebendzellmikroskopie-Analysen und in Kolonienbildungs-Assays inhibiert. Dies zeigt, dass FAM57A in Zervixkarzinomzellen pro-proliferativ wirkt. Zudem offenbaren Wundheilung-Analysen, dass eine FAM57A-Repression die Zellmigration hemmt. „Mammalian Two-Hybrid“-Assays zeigen, dass FAM57A intrazellulär mit seinem putativen Bindungspartner SLC3A2 interagieren kann. Diese Wechselwirkung beeinflusst aber weder die Expressionsspiegel der beiden Bindungspartner, noch scheint sie der pro-proliferativen Wirkung von FAM57A zugrunde zu liegen. Bemerkenswerterweise ist aber eine FAM57A-Hemmung mit einer Herunterregulierung von Faktoren des YAP/TAZ-Signalwegs verbunden. Dies impliziert, dass dieser Signalweg, der an der Kontrolle der Zellproliferation und -migration beteiligt ist, direkt oder indirekt durch FAM57A stimuliert werden kann. Zusammenfassend zeigen diese Resultate, dass FAM57A in Zervixkarzinomzellen ein stark Zelldichte-abhängiges Expressionsmuster aufweist, was die erhöhten FAM57A-Spiegel in hypoxischen Zellen erklärt. Mechanistisch könnte FAM57A den YAP/TAZ-Signalweg stimulieren, was in zukünftigen Studien weiter erhärtet werden sollte. FAM57A stellt einen neu identifizierten Faktor mit einer signifikanten Wirkung auf den Phänotyp von Zervixkarzinomzellen dar, der ihre Proliferation und Migration fördert und möglicherweise als ein neues therapeutisches Angriffsziel dienen könnte.

10. References

- Al Tameemi, W., Dale, T. P., Al-Jumaily, R. M. K. and Forsyth, N. R. (2019). **Hypoxia-Modified Cancer Cell Metabolism**. *Front Cell Dev Biol* 7, 4, doi: 10.3389/fcell.2019.00004.
- Albadari, N., Deng, S. and Li, W. (2019). **The transcriptional factors HIF-1 and HIF-2 and their novel inhibitors in cancer therapy**. *Expert Opin Drug Discov* 14 (7), 667-682, doi: 10.1080/17460441.2019.1613370.
- Aragona, M., Panciera, T., Manfrin, A., Giulitti, S., Michielin, F., Elvassore, N., Dupont, S. and Piccolo, S. (2013). **A mechanical checkpoint controls multicellular growth through YAP/TAZ regulation by actin-processing factors**. *Cell* 154 (5), 1047-1059, doi: 10.1016/j.cell.2013.07.042.
- Avci, D. and Lemberg, M. K. (2015). **Clipping or Extracting: Two Ways to Membrane Protein Degradation**. *Trends Cell Biol* 25 (10), 611-622, doi: 10.1016/j.tcb.2015.07.003.
- Bahrami, A., Hasanzadeh, M., Hassanian, S. M., ShahidSales, S., Ghayour-Mobarhan, M., Ferns, G. A. and Avan, A. (2017). **The Potential Value of the PI3K/Akt/mTOR Signaling Pathway for Assessing Prognosis in Cervical Cancer and as a Target for Therapy**. *J Cell Biochem* 118 (12), 4163-4169, doi: 10.1002/jcb.26118.
- Baltaci, E., Ekizoglu, S., Sari, E., Karaman, E., Ulutin, T. and Buyru, N. (2015). **CT120A Acts as an Oncogene in Head and Neck Squamous Cell Carcinoma**. *J Cancer* 6 (12), 1255-1259, doi: 10.7150/jca.12969.
- Baltaci, E., Seyhan, B., Baykara, O. and Buyru, N. (2017). **CT120: A New Potential Target for c-Myc in Head and Neck Cancers**. *J Cancer* 8 (5), 880-886, doi: 10.7150/jca.18207.
- Bisaria, A., Hayer, A., Garbett, D., Cohen, D. and Meyer, T. (2020). **Membrane-proximal F-actin restricts local membrane protrusions and directs cell migration**. *Science* 368 (6496), 1205-1210, doi: 10.1126/science.aay7794.
- Bossler, F., Hoppe-Seyler, K. and Hoppe-Seyler, F. (2019a). **PI3K/AKT/mTOR Signaling Regulates the Virus/Host Cell Crosstalk in HPV-Positive Cervical Cancer Cells**. *Int J Mol Sci* 20 (9), doi: 10.3390/ijms20092188.
- Bossler, F., Kuhn, B. J., Gunther, T., Kraemer, S. J., Khalkar, P., Adrian, S., Lohrey, C., Holzer, A., Shimobayashi, M., Durst, M., Mayer, A., Rosl, F., Grundhoff, A., Krijgsveld, J., Hoppe-Seyler, K. and Hoppe-Seyler, F. (2019b). **Repression of Human Papillomavirus Oncogene Expression under Hypoxia Is Mediated by PI3K/mTORC2/AKT Signaling**. *MBio* 10 (1), doi: 10.1128/mBio.02323-18.
- Boukamp, P., Petrussevska, R. T., Breitkreutz, D., Hornung, J., Markham, A. and Fusenig, N. E. (1988). **Normal keratinization in a spontaneously immortalized aneuploid human keratinocyte cell line**. *J Cell Biol* 106 (3), 761-771, doi: 10.1083/jcb.106.3.761.

- Bouleftour, W., Rowinski, E., Louati, S., Sotton, S., Wozny, A. S., Moreno-Acosta, P., Mery, B., Rodriguez-Lafrasse, C. and Magne, N. (2021). **A Review of the Role of Hypoxia in Radioresistance in Cancer Therapy**. *Med Sci Monit* 27, e934116, doi: 10.12659/MSM.934116.
- Bouthelier, A. and Aragones, J. (2020). **Role of the HIF oxygen sensing pathway in cell defense and proliferation through the control of amino acid metabolism**. *Biochim Biophys Acta Mol Cell Res* 1867 (9), 118733, doi: 10.1016/j.bbamcr.2020.118733.
- Brill, E., Gobble, R., Angeles, C., Lagos-Quintana, M., Crago, A., Laxa, B., Decarolis, P., Zhang, L., Antonescu, C., Socci, N. D., Taylor, B. S., Sander, C., Koff, A. and Singer, S. (2010). **ZIC1 overexpression is oncogenic in liposarcoma**. *Cancer Res* 70 (17), 6891-6901, doi: 10.1158/0008-5472.CAN-10-0745.
- Broer, A., Friedrich, B., Wagner, C. A., Fillon, S., Ganapathy, V., Lang, F. and Broer, S. (2001). **Association of 4F2hc with light chains LAT1, LAT2 or y+LAT2 requires different domains**. *Biochem J* 355 (Pt 3), 725-731, doi: 10.1042/bj3550725.
- Bruick, R. K. and McKnight, S. L. (2001). **A conserved family of prolyl-4-hydroxylases that modify HIF**. *Science* 294 (5545), 1337-1340, doi: 10.1126/science.1066373.
- Brummelkamp, T. R., Bernards, R. and Agami, R. (2002). **A system for stable expression of short interfering RNAs in mammalian cells**. *Science* 296 (5567), 550-553, doi: 10.1126/science.1068999.
- Bui, T. T., Nitta, R. T., Kahn, S. A., Razavi, S. M., Agarwal, M., Aujla, P., Gholamin, S., Recht, L. and Li, G. (2015). **gamma-Glutamyl transferase 7 is a novel regulator of glioblastoma growth**. *BMC Cancer* 15, 225, doi: 10.1186/s12885-015-1232-y.
- Cano-Crespo, S., Chillaron, J., Junza, A., Fernandez-Miranda, G., Garcia, J., Polte, C., L, R. d. I. B., Ignatova, Z., Yanes, O., Zorzano, A., Stephan-Otto Attolini, C. and Palacin, M. (2019). **CD98hc (SLC3A2) sustains amino acid and nucleotide availability for cell cycle progression**. *Sci Rep* 9 (1), 14065, doi: 10.1038/s41598-019-50547-9.
- Capuana, L., Bostrom, A. and Etienne-Manneville, S. (2020). **Multicellular scale front-to-rear polarity in collective migration**. *Curr Opin Cell Biol* 62, 114-122, doi: 10.1016/j.ceb.2019.10.001.
- Castellsague, X., Giuliano, A. R., Goldstone, S., Guevara, A., Mogensen, O., Palefsky, J. M., Group, T., Shields, C., Liu, K., Maansson, R., Luxembourg, A. and Kaplan, S. S. (2015). **Immunogenicity and safety of the 9-valent HPV vaccine in men**. *Vaccine* 33 (48), 6892-6901, doi: 10.1016/j.vaccine.2015.06.088.
- Chaneton, B., Hillmann, P., Zheng, L., Martin, A. C. L., Maddocks, O. D. K., Chokkathukalam, A., Coyle, J. E., Jankevics, A., Holding, F. P., Vousden, K. H., Frezza, C., O'Reilly, M. and Gottlieb, E. (2012).

10. References

- Serine is a natural ligand and allosteric activator of pyruvate kinase M2.** *Nature* 491 (7424), 458-462, doi: 10.1038/nature11540.
- Chaour, B. and Goppelt-Struebe, M. (2006). **Mechanical regulation of the Cyr61/CCN1 and CTGF/CCN2 proteins.** *FEBS J* 273 (16), 3639-3649, doi: 10.1111/j.1742-4658.2006.05360.x.
- Chazotte, B. (2010). **Labeling cytoskeletal F-actin with rhodamine phalloidin or fluorescein phalloidin for imaging.** *Cold Spring Harb Protoc* 2010 (5), pdb prot4947, doi: 10.1101/pdb.prot4947.
- Chen, C. and Okayama, H. (1987). **High-efficiency transformation of mammalian cells by plasmid DNA.** *Mol Cell Biol* 7 (8), 2745-2752, doi: 10.1128/mcb.7.8.2745-2752.1987.
- Ciccarelli, C., Di Rocco, A., Gravina, G. L., Mauro, A., Festuccia, C., Del Fattore, A., Berardinelli, P., De Felice, F., Musio, D., Bouche, M., Tombolini, V., Zani, B. M. and Marampon, F. (2018). **Disruption of MEK/ERK/c-Myc signaling radiosensitizes prostate cancer cells in vitro and in vivo.** *J Cancer Res Clin Oncol* 144 (9), 1685-1699, doi: 10.1007/s00432-018-2696-3.
- Ciechanover, A. (2005). **Proteolysis: from the lysosome to ubiquitin and the proteasome.** *Nat Rev Mol Cell Biol* 6 (1), 79-87, doi: 10.1038/nrm1552.
- Cosper, P. F., Bradley, S., Luo, L. and Kimple, R. J. (2021). **Biology of HPV Mediated Carcinogenesis and Tumor Progression.** *Semin Radiat Oncol* 31 (4), 265-273, doi: 10.1016/j.semradonc.2021.02.006.
- Crook, T., Fisher, C., Masterson, P. J. and Vousden, K. H. (1994). **Modulation of transcriptional regulatory properties of p53 by HPV E6.** *Oncogene* 9 (4), 1225-1230.
- de Martel, C., Georges, D., Bray, F., Ferlay, J. and Clifford, G. M. (2020). **Global burden of cancer attributable to infections in 2018: a worldwide incidence analysis.** *Lancet Glob Health* 8 (2), e180-e190, doi: 10.1016/S2214-109X(19)30488-7.
- DeBerardinis, R. J., Lum, J. J., Hatzivassiliou, G. and Thompson, C. B. (2008). **The biology of cancer: metabolic reprogramming fuels cell growth and proliferation.** *Cell Metab* 7 (1), 11-20, doi: 10.1016/j.cmet.2007.10.002.
- Degirmenci, U., Wang, M. and Hu, J. (2020). **Targeting Aberrant RAS/RAF/MEK/ERK Signaling for Cancer Therapy.** *Cells* 9 (1), doi: 10.3390/cells9010198.
- Della Fera, A. N., Warburton, A., Coursey, T. L., Khurana, S. and McBride, A. A. (2021). **Persistent Human Papillomavirus Infection.** *Viruses* 13 (2), doi: 10.3390/v13020321.
- Deng, S., Leong, H. C., Datta, A., Gopal, V., Kumar, A. P. and Yap, C. T. (2022). **PI3K/AKT Signaling Tips the Balance of Cytoskeletal Forces for Cancer Progression.** *Cancers (Basel)* 14 (7), doi: 10.3390/cancers14071652.

- Denko, N. C. (2008). **Hypoxia, HIF1 and glucose metabolism in the solid tumour**. *Nat Rev Cancer* 8 (9), 705-713, doi: 10.1038/nrc2468.
- Digomann, D., Kurth, I., Tyutyunnykova, A., Chen, O., Lock, S., Gorodetska, I., Peitzsch, C., Skvortsova, II, Negro, G., Aschenbrenner, B., Eisenhofer, G., Richter, S., Heiden, S., Porrmann, J., Klink, B., Schwager, C., Dowle, A. A., Hein, L., Kunz-Schughart, L. A., Abdollahi, A., Lohaus, F., Krause, M., Baumann, M., Linge, A. and Dubrovskaya, A. (2019a). **The CD98 Heavy Chain Is a Marker and Regulator of Head and Neck Squamous Cell Carcinoma Radiosensitivity**. *Clin Cancer Res* 25 (10), 3152-3163, doi: 10.1158/1078-0432.CCR-18-2951.
- Digomann, D., Linge, A. and Dubrovskaya, A. (2019b). **SLC3A2/CD98hc, autophagy and tumor radioresistance: a link confirmed**. *Autophagy* 15 (10), 1850-1851, doi: 10.1080/15548627.2019.1639302.
- Dupont, S., Morsut, L., Aragona, M., Enzo, E., Giulitti, S., Cordenonsi, M., Zanconato, F., Le Digabel, J., Forcato, M., Bicciato, S., Elvassore, N. and Piccolo, S. (2011). **Role of YAP/TAZ in mechanotransduction**. *Nature* 474 (7350), 179-183, doi: 10.1038/nature10137.
- Ebner, H. L., Blatzer, M., Nawaz, M. and Krumschnabel, G. (2007). **Activation and nuclear translocation of ERK in response to ligand-dependent and -independent stimuli in liver and gill cells from rainbow trout**. *J Exp Biol* 210 (Pt 6), 1036-1045, doi: 10.1242/jeb.02719.
- Eichten, A., Rud, D. S., Grace, M., Piboonniyom, S. O., Zacny, V. and Munger, K. (2004). **Molecular pathways executing the "trophic sentinel" response in HPV-16 E7-expressing normal human diploid fibroblasts upon growth factor deprivation**. *Virology* 319 (1), 81-93, doi: 10.1016/j.virol.2003.11.008.
- Einstein, M. H., Baron, M., Levin, M. J., Chatterjee, A., Fox, B., Scholar, S., Rosen, J., Chakhtoura, N., Lebacqz, M., van der Most, R., Moris, P., Giannini, S. L., Schuind, A., Datta, S. K., Descamps, D. and Group, H. P. V. S. (2011). **Comparison of the immunogenicity of the human papillomavirus (HPV)-16/18 vaccine and the HPV-6/11/16/18 vaccine for oncogenic non-vaccine types HPV-31 and HPV-45 in healthy women aged 18-45 years**. *Hum Vaccin* 7 (12), 1359-1373, doi: 10.4161/hv.7.12.18282.
- Ema, M., Taya, S., Yokotani, N., Sogawa, K., Matsuda, Y. and Fujii-Kuriyama, Y. (1997). **A novel bHLH-PAS factor with close sequence similarity to hypoxia-inducible factor 1alpha regulates the VEGF expression and is potentially involved in lung and vascular development**. *Proc Natl Acad Sci U S A* 94 (9), 4273-4278, doi: 10.1073/pnas.94.9.4273.
- Engelman, J. A. (2009). **Targeting PI3K signalling in cancer: opportunities, challenges and limitations**. *Nat Rev Cancer* 9 (8), 550-562, doi: 10.1038/nrc2664.
- Epstein, A. C., Gleadle, J. M., McNeill, L. A., Hewitson, K. S., O'Rourke, J., Mole, D. R., Mukherji, M., Metzen, E., Wilson, M. I., Dhanda, A., Tian, Y. M., Masson, N., Hamilton, D. L., Jaakkola, P., Barstead, R., Hodgkin, J., Maxwell, P. H., Pugh, C. W., Schofield, C. J. and Ratcliffe, P. J. (2001).

- C. elegans EGL-9 and mammalian homologs define a family of dioxygenases that regulate HIF by prolyl hydroxylation.** *Cell* 107 (1), 43-54, doi: 10.1016/s0092-8674(01)00507-4.
- Estrach, S., Lee, S. A., Boulter, E., Pisano, S., Errante, A., Tissot, F. S., Cailleteau, L., Pons, C., Ginsberg, M. H. and Feral, C. C. (2014). **CD98hc (SLC3A2) loss protects against ras-driven tumorigenesis by modulating integrin-mediated mechanotransduction.** *Cancer Res* 74 (23), 6878-6889, doi: 10.1158/0008-5472.CAN-14-0579.
- Falcaro, M., Castanon, A., Ndlela, B., Checchi, M., Soldan, K., Lopez-Bernal, J., Elliss-Brookes, L. and Sasieni, P. (2021). **The effects of the national HPV vaccination programme in England, UK, on cervical cancer and grade 3 cervical intraepithelial neoplasia incidence: a register-based observational study.** *Lancet* 398 (10316), 2084-2092, doi: 10.1016/S0140-6736(21)02178-4.
- Fang, J., Zhang, H. and Jin, S. (2014). **Epigenetics and cervical cancer: from pathogenesis to therapy.** *Tumour Biol* 35 (6), 5083-5093, doi: 10.1007/s13277-014-1737-z.
- Feral, C. C., Nishiya, N., Fenczik, C. A., Stuhlmann, H., Slepak, M. and Ginsberg, M. H. (2005). **CD98hc (SLC3A2) mediates integrin signaling.** *Proc Natl Acad Sci U S A* 102 (2), 355-360, doi: 10.1073/pnas.0404852102.
- Fjeldbo, C. S., Aarnes, E. K., Malinen, E., Kristensen, G. B. and Lyng, H. (2016). **Identification and Validation of Reference Genes for RT-qPCR Studies of Hypoxia in Squamous Cervical Cancer Patients.** *PLoS One* 11 (5), e0156259, doi: 10.1371/journal.pone.0156259.
- Flamme, I., Frohlich, T., von Reutern, M., Kappel, A., Damert, A. and Risau, W. (1997). **HRF, a putative basic helix-loop-helix-PAS-domain transcription factor is closely related to hypoxia-inducible factor-1 alpha and developmentally expressed in blood vessels.** *Mech Dev* 63 (1), 51-60, doi: 10.1016/s0925-4773(97)00674-6.
- Fontham, E. T. H., Wolf, A. M. D., Church, T. R., Etzioni, R., Flowers, C. R., Herzig, A., Guerra, C. E., Oeffinger, K. C., Shih, Y. T., Walter, L. C., Kim, J. J., Andrews, K. S., DeSantis, C. E., Fedewa, S. A., Manassaram-Baptiste, D., Saslow, D., Wender, R. C. and Smith, R. A. (2020). **Cervical cancer screening for individuals at average risk: 2020 guideline update from the American Cancer Society.** *CA Cancer J Clin* 70 (5), 321-346, doi: 10.3322/caac.21628.
- Fort, J., Nicolas-Arago, A. and Palacin, M. (2021). **The Ectodomains of rBAT and 4F2hc Are Fake or Orphan alpha-Glucosidases.** *Molecules* 26 (20), doi: 10.3390/molecules26206231.
- Franco, S. J. and Huttenlocher, A. (2005). **Regulating cell migration: calpains make the cut.** *J Cell Sci* 118 (Pt 17), 3829-3838, doi: 10.1242/jcs.02562.
- Fukuda, R., Zhang, H., Kim, J. W., Shimoda, L., Dang, C. V. and Semenza, G. L. (2007). **HIF-1 regulates cytochrome oxidase subunits to optimize efficiency of respiration in hypoxic cells.** *Cell* 129 (1), 111-122, doi: 10.1016/j.cell.2007.01.047.

- Ganti, K., Broniarczyk, J., Manoubi, W., Massimi, P., Mittal, S., Pim, D., Szalmas, A., Thatte, J., Thomas, M., Tomaic, V. and Banks, L. (2015). **The Human Papillomavirus E6 PDZ Binding Motif: From Life Cycle to Malignancy**. *Viruses* 7 (7), 3530-3551, doi: 10.3390/v7072785.
- Ganti, K., Massimi, P., Manzo-Merino, J., Tomaic, V., Pim, D., Playford, M. P., Lizano, M., Roberts, S., Kranjec, C., Doorbar, J. and Banks, L. (2016). **Interaction of the Human Papillomavirus E6 Oncoprotein with Sorting Nexin 27 Modulates Endocytic Cargo Transport Pathways**. *PLoS Pathog* 12 (9), e1005854, doi: 10.1371/journal.ppat.1005854.
- Giaccia, A. J. and Kastan, M. B. (1998). **The complexity of p53 modulation: emerging patterns from divergent signals**. *Genes Dev* 12 (19), 2973-2983, doi: 10.1101/gad.12.19.2973.
- Giuliano, A. R., Palefsky, J. M., Goldstone, S., Moreira, E. D., Jr., Penny, M. E., Aranda, C., Vardas, E., Moi, H., Jessen, H., Hillman, R., Chang, Y. H., Ferris, D., Rouleau, D., Bryan, J., Marshall, J. B., Vuocolo, S., Barr, E., Radley, D., Haupt, R. M. and Guris, D. (2011). **Efficacy of quadrivalent HPV vaccine against HPV Infection and disease in males**. *N Engl J Med* 364 (5), 401-411, doi: 10.1056/NEJMoa0909537.
- Goll, D. E., Thompson, V. F., Li, H., Wei, W. and Cong, J. (2003). **The calpain system**. *Physiol Rev* 83 (3), 731-801, doi: 10.1152/physrev.00029.2002.
- Gumbiner, B. M. and Kim, N. G. (2014). **The Hippo-YAP signaling pathway and contact inhibition of growth**. *J Cell Sci* 127 (Pt 4), 709-717, doi: 10.1242/jcs.140103.
- Guo, Y. J., Pan, W. W., Liu, S. B., Shen, Z. F., Xu, Y. and Hu, L. L. (2020). **ERK/MAPK signalling pathway and tumorigenesis**. *Exp Ther Med* 19 (3), 1997-2007, doi: 10.3892/etm.2020.8454.
- Hanahan, D. (1983). **Studies on transformation of Escherichia coli with plasmids**. *J Mol Biol* 166 (4), 557-580, doi: 10.1016/s0022-2836(83)80284-8.
- Hanahan, D. and Weinberg, R. A. (2011). **Hallmarks of cancer: the next generation**. *Cell* 144 (5), 646-674, doi: 10.1016/j.cell.2011.02.013.
- Hanigan, M. H. (2014). **Gamma-glutamyl transpeptidase: redox regulation and drug resistance**. *Adv Cancer Res* 122, 103-141, doi: 10.1016/B978-0-12-420117-0.00003-7.
- Harden, M. E. and Munger, K. (2017). **Human papillomavirus molecular biology**. *Mutat Res Rev Mutat Res* 772, 3-12, doi: 10.1016/j.mrrev.2016.07.002.
- He, X., Di, Y., Li, J., Xie, Y., Tang, Y., Zhang, F., Wei, L., Zhang, Y., Qin, W., Huo, K., Li, Y., Wan, D. and Gu, J. (2002). **Molecular cloning and characterization of CT120, a novel membrane-associated gene involved in amino acid transport and glutathione metabolism**. *Biochem Biophys Res Commun* 297 (3), 528-536, doi: 10.1016/s0006-291x(02)02227-1.

10. References

- He, X. H., Li, J. J., Xie, Y. H., Tang, Y. T., Yao, G. F., Qin, W. X., Wan, D. F. and Gu, J. R. (2004). **Altered gene expression profiles of NIH3T3 cells regulated by human lung cancer associated gene CT120**. *Cell Res* 14 (6), 487-496, doi: 10.1038/sj.cr.7290252.
- He, X. H., Li, J. J., Xie, Y. H., Zhang, F. R., Qu, S. M., Tang, Y. T., Qin, W. X., Wan, D. F. and Gu, J. R. (2003). **[Expression of human novel gene CT120 in lung cancer and its effects on cell growth]**. *Ai Zheng* 22 (2), 113-118.
- Heckman, C. A. and Plummer, H. K., 3rd (2013). **Filopodia as sensors**. *Cell Signal* 25 (11), 2298-2311, doi: 10.1016/j.cellsig.2013.07.006.
- Heikkila, M., Pasanen, A., Kivirikko, K. I. and Myllyharju, J. (2011). **Roles of the human hypoxia-inducible factor (HIF)-3alpha variants in the hypoxia response**. *Cell Mol Life Sci* 68 (23), 3885-3901, doi: 10.1007/s00018-011-0679-5.
- Heisterkamp, N., Groffen, J., Warburton, D. and Sneddon, T. P. (2008). **The human gamma-glutamyltransferase gene family**. *Hum Genet* 123 (4), 321-332, doi: 10.1007/s00439-008-0487-7.
- Henderson, N. C., Collis, E. A., Mackinnon, A. C., Simpson, K. J., Haslett, C., Zent, R., Ginsberg, M. and Sethi, T. (2004). **CD98hc (SLC3A2) interaction with beta 1 integrins is required for transformation**. *J Biol Chem* 279 (52), 54731-54741, doi: 10.1074/jbc.M408700200.
- Hoppe-Seyler, K., Bossler, F., Lohrey, C., Bulkescher, J., Rosl, F., Jansen, L., Mayer, A., Vaupel, P., Durst, M. and Hoppe-Seyler, F. (2017a). **Induction of dormancy in hypoxic human papillomavirus-positive cancer cells**. *Proc Natl Acad Sci U S A* 114 (6), E990-E998, doi: 10.1073/pnas.1615758114.
- Hoppe-Seyler, K., Herrmann, A. L., Daschle, A., Kuhn, B. J., Strobel, T. D., Lohrey, C., Bulkescher, J., Krijgsveld, J. and Hoppe-Seyler, F. (2021). **Effects of Metformin on the virus/host cell crosstalk in human papillomavirus-positive cancer cells**. *Int J Cancer* 149 (5), 1137-1149, doi: 10.1002/ijc.33594.
- Hoppe-Seyler, K., Mandl, J., Adrian, S., Kuhn, B. J. and Hoppe-Seyler, F. (2017b). **Virus/Host Cell Crosstalk in Hypoxic HPV-Positive Cancer Cells**. *Viruses* 9 (7), doi: 10.3390/v9070174.
- Hu, C. J., Wang, L. Y., Chodosh, L. A., Keith, B. and Simon, M. C. (2003). **Differential roles of hypoxia-inducible factor 1alpha (HIF-1alpha) and HIF-2alpha in hypoxic gene regulation**. *Mol Cell Biol* 23 (24), 9361-9374, doi: 10.1128/MCB.23.24.9361-9374.2003.
- Huang, Li, T., Li, X., Zhang, L., Sun, L., He, X., Zhong, X., Jia, D., Song, L., Semenza, G. L., Gao, P. and Zhang, H. (2014). **HIF-1-mediated suppression of acyl-CoA dehydrogenases and fatty acid oxidation is critical for cancer progression**. *Cell Rep* 8 (6), 1930-1942, doi: 10.1016/j.celrep.2014.08.028.

- Huang, L. E., Arany, Z., Livingston, D. M. and Bunn, H. F. (1996). **Activation of hypoxia-inducible transcription factor depends primarily upon redox-sensitive stabilization of its alpha subunit.** *J Biol Chem* 271 (50), 32253-32259, doi: 10.1074/jbc.271.50.32253.
- Ishiji, T., Lace, M. J., Parkkinen, S., Anderson, R. D., Haugen, T. H., Cripe, T. P., Xiao, J. H., Davidson, I., Chambon, P. and Turek, L. P. (1992). **Transcriptional enhancer factor (TEF)-1 and its cell-specific co-activator activate human papillomavirus-16 E6 and E7 oncogene transcription in keratinocytes and cervical carcinoma cells.** *EMBO J* 11 (6), 2271-2281, doi: 10.1002/j.1460-2075.1992.tb05286.x.
- Ivan, M., Kondo, K., Yang, H., Kim, W., Valiando, J., Ohh, M., Salic, A., Asara, J. M., Lane, W. S. and Kaelin, W. G., Jr. (2001). **HIFalpha targeted for VHL-mediated destruction by proline hydroxylation: implications for O₂ sensing.** *Science* 292 (5516), 464-468, doi: 10.1126/science.1059817.
- Jaakkola, P., Mole, D. R., Tian, Y. M., Wilson, M. I., Gielbert, J., Gaskell, S. J., von Kriegsheim, A., Hebestreit, H. F., Mukherji, M., Schofield, C. J., Maxwell, P. H., Pugh, C. W. and Ratcliffe, P. J. (2001). **Targeting of HIF-alpha to the von Hippel-Lindau ubiquitylation complex by O₂-regulated prolyl hydroxylation.** *Science* 292 (5516), 468-472, doi: 10.1126/science.1059796.
- Jing, X., Yang, F., Shao, C., Wei, K., Xie, M., Shen, H. and Shu, Y. (2019). **Role of hypoxia in cancer therapy by regulating the tumor microenvironment.** *Mol Cancer* 18 (1), 157, doi: 10.1186/s12943-019-1089-9.
- Jones, D. L., Thompson, D. A. and Munger, K. (1997). **Destabilization of the RB tumor suppressor protein and stabilization of p53 contribute to HPV type 16 E7-induced apoptosis.** *Virology* 239 (1), 97-107, doi: 10.1006/viro.1997.8851.
- Joura, E. A., Giuliano, A. R., Iversen, O. E., Bouchard, C., Mao, C., Mehlsen, J., Moreira, E. D., Jr., Ngan, Y., Petersen, L. K., Lazcano-Ponce, E., Pitisuttithum, P., Restrepo, J. A., Stuart, G., Woelber, L., Yang, Y. C., Cuzick, J., Garland, S. M., Huh, W., Kjaer, S. K., Bautista, O. M., Chan, I. S., Chen, J., Gesser, R., Moeller, E., Ritter, M., Vuocolo, S., Luxembourg, A. and Broad Spectrum, H. P. V. V. S. (2015). **A 9-valent HPV vaccine against infection and intraepithelial neoplasia in women.** *N Engl J Med* 372 (8), 711-723, doi: 10.1056/NEJMoa1405044.
- Julien, O. and Wells, J. A. (2017). **Caspases and their substrates.** *Cell Death Differ* 24 (8), 1380-1389, doi: 10.1038/cdd.2017.44.
- Justus, C. R., Leffler, N., Ruiz-Echevarria, M. and Yang, L. V. (2014). **In vitro cell migration and invasion assays.** *J Vis Exp* (88), doi: 10.3791/51046.
- Kabakov, A. E. and Yakimova, A. O. (2021). **Hypoxia-Induced Cancer Cell Responses Driving Radioresistance of Hypoxic Tumors: Approaches to Targeting and Radiosensitizing.** *Cancers (Basel)* 13 (5), doi: 10.3390/cancers13051102.

10. References

- Kantipudi, S., Jeckelmann, J. M., Ucurum, Z., Bosshart, P. D. and Fotiadis, D. (2020). **The Heavy Chain 4F2hc Modulates the Substrate Affinity and Specificity of the Light Chains LAT1 and LAT2.** *Int J Mol Sci* *21* (20), doi: 10.3390/ijms21207573.
- Kapitsinou, P. P., Liu, Q., Unger, T. L., Rha, J., Davidoff, O., Keith, B., Epstein, J. A., Moores, S. L., Erickson-Miller, C. L. and Haase, V. H. (2010). **Hepatic HIF-2 regulates erythropoietic responses to hypoxia in renal anemia.** *Blood* *116* (16), 3039-3048, doi: 10.1182/blood-2010-02-270322.
- Kierans, S. J. and Taylor, C. T. (2021). **Regulation of glycolysis by the hypoxia-inducible factor (HIF): implications for cellular physiology.** *J Physiol* *599* (1), 23-37, doi: 10.1113/JP280572.
- Kim, H., Son, S. and Shin, I. (2018). **Role of the CCN protein family in cancer.** *BMB Rep* *51* (10), 486-492.
- Kisselev, A. F. (2021). **Site-Specific Proteasome Inhibitors.** *Biomolecules* *12* (1), doi: 10.3390/biom12010054.
- Koh, W. J., Greer, B. E., Abu-Rustum, N. R., Apte, S. M., Campos, S. M., Cho, K. R., Chu, C., Cohn, D., Crispens, M. A., Dorigo, O., Eifel, P. J., Fisher, C. M., Frederick, P., Gaffney, D. K., Han, E., Huh, W. K., Lurain, J. R., 3rd, Mutch, D., Fader, A. N., Remmenga, S. W., Reynolds, R. K., Teng, N., Tillmanns, T., Valea, F. A., Yashar, C. M., McMillian, N. R. and Scavone, J. L. (2015). **Cervical Cancer, Version 2.2015.** *J Natl Compr Canc Netw* *13* (4), 395-404; quiz 404, doi: 10.6004/jnccn.2015.0055.
- Kohler, G. and Milstein, C. (1975). **Continuous cultures of fused cells secreting antibody of predefined specificity.** *Nature* *256* (5517), 495-497, doi: 10.1038/256495a0.
- Koo, J. H. and Guan, K. L. (2018). **Interplay between YAP/TAZ and Metabolism.** *Cell Metab* *28* (2), 196-206, doi: 10.1016/j.cmet.2018.07.010.
- Kozera, B. and Rapacz, M. (2013). **Reference genes in real-time PCR.** *J Appl Genet* *54* (4), 391-406, doi: 10.1007/s13353-013-0173-x.
- Kuhnle, N., Dederer, V. and Lemberg, M. K. (2019). **Intramembrane proteolysis at a glance: from signalling to protein degradation.** *J Cell Sci* *132* (16), doi: 10.1242/jcs.217745.
- Kumar, A., Zhao, Y., Meng, G., Zeng, M., Srinivasan, S., Delmolino, L. M., Gao, Q., Dimri, G., Weber, G. F., Wazer, D. E., Band, H. and Band, V. (2002). **Human papillomavirus oncoprotein E6 inactivates the transcriptional coactivator human ADA3.** *Mol Cell Biol* *22* (16), 5801-5812, doi: 10.1128/MCB.22.16.5801-5812.2002.
- Lavoie, H., Gagnon, J. and Therrien, M. (2020). **ERK signalling: a master regulator of cell behaviour, life and fate.** *Nat Rev Mol Cell Biol* *21* (10), 607-632, doi: 10.1038/s41580-020-0255-7.

- Lechner, M. S. and Laimins, L. A. (1994). **Inhibition of p53 DNA binding by human papillomavirus E6 proteins.** *J Virol* 68 (7), 4262-4273, doi: 10.1128/JVI.68.7.4262-4273.1994.
- Li, D., Zhou, L., Huang, J. and Xiao, X. (2016). **Effect of multidrug resistance 1/P-glycoprotein on the hypoxia-induced multidrug resistance of human laryngeal cancer cells.** *Oncol Lett* 12 (2), 1569-1574, doi: 10.3892/ol.2016.4749.
- Li, Z., Shao, S., Xie, S., Jiao, F., Ma, Y. and Shi, S. (2010). **Silencing of CT120 by antisense oligonucleotides could inhibit the lung cancer cells growth.** *Ir J Med Sci* 179 (2), 217-223, doi: 10.1007/s11845-009-0418-1.
- Liang, J. and Sun, Z. (2021). **Overexpression of membranal SLC3A2 regulates the proliferation of oral squamous cancer cells and affects the prognosis of oral cancer patients.** *J Oral Pathol Med* 50 (4), 371-377, doi: 10.1111/jop.13132.
- Lin, L., Li, K., Yu, M., Fan, B., Yerle, M. and Liu, B. (2005). **Isolation, polymorphism studies and radiation hybrid mapping of the porcine homologue of human membrane-associated protein (CT120) gene.** *Anim Genet* 36 (1), 73-74, doi: 10.1111/j.1365-2052.2004.01216.x.
- Linge, A., Lock, S., Gudziol, V., Nowak, A., Lohaus, F., von Neubeck, C., Jutz, M., Abdollahi, A., Debus, J., Tinhofer, I., Budach, V., Sak, A., Stuschke, M., Balermipas, P., Rodel, C., Avlar, M., Grosu, A. L., Bayer, C., Belka, C., Pigorsch, S., Combs, S. E., Welz, S., Zips, D., Buchholz, F., Aust, D. E., Baretton, G. B., Thames, H. D., Dubrovskaya, A., Alsner, J., Overgaard, J., Baumann, M., Krause, M. and Dtk, R. O. G. (2016a). **Low Cancer Stem Cell Marker Expression and Low Hypoxia Identify Good Prognosis Subgroups in HPV(-) HNSCC after Postoperative Radiochemotherapy: A Multicenter Study of the DTK-ROG.** *Clin Cancer Res* 22 (11), 2639-2649, doi: 10.1158/1078-0432.CCR-15-1990.
- Linge, A., Lock, S., Krenn, C., Appold, S., Lohaus, F., Nowak, A., Gudziol, V., Baretton, G. B., Buchholz, F., Baumann, M. and Krause, M. (2016b). **Independent validation of the prognostic value of cancer stem cell marker expression and hypoxia-induced gene expression for patients with locally advanced HNSCC after postoperative radiotherapy.** *Clin Transl Radiat Oncol* 1, 19-26, doi: 10.1016/j.ctro.2016.10.002.
- Linge, A., Lohaus, F., Lock, S., Nowak, A., Gudziol, V., Valentini, C., von Neubeck, C., Jutz, M., Tinhofer, I., Budach, V., Sak, A., Stuschke, M., Balermipas, P., Rodel, C., Grosu, A. L., Abdollahi, A., Debus, J., Ganswindt, U., Belka, C., Pigorsch, S., Combs, S. E., Monnich, D., Zips, D., Buchholz, F., Aust, D. E., Baretton, G. B., Thames, H. D., Dubrovskaya, A., Alsner, J., Overgaard, J., Krause, M., Baumann, M. and Dtk, R. O. G. (2016c). **HPV status, cancer stem cell marker expression, hypoxia gene signatures and tumour volume identify good prognosis subgroups in patients with HNSCC after primary radiochemotherapy: A multicentre retrospective study of the German Cancer Consortium Radiation Oncology Group (DKTK-ROG).** *Radiother Oncol* 121 (3), 364-373, doi: 10.1016/j.radonc.2016.11.008.
- Liu, J., Xia, X. and Huang, P. (2020a). **xCT: A Critical Molecule That Links Cancer Metabolism to Redox Signaling.** *Mol Ther* 28 (11), 2358-2366, doi: 10.1016/j.ymthe.2020.08.021.

- Liu, T., Liu, Y., Gao, H., Meng, F., Yang, S. and Lou, G. (2013). **Clinical significance of yes-associated protein overexpression in cervical carcinoma: the differential effects based on histotypes.** *Int J Gynecol Cancer* 23 (4), 735-742, doi: 10.1097/IGC.0b013e31828c8619.
- Liu, X., Meng, L., Li, X., Li, D., Liu, Q., Chen, Y., Li, X., Bu, W. and Sun, H. (2020b). **Regulation of FN1 degradation by the p62/SQSTM1-dependent autophagy-lysosome pathway in HNSCC.** *Int J Oral Sci* 12 (1), 34, doi: 10.1038/s41368-020-00101-5.
- Liu, Y., Ren, M., Tan, X. and Hu, L. (2018). **Distinct Changes in the Expression TAZ are Associated with Normal Cervix and Human Cervical Cancer.** *J Cancer* 9 (22), 4263-4270, doi: 10.7150/jca.26623.
- Liu, Y., Zhao, R., Qin, X., Mao, X., Li, Q. and Fang, S. (2022). **Cobimetinib Sensitizes Cervical Cancer to Paclitaxel via Suppressing Paclitaxel-Induced ERK Activation.** *Pharmacology*, 1-8, doi: 10.1159/000524305.
- Livak, K. J. and Schmittgen, T. D. (2001). **Analysis of relative gene expression data using real-time quantitative PCR and the 2(-Delta Delta C(T)) Method.** *Methods* 25 (4), 402-408, doi: 10.1006/meth.2001.1262.
- Lock, S., Linge, A., Lohaus, F., Ebert, N., Gudziol, V., Nowak, A., Tinhofer, I., Kalinauskaite, G., Guberina, M., Stuschke, M., Balermipas, P., von der Grun, J., Grosu, A. L., Debus, J., Ganswindt, U., Belka, C., Peeken, J. C., Combs, S. E., De-Colle, C., Zips, D., Baretton, G. B., Krause, M., Baumann, M. and Dtkk, R. O. G. (2022). **Biomarker signatures for primary radiochemotherapy of locally advanced HNSCC - Hypothesis generation on a multicentre cohort of the DKTK-ROG.** *Radiother Oncol* 169, 8-14, doi: 10.1016/j.radonc.2022.02.009.
- Lu, S. C. (2013). **Glutathione synthesis.** *Biochim Biophys Acta* 1830 (5), 3143-3153, doi: 10.1016/j.bbagen.2012.09.008.
- Luna, A. J., Sterk, R. T., Griego-Fisher, A. M., Chung, J. Y., Berggren, K. L., Bondu, V., Barraza-Flores, P., Cowan, A. T., Gan, G. N., Yilmaz, E., Cho, H., Kim, J. H., Hewitt, S. M., Bauman, J. E. and Ozbun, M. A. (2021). **MEK/ERK signaling is a critical regulator of high-risk human papillomavirus oncogene expression revealing therapeutic targets for HPV-induced tumors.** *PLoS Pathog* 17 (1), e1009216, doi: 10.1371/journal.ppat.1009216.
- Machesky, L. M. (2008). **Lamellipodia and filopodia in metastasis and invasion.** *FEBS Lett* 582 (14), 2102-2111, doi: 10.1016/j.febslet.2008.03.039.
- Maehama, T., Nishio, M., Otani, J., Mak, T. W. and Suzuki, A. (2021). **The role of Hippo-YAP signaling in squamous cell carcinomas.** *Cancer Sci* 112 (1), 51-60, doi: 10.1111/cas.14725.
- Mandl, M. and Depping, R. (2014). **Hypoxia-inducible aryl hydrocarbon receptor nuclear translocator (ARNT) (HIF-1beta): is it a rare exception?** *Mol Med* 20, 215-220, doi: 10.2119/molmed.2014.00032.

- Manning, B. D. and Cantley, L. C. (2007). **AKT/PKB signaling: navigating downstream**. *Cell* 129 (7), 1261-1274, doi: 10.1016/j.cell.2007.06.009.
- Mantovani, F. and Banks, L. (2001). **The human papillomavirus E6 protein and its contribution to malignant progression**. *Oncogene* 20 (54), 7874-7887, doi: 10.1038/sj.onc.1204869.
- Manzo-Merino, J., Contreras-Paredes, A., Vazquez-Ulloa, E., Rocha-Zavaleta, L., Fuentes-Gonzalez, A. M. and Lizano, M. (2014). **The role of signaling pathways in cervical cancer and molecular therapeutic targets**. *Arch Med Res* 45 (7), 525-539, doi: 10.1016/j.arcmed.2014.10.008.
- Marth, C., Landoni, F., Mahner, S., McCormack, M., Gonzalez-Martin, A., Colombo, N. and Committee, E. G. (2017). **Cervical cancer: ESMO Clinical Practice Guidelines for diagnosis, treatment and follow-up**. *Ann Oncol* 28 (suppl_4), iv72-iv83, doi: 10.1093/annonc/mdx220.
- Mason, D. E., Collins, J. M., Dawahare, J. H., Nguyen, T. D., Lin, Y., Voytik-Harbin, S. L., Zorlutuna, P., Yoder, M. C. and Boerckel, J. D. (2019). **YAP and TAZ limit cytoskeletal and focal adhesion maturation to enable persistent cell motility**. *J Cell Biol* 218 (4), 1369-1389, doi: 10.1083/jcb.201806065.
- Matsumoto, H., Haniu, H. and Komori, N. (2019). **Determination of Protein Molecular Weights on SDS-PAGE**. *Methods Mol Biol* 1855, 101-105, doi: 10.1007/978-1-4939-8793-1_10.
- Maxwell, P. H., Wiesener, M. S., Chang, G. W., Clifford, S. C., Vaux, E. C., Cockman, M. E., Wykoff, C. C., Pugh, C. W., Maher, E. R. and Ratcliffe, P. J. (1999). **The tumour suppressor protein VHL targets hypoxia-inducible factors for oxygen-dependent proteolysis**. *Nature* 399 (6733), 271-275, doi: 10.1038/20459.
- McFate, T., Mohyeldin, A., Lu, H., Thakar, J., Henriques, J., Halim, N. D., Wu, H., Schell, M. J., Tsang, T. M., Teahan, O., Zhou, S., Califano, J. A., Jeoung, N. H., Harris, R. A. and Verma, A. (2008). **Pyruvate dehydrogenase complex activity controls metabolic and malignant phenotype in cancer cells**. *J Biol Chem* 283 (33), 22700-22708, doi: 10.1074/jbc.M801765200.
- McKeown, S. R. (2014). **Defining normoxia, physoxia and hypoxia in tumours-implications for treatment response**. *Br J Radiol* 87 (1035), 20130676, doi: 10.1259/bjr.20130676.
- Millis, S. Z., Ikeda, S., Reddy, S., Gatalica, Z. and Kurzrock, R. (2016). **Landscape of Phosphatidylinositol-3-Kinase Pathway Alterations Across 19784 Diverse Solid Tumors**. *JAMA Oncol* 2 (12), 1565-1573, doi: 10.1001/jamaoncol.2016.0891.
- Moesslacher, C. S., Kohlmayr, J. M. and Stelzl, U. (2021). **Exploring absent protein function in yeast: assaying post translational modification and human genetic variation**. *Microb Cell* 8 (8), 164-183, doi: 10.15698/mic2021.08.756.

10. References

- Moody, C. (2017). **Mechanisms by which HPV Induces a Replication Competent Environment in Differentiating Keratinocytes**. *Viruses* 9 (9), doi: 10.3390/v9090261.
- Mori, S., Takeuchi, T., Ishii, Y., Yugawa, T., Kiyono, T., Nishina, H. and Kukimoto, I. (2017). **Human Papillomavirus 16 E6 Upregulates APOBEC3B via the TEAD Transcription Factor**. *J Virol* 91 (6), doi: 10.1128/JVI.02413-16.
- Munger, K., Basile, J. R., Duensing, S., Eichten, A., Gonzalez, S. L., Grace, M. and Zacny, V. L. (2001). **Biological activities and molecular targets of the human papillomavirus E7 oncoprotein**. *Oncogene* 20 (54), 7888-7898, doi: 10.1038/sj.onc.1204860.
- Narisawa-Saito, M. and Kiyono, T. (2007). **Basic mechanisms of high-risk human papillomavirus-induced carcinogenesis: roles of E6 and E7 proteins**. *Cancer Sci* 98 (10), 1505-1511, doi: 10.1111/j.1349-7006.2007.00546.x.
- Noorolyai, S., Shajari, N., Baghbani, E., Sadreddini, S. and Baradaran, B. (2019). **The relation between PI3K/AKT signalling pathway and cancer**. *Gene* 698, 120-128, doi: 10.1016/j.gene.2019.02.076.
- Ohno, H., Nakatsu, Y., Sakoda, H., Kushiya, A., Ono, H., Fujishiro, M., Otani, Y., Okubo, H., Yoneda, M., Fukushima, T., Tsuchiya, Y., Kamata, H., Nishimura, F., Kurihara, H., Katagiri, H., Oka, Y. and Asano, T. (2011). **4F2hc stabilizes GLUT1 protein and increases glucose transport activity**. *Am J Physiol Cell Physiol* 300 (5), C1047-1054, doi: 10.1152/ajpcell.00416.2010.
- Olmedo-Nieva, L., Munoz-Bello, J. O., Manzo-Merino, J. and Lizano, M. (2020). **New insights in Hippo signalling alteration in human papillomavirus-related cancers**. *Cell Signal* 76, 109815, doi: 10.1016/j.cellsig.2020.109815.
- Palacin, M., Bertran, J., Chillaron, J., Estevez, R. and Zorzano, A. (2004). **Lysinuric protein intolerance: mechanisms of pathophysiology**. *Mol Genet Metab* 81 Suppl 1, S27-37, doi: 10.1016/j.ymgme.2003.11.015.
- Pan, D., Wei, L., Yao, M., Wan, D. and Gu, J. (2006). **Down-regulation of CT120A by RNA interference suppresses lung cancer cells growth and sensitizes to ultraviolet-induced apoptosis**. *Cancer Lett* 235 (1), 26-33, doi: 10.1016/j.canlet.2005.03.045.
- Pan, D. N., Li, J. J., Wei, L., Yao, M., Wan, D. F. and Gu, J. R. (2005). **Inhibitory effect of CT120B, an alternative splice variant of CT120A, on lung cancer cell growth**. *Acta Biochim Biophys Sin (Shanghai)* 37 (9), 588-592, doi: 10.1111/j.1745-7270.2005.00091.x.
- Parham, J. H., Kost, T. and Hutchins, J. T. (2001). **Effects of pCIneo and pCEP4 expression vectors on transient and stable protein production in human and simian cell lines**. *Cytotechnology* 35 (3), 181-187, doi: 10.1023/A:1013131415382.
- Pasanen, A., Heikkila, M., Rautavuoma, K., Hirsila, M., Kivirikko, K. I. and Myllyharju, J. (2010). **Hypoxia-inducible factor (HIF)-3alpha is subject to extensive alternative splicing in human**

- tissues and cancer cells and is regulated by HIF-1 but not HIF-2.** *Int J Biochem Cell Biol* 42 (7), 1189-1200, doi: 10.1016/j.biocel.2010.04.008.
- Patel, D., Huang, S. M., Baglia, L. A. and McCance, D. J. (1999). **The E6 protein of human papillomavirus type 16 binds to and inhibits co-activation by CBP and p300.** *EMBO J* 18 (18), 5061-5072, doi: 10.1093/emboj/18.18.5061.
- Pavel, M., Renna, M., Park, S. J., Menzies, F. M., Ricketts, T., Fullgrabe, J., Ashkenazi, A., Frake, R. A., Lombarte, A. C., Bento, C. F., Franze, K. and Rubinsztein, D. C. (2018). **Contact inhibition controls cell survival and proliferation via YAP/TAZ-autophagy axis.** *Nat Commun* 9 (1), 2961, doi: 10.1038/s41467-018-05388-x.
- Phelan, M. C. and Lawler, G. (2001). **Cell counting.** *Curr Protoc Cytom Appendix 3*, Appendix 3A, doi: 10.1002/0471142956.cya03as00.
- Piccolo, S., Dupont, S. and Cordenonsi, M. (2014). **The biology of YAP/TAZ: hippo signaling and beyond.** *Physiol Rev* 94 (4), 1287-1312, doi: 10.1152/physrev.00005.2014.
- Plummer, M., Schiffman, M., Castle, P. E., Maucort-Boulch, D., Wheeler, C. M. and Group, A. (2007). **A 2-year prospective study of human papillomavirus persistence among women with a cytological diagnosis of atypical squamous cells of undetermined significance or low-grade squamous intraepithelial lesion.** *J Infect Dis* 195 (11), 1582-1589, doi: 10.1086/516784.
- Pobbati, A. V. and Hong, W. (2020). **A combat with the YAP/TAZ-TEAD oncoproteins for cancer therapy.** *Theranostics* 10 (8), 3622-3635, doi: 10.7150/thno.40889.
- Pocaterra, A., Romani, P. and Dupont, S. (2020). **YAP/TAZ functions and their regulation at a glance.** *J Cell Sci* 133 (2), doi: 10.1242/jcs.230425.
- Prager, G. W., Feral, C. C., Kim, C., Han, J. and Ginsberg, M. H. (2007). **CD98hc (SLC3A2) interaction with the integrin beta subunit cytoplasmic domain mediates adhesive signaling.** *J Biol Chem* 282 (33), 24477-24484, doi: 10.1074/jbc.M702877200.
- Ramanand, S. G., Chen, Y., Yuan, J., Daescu, K., Lambros, M. B., Houlahan, K. E., Carreira, S., Yuan, W., Baek, G., Sharp, A., Paschalis, A., Kanchwala, M., Gao, Y., Aslam, A., Safdar, N., Zhan, X., Raj, G. V., Xing, C., Boutros, P. C., de Bono, J., Zhang, M. Q. and Mani, R. S. (2020). **The landscape of RNA polymerase II-associated chromatin interactions in prostate cancer.** *J Clin Invest* 130 (8), 3987-4005, doi: 10.1172/JCI134260.
- Rasi Bonab, F., Baghbanzadeh, A., Ghaseminia, M., Bolandi, N., Mokhtarzadeh, A., Amini, M., Dadashzadeh, K., Hajiasgharzadeh, K., Baradaran, B. and Bannazadeh Baghi, H. (2021). **Molecular pathways in the development of HPV-induced cervical cancer.** *EXCLI J* 20, 320-337, doi: 10.17179/excli2021-3365.

10. References

- Ren, N., Liu, Q., Yan, L. and Huang, Q. (2021). **Parallel Reporter Assays Identify Altered Regulatory Role of rs684232 in Leading to Prostate Cancer Predisposition.** *Int J Mol Sci* 22 (16), doi: 10.3390/ijms22168792.
- Revathidevi, S. and Munirajan, A. K. (2019). **Akt in cancer: Mediator and more.** *Semin Cancer Biol* 59, 80-91, doi: 10.1016/j.semcancer.2019.06.002.
- Rodriguez, A. C., Schiffman, M., Herrero, R., Wacholder, S., Hildesheim, A., Castle, P. E., Solomon, D., Burk, R. and Proyecto Epidemiologico Guanacaste, G. (2008). **Rapid clearance of human papillomavirus and implications for clinical focus on persistent infections.** *J Natl Cancer Inst* 100 (7), 513-517, doi: 10.1093/jnci/djn044.
- Rodriguez, C. F., Escudero-Bravo, P., Diaz, L., Bartoccioni, P., Garcia-Martin, C., Gilabert, J. G., Boskovic, J., Guallar, V., Errasti-Murugarren, E., Llorca, O. and Palacin, M. (2021). **Structural basis for substrate specificity of heteromeric transporters of neutral amino acids.** *Proc Natl Acad Sci U S A* 118 (49), doi: 10.1073/pnas.2113573118.
- Rodriguez, L. G., Wu, X. and Guan, J. L. (2005). **Wound-healing assay.** *Methods Mol Biol* 294, 23-29, doi: 10.1385/1-59259-860-9:023.
- Rohwer, N. and Cramer, T. (2011). **Hypoxia-mediated drug resistance: novel insights on the functional interaction of HIFs and cell death pathways.** *Drug Resist Updat* 14 (3), 191-201, doi: 10.1016/j.drug.2011.03.001.
- Santarpia, L., Lippman, S. M. and El-Naggar, A. K. (2012). **Targeting the MAPK-RAS-RAF signaling pathway in cancer therapy.** *Expert Opin Ther Targets* 16 (1), 103-119, doi: 10.1517/14728222.2011.645805.
- Saxton, R. A. and Sabatini, D. M. (2017). **mTOR Signaling in Growth, Metabolism, and Disease.** *Cell* 168 (6), 960-976, doi: 10.1016/j.cell.2017.02.004.
- Schaks, M., Giannone, G. and Rottner, K. (2019). **Actin dynamics in cell migration.** *Essays Biochem* 63 (5), 483-495, doi: 10.1042/EBC20190015.
- Schiffman, M., Castle, P. E., Jeronimo, J., Rodriguez, A. C. and Wacholder, S. (2007). **Human papillomavirus and cervical cancer.** *Lancet* 370 (9590), 890-907, doi: 10.1016/S0140-6736(07)61416-0.
- Schiffman, M., Doorbar, J., Wentzensen, N., de Sanjose, S., Fakhry, C., Monk, B. J., Stanley, M. A. and Franceschi, S. (2016). **Carcinogenic human papillomavirus infection.** *Nat Rev Dis Primers* 2, 16086, doi: 10.1038/nrdp.2016.86.
- Schneider-Poetsch, T., Ju, J., Eyler, D. E., Dang, Y., Bhat, S., Merrick, W. C., Green, R., Shen, B. and Liu, J. O. (2010). **Inhibition of eukaryotic translation elongation by cycloheximide and lactimidomycin.** *Nat Chem Biol* 6 (3), 209-217, doi: 10.1038/nchembio.304.

- Semenza, G. L. (2003). **Targeting HIF-1 for cancer therapy**. *Nat Rev Cancer* 3 (10), 721-732, doi: 10.1038/nrc1187.
- Semenza, G. L. (2010). **HIF-1: upstream and downstream of cancer metabolism**. *Curr Opin Genet Dev* 20 (1), 51-56, doi: 10.1016/j.gde.2009.10.009.
- Shi, R., Liao, C. and Zhang, Q. (2021). **Hypoxia-Driven Effects in Cancer: Characterization, Mechanisms, and Therapeutic Implications**. *Cells* 10 (3), doi: 10.3390/cells10030678.
- Small, W., Jr., Bacon, M. A., Bajaj, A., Chuang, L. T., Fisher, B. J., Harkenrider, M. M., Jhingran, A., Kitchener, H. C., Mileskin, L. R., Viswanathan, A. N. and Gaffney, D. K. (2017). **Cervical cancer: A global health crisis**. *Cancer* 123 (13), 2404-2412, doi: 10.1002/cncr.30667.
- Soto, D., Song, C. and McLaughlin-Drubin, M. E. (2017). **Epigenetic Alterations in Human Papillomavirus-Associated Cancers**. *Viruses* 9 (9), doi: 10.3390/v9090248.
- Stanley, M., Pinto, L. A. and Trimble, C. (2012). **Human papillomavirus vaccines--immune responses**. *Vaccine* 30 Suppl 5, F83-87, doi: 10.1016/j.vaccine.2012.04.106.
- Steinbach, A. and Riemer, A. B. (2018). **Immune evasion mechanisms of human papillomavirus: An update**. *Int J Cancer* 142 (2), 224-229, doi: 10.1002/ijc.31027.
- Stutz, C., Reinz, E., Honegger, A., Bulkescher, J., Schweizer, J., Zanier, K., Trave, G., Lohrey, C., Hoppe-Seyler, K. and Hoppe-Seyler, F. (2015). **Intracellular Analysis of the Interaction between the Human Papillomavirus Type 16 E6 Oncoprotein and Inhibitory Peptides**. *PLoS One* 10 (7), e0132339, doi: 10.1371/journal.pone.0132339.
- Sun, F., Wang, J., Sun, Q., Li, F., Gao, H., Xu, L., Zhang, J., Sun, X., Tian, Y., Zhao, Q., Shen, H., Zhang, K. and Liu, J. (2019). **Interleukin-8 promotes integrin beta3 upregulation and cell invasion through PI3K/Akt pathway in hepatocellular carcinoma**. *J Exp Clin Cancer Res* 38 (1), 449, doi: 10.1186/s13046-019-1455-x.
- Sung, H., Ferlay, J., Siegel, R. L., Laversanne, M., Soerjomataram, I., Jemal, A. and Bray, F. (2021). **Global Cancer Statistics 2020: GLOBOCAN Estimates of Incidence and Mortality Worldwide for 36 Cancers in 185 Countries**. *CA Cancer J Clin* 71 (3), 209-249, doi: 10.3322/caac.21660.
- Tavares, S., Vieira, A. F., Taubenberger, A. V., Araujo, M., Martins, N. P., Bras-Pereira, C., Polonia, A., Herbig, M., Barreto, C., Otto, O., Cardoso, J., Pereira-Leal, J. B., Guck, J., Paredes, J. and Janody, F. (2017). **Actin stress fiber organization promotes cell stiffening and proliferation of pre-invasive breast cancer cells**. *Nat Commun* 8, 15237, doi: 10.1038/ncomms15237.
- Thews, O., Riemann, A., Nowak, M. and Gekle, M. (2014). **Impact of hypoxia-related tumor acidosis on cytotoxicity of different chemotherapeutic drugs in vitro and in vivo**. *Adv Exp Med Biol* 812, 51-58, doi: 10.1007/978-1-4939-0620-8_7.

10. References

- Thomas, M., Narayan, N., Pim, D., Tomaic, V., Massimi, P., Nagasaka, K., Kranjec, C., Gammoh, N. and Banks, L. (2008). **Human papillomaviruses, cervical cancer and cell polarity**. *Oncogene* 27 (55), 7018-7030, doi: 10.1038/onc.2008.351.
- Thompson, B. J. (2020). **YAP/TAZ: Drivers of Tumor Growth, Metastasis, and Resistance to Therapy**. *Bioessays* 42 (5), e1900162, doi: 10.1002/bies.201900162.
- Tian, H., McKnight, S. L. and Russell, D. W. (1997). **Endothelial PAS domain protein 1 (EPAS1), a transcription factor selectively expressed in endothelial cells**. *Genes Dev* 11 (1), 72-82, doi: 10.1101/gad.11.1.72.
- Tian, S., Li, J., Guo, Y., Dong, W. and Zheng, X. (2021). **Expression Status and Prognostic Significance of Gamma-Glutamyl Transpeptidase Family Genes in Hepatocellular Carcinoma**. *Front Oncol* 11, 731144, doi: 10.3389/fonc.2021.731144.
- Torre, L. A., Bray, F., Siegel, R. L., Ferlay, J., Lortet-Tieulent, J. and Jemal, A. (2015). **Global cancer statistics, 2012**. *CA Cancer J Clin* 65 (2), 87-108, doi: 10.3322/caac.21262.
- Totaro, A., Panciera, T. and Piccolo, S. (2018). **YAP/TAZ upstream signals and downstream responses**. *Nat Cell Biol* 20 (8), 888-899, doi: 10.1038/s41556-018-0142-z.
- Tsai, W. B., Aiba, I., Long, Y., Lin, H. K., Feun, L., Savaraj, N. and Kuo, M. T. (2012). **Activation of Ras/PI3K/ERK pathway induces c-Myc stabilization to upregulate argininosuccinate synthetase, leading to arginine deiminase resistance in melanoma cells**. *Cancer Res* 72 (10), 2622-2633, doi: 10.1158/0008-5472.CAN-11-3605.
- Ullah, M. S., Davies, A. J. and Halestrap, A. P. (2006). **The plasma membrane lactate transporter MCT4, but not MCT1, is up-regulated by hypoxia through a HIF-1alpha-dependent mechanism**. *J Biol Chem* 281 (14), 9030-9037, doi: 10.1074/jbc.M511397200.
- van der Heijden, M., Essers, P. B. M., de Jong, M. C., de Roest, R. H., Sanduleanu, S., Verhagen, C. V. M., Hamming-Vrieze, O., Hoebors, F., Lambin, P., Bartelink, H., Leemans, C. R., Verheij, M., Brakenhoff, R. H., van den Brekel, M. W. M. and Vens, C. (2019). **Biological Determinants of Chemo-Radiotherapy Response in HPV-Negative Head and Neck Cancer: A Multicentric External Validation**. *Front Oncol* 9, 1470, doi: 10.3389/fonc.2019.01470.
- Vang Mouritzen, M. and Jenssen, H. (2018). **Optimized Scratch Assay for In Vitro Testing of Cell Migration with an Automated Optical Camera**. *J Vis Exp* (138), doi: 10.3791/57691.
- Vaupel, P. and Mayer, A. (2007). **Hypoxia in cancer: significance and impact on clinical outcome**. *Cancer Metastasis Rev* 26 (2), 225-239, doi: 10.1007/s10555-007-9055-1.
- Viallard, C. and Larrivee, B. (2017). **Tumor angiogenesis and vascular normalization: alternative therapeutic targets**. *Angiogenesis* 20 (4), 409-426, doi: 10.1007/s10456-017-9562-9.

- Vineis, P. and Wild, C. P. (2014). **Global cancer patterns: causes and prevention**. *Lancet* 383 (9916), 549-557, doi: 10.1016/S0140-6736(13)62224-2.
- Wang, D., He, J., Dong, J., Meyer, T. F. and Xu, T. (2020). **The HIPPO pathway in gynecological malignancies**. *Am J Cancer Res* 10 (2), 610-629.
- Wang, H., Jiang, H., Van De Gucht, M. and De Ridder, M. (2019). **Hypoxic Radioresistance: Can ROS Be the Key to Overcome It?** *Cancers (Basel)* 11 (1), doi: 10.3390/cancers11010112.
- Wang, S., Wang, X., Ma, L., Lin, X., Zhang, D., Li, Z., Wu, Y., Zheng, C., Feng, X., Liao, S., Feng, Y., Chen, J., Hu, X., Wang, M. and Han, C. (2016). **Retinoic Acid Is Sufficient for the In Vitro Induction of Mouse Spermatocytes**. *Stem Cell Reports* 7 (1), 80-94, doi: 10.1016/j.stemcr.2016.05.013.
- Wei, J., Liu, Y. and Zhao, C. (2021). **Integrated Analysis of FAM57A Expression and Its Potential Roles in Hepatocellular Carcinoma**. *Front Oncol* 11, 719973, doi: 10.3389/fonc.2021.719973.
- Welf, E. S., Miles, C. E., Huh, J., Sapoznik, E., Chi, J., Driscoll, M. K., Isogai, T., Noh, J., Weems, A. D., Pohlkamp, T., Dean, K., Fiolka, R., Mogilner, A. and Danuser, G. (2020). **Actin-Membrane Release Initiates Cell Protrusions**. *Dev Cell* 55 (6), 723-736 e728, doi: 10.1016/j.devcel.2020.11.024.
- Wigerup, C., Pahlman, S. and Bexell, D. (2016). **Therapeutic targeting of hypoxia and hypoxia-inducible factors in cancer**. *Pharmacol Ther* 164, 152-169, doi: 10.1016/j.pharmthera.2016.04.009.
- Wu, F., Xiong, G., Chen, Z., Lei, C., Liu, Q. and Bai, Y. (2022). **SLC3A2 inhibits ferroptosis in laryngeal carcinoma via mTOR pathway**. *Hereditas* 159 (1), 6, doi: 10.1186/s41065-022-00225-0.
- Wu, X., Cai, J., Zuo, Z. and Li, J. (2019). **Collagen facilitates the colorectal cancer stemness and metastasis through an integrin/PI3K/AKT/Snail signaling pathway**. *Biomed Pharmacother* 114, 108708, doi: 10.1016/j.biopha.2019.108708.
- Xu, W., Yang, Z. and Lu, N. (2015). **A new role for the PI3K/Akt signaling pathway in the epithelial-mesenchymal transition**. *Cell Adh Migr* 9 (4), 317-324, doi: 10.1080/19336918.2015.1016686.
- Yamaguchi, H. and Taouk, G. M. (2020). **A Potential Role of YAP/TAZ in the Interplay Between Metastasis and Metabolic Alterations**. *Front Oncol* 10, 928, doi: 10.3389/fonc.2020.00928.
- Yan, R., Zhao, X., Lei, J. and Zhou, Q. (2019). **Structure of the human LAT1-4F2hc heteromeric amino acid transporter complex**. *Nature* 568 (7750), 127-130, doi: 10.1038/s41586-019-1011-z.

10. References

- Zahra, K., Dey, T., Ashish, Mishra, S. P. and Pandey, U. (2020). **Pyruvate Kinase M2 and Cancer: The Role of PKM2 in Promoting Tumorigenesis**. *Front Oncol* 10, 159, doi: 10.3389/fonc.2020.00159.
- Zhang, H., Bosch-Marce, M., Shimoda, L. A., Tan, Y. S., Baek, J. H., Wesley, J. B., Gonzalez, F. J. and Semenza, G. L. (2008). **Mitochondrial autophagy is an HIF-1-dependent adaptive metabolic response to hypoxia**. *J Biol Chem* 283 (16), 10892-10903, doi: 10.1074/jbc.M800102200.
- Zhang, Q. S., Li, Y. H., Wang, B. B. and Ma, S. S. (2020). **Expression of TAZ, YAP, and beta-catenin in cervical squamous cell carcinoma and their clinical significance**. *Int J Clin Exp Pathol* 13 (7), 1560-1568.
- Zhu, B., Cheng, D., Hou, L., Zhou, S., Ying, T. and Yang, Q. (2017). **SLC3A2 is upregulated in human osteosarcoma and promotes tumor growth through the PI3K/Akt signaling pathway**. *Oncol Rep* 37 (5), 2575-2582, doi: 10.3892/or.2017.5530.
- Zimmermann, H., Degenkolbe, R., Bernard, H. U. and O'Connor, M. J. (1999). **The human papillomavirus type 16 E6 oncoprotein can down-regulate p53 activity by targeting the transcriptional coactivator CBP/p300**. *J Virol* 73 (8), 6209-6219, doi: 10.1128/JVI.73.8.6209-6219.1999.

11. Curriculum Vitae

Personal information

Family name:	Yang
First name:	Dongyun
Gender:	Female
Date of Birth:	28.12.1992
Place of Birth:	Anhui, China
Nationality:	Chinese

Education:

Sep. 2018 - present:	Research Group Molecular Therapy of Virus-Associated Cancers, German Cancer Research Center (DKFZ), Heidelberg University, Heidelberg, Germany MD candidate
Sep. 2015 – Jun. 2018	Obstetrics and Gynecology, Huazhong University of Science and Technology, Wuhan, China granted Master degree
Sep.2010 – Jun. 2015	Clinical medicine, Huazhong University of Science and Technology, Wuhan, China granted Bachelor degree
Sep. 2007 – Jun. 2010	Hefei No.6 High School, Hefei, China graduation

12. Acknowledgments

This dissertation was conducted at the German Cancer Research Center (DKFZ) in Heidelberg, Germany, in the Research Group “Molecular Therapy of Virus-Associated Cancers” headed by Prof. Dr. Felix Hoppe-Seyler.

First and foremost, I would like to express my sincere gratitude to Prof. Dr. Felix Hoppe-Seyler for giving me the precious opportunity to work on this project in his team and for constant guidance, support and encouragement. In addition, I am extremely grateful to Prof. Dr. Karin Hoppe-Seyler for patient mentoring and discussions and for inspiring me in my scientific research and daily life.

I would like to acknowledge to Prof. Dr. Frank Rösl (DKFZ) and PD Dr. Martin Volkmann (MVZ Labor PD Dr. Volkmann und Kollegen, Karlsruhe) for being members of my Thesis Advisory Committee.

I would also like to thank Claudia Tessmer and Prof. Dr. Ilse Hofmann (DKFZ) for their contributions to the development of anti-FAM57A antibody.

Importantly, I wish to express my warmest gratitude to all members of the F065 team, not only for their valuable and productive advice regarding my laboratory routine, but also for creating the friendly and supportive working atmosphere. I would thank Angela Holzer, Claudia Lohrey, and especially Julia Bulkescher for their excellent assistance at the workbench and for their patience in answering all my questions. My gratitude also goes to Svenja Adrian, Alicia Avenhaus, Felicitas Bossler, Julia Braun, Antonia Däschle, Kristin Frensemeier, Nora Heber, Anja Herrmann, Julia Mändl, Tobias Strobel, Milica Velimirović and Maria Weber. In addition, I would also thank Thomas Holz for his support concerning any IT problems. It was a great and memorable experience working with you all.

Furthermore, many thanks go to my friends in Heidelberg for being with me and for giving me many wonderful memories during the 4-year research life. I would also like to be thankful to my friends in China for their words of comfort, encouragement and support, particularly during the tough time of COVID-19.

I would also appreciate the support from the China Scholarship Council (CSC) and the help from the General Consulate of the People’s Republic of China in Frankfurt am Main.

Finally, I am deeply grateful to my beloved family, especially to my parents Chunhai Yang and Yuhong Yang. Thank you for all of your care and love, as well as for your understanding and support through these years. I am lucky and happy to have you in my life.

13. Eidesstattliche Versicherung

1. Bei der eingereichten Dissertation zu dem Thema

Expression and Function of FAM57A (Family with Sequence Similarity 57 Member A) in Human Papillomavirus-Positive Cervical Cancer Cells

handelt es sich um meine eigenständig erbrachte Leistung.

2. Ich habe nur die angegebenen Quellen und Hilfsmittel benutzt und mich keiner unzulässigen Hilfe Dritter bedient. Insbesondere habe ich wörtlich oder sinngemäß aus anderen Werken übernommene Inhalte als solche kenntlich gemacht.

3. Die Arbeit oder Teile davon habe ich bislang nicht an einer Hochschule des In- oder Auslands als Bestandteil einer Prüfungs- oder Qualifikationsleistung vorgelegt.

4. Die Richtigkeit der vorstehenden Erklärungen bestätige ich.

5. Die Bedeutung der eidesstattlichen Versicherung und die strafrechtlichen Folgen einer unrichtigen oder unvollständigen eidesstattlichen Versicherung sind mir bekannt. Ich versichere an Eides statt, dass ich nach bestem Wissen die reine Wahrheit erklärt und nichts verschwiegen habe.

Ort und Datum

Unterschrift